University of Stavanger

Faculty of Science and Technology

MASTER'S THESIS

Study program/ Specialization: Petroleum Geosciences Engineering	Spring semester, 2015 Open
Writer: Nina Egeland	…… (Writer's signature)
Faculty supervisor: Dr. Udo Zimmermann Co-supervisor(s): Laura Borromeo (Ph.D. candidate)	
Thesis title: Raman Spectroscopy Applied To Enhanced Oil Recovery Research	
Credits (ECTS): 30	
Key words: Raman spectroscopy, Enhanced oil recovery, EOR, Liège chalk, Gulpen Formation, Long term test, Ultra long term test, Alteration front	Pages: …… + enclosure: …… Stavanger, …….. Date/year

Raman Spectroscopy Applied To Enhanced Oil Recovery Research

by

Nina Egeland

MSc Thesis

Presented to the Faculty of Science and Technology

University of Stavanger

Norway

University of Stavanger

June 2015

ACKNOWLEDGEMENTS

Foremost, I would like to express my immense gratitude to my supervisor Dr. Udo Zimmermann for providing me with the possibility to conduct and complete this thesis. His continuous support and engagement have helped me in the time of research and writing. His dedication to geology has deeply inspired me and it gives me great pleasure acknowledging Dr. Zimmermann as an outstanding teacher and mentor throughout my five years of study at the University of Stavanger.

Besides, I would like to thank my co-supervisor Laura Borromeo, Ph.D. candidate at the University of Stavanger for training in use of Raman spectrometer. This thesis would not have been completed without your knowledge. Your encouraging words have meant a lot to me through the process of writing this thesis. I would also like to thank Dr. Eduardo Garzanti and Dr. Sergio Andò by the Dipartimento di Scienze Geologiche e Geotecnologie Università di Milano-Bicocca in Italy, for giving me the opportunity to use their Raman spectrometer.

I would like to thank Reidar I. Korsnes and Anders Nermoen, who were in charge of the flooding experiment performed on the two samples in this study. I would also like to thank Andreas Habel for providing me with the necessary software and making it easy for me to work on different locations. I want to express my gratitude to the National IOR Centre for funding this study.

Finally, I want to thank my husband, family, and friends for the support and encouragement throughout the completion of my Master's Degree in Petroleum Geosciences Engineering at the University of Stavanger.

ABSTRACT

It is well established that aqueous chemistry affects the mechanical strength of chalk. Seawater tends to weaken chalk at reservoir temperatures and consequently the recovery rate. As more than 50 % of the oil in existing fields on the Norwegian Continental Shelf cannot be produced with current methods, many research projects concerning enhanced oil recovery (EOR) have been initiated, which is also the background for this study.

Raman spectroscopy is a non-destructive, quick, analytical method getting more and more attention in the oil industry. The objectives of this study were to describe the methodology of Raman spectroscopy, and to apply this methodology to two core samples of chalk flooded with $MgCl_2$ in order to describe and quantify the effects of flooding processes. When chalk is injected with $MgCl_2$, ion exchange will take place and may result in growth of new mineral phases. Magnesite ($MgCO_3$) was identified as the major newly grown mineral phase in these samples. The extent of the injection period was different for the two samples from chalk exposures close to Liège (Belgium) of Upper Cretaceous age; LTT was flooded for 1.5 years and ULTT for 3 years.

Raman spectroscopy quickly confirmed that in the ULTT sample sufficient amount of Mg^{2+} was exposed to ion exchange to form magnesite throughout the whole injection period, resulting in a magnesite content of 81 %. Raman spectroscopy could identify a decreasing occurrence of magnesite along the core of LTT. The magnesite abundance decreases from 51 % to 15 % within the first 4 cm of the core (slice 1-4). In previous research, magnesite was traced up to slice 3, while in this study magnesite was detected in slice 4, suggesting the alteration front to be located within this slice.

These results strengthen the possibility of the application of Raman spectroscopy as a quick, cheap, and effective methodology for the study of mineral compositions and even fine-grained rock material like chalk.

TABLE OF CONTENTS

TABLE OF FIGURES

TABLE OF TABLES

1. INTRODUCTION

1.1. Enhanced Oil Recovery (EOR)

Enhanced oil recovery (EOR) is a topic of high interest for the Norwegian government as more than 50 % of the oil in existing fields on the Norwegian Continental Shelf (NCS) cannot be produced with current methods (Figure 1) (Norwegian Petroleum Directorate, 2011). Either the oil is immobile or chosen injection strategies lead to insufficient sweep efficiency (Norwegian Petroleum Directorate, 2014). The average oil recovery rate on NCS is currently about 47 % and the aim is to further increase this factor. Only a slight increase in the recovery rate can result in huge economical rewards. Several research projects concerning improved oil recovery (IOR) have therefore been initiated and the National IOR Centre of Norway (NIOR), which was established in 2013, is one of them. This study is part of a larger research project at NIOR.

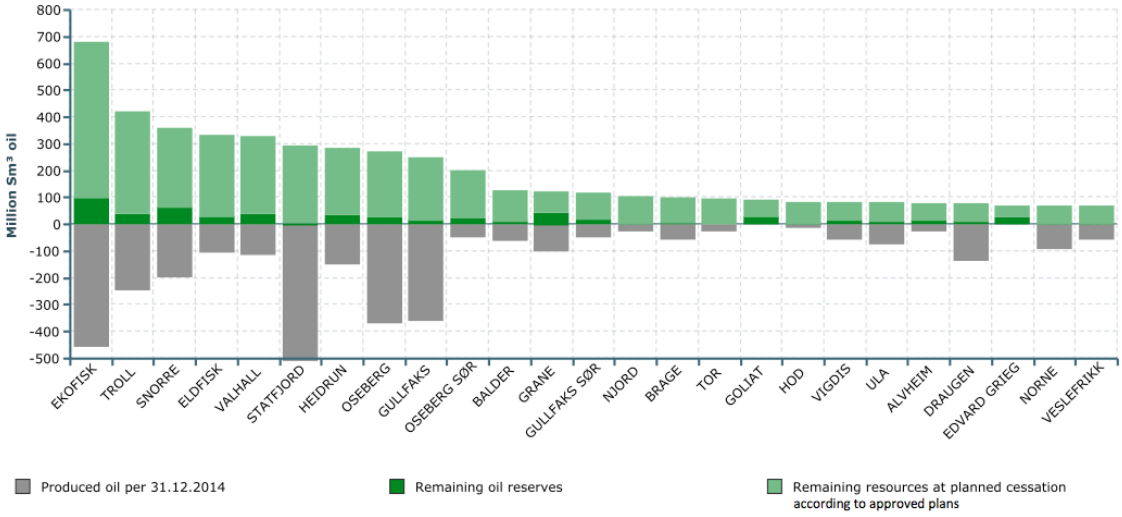

Figure 1: Distribution of oil reserves and resources for the largest oil producing fields on the Norwegian Continental Shelf as of 31 December 2014 (Norwegian Petroleum Directorate, 2015).

The effect of aqueous chemistry on the mechanical strength of chalk is extensively studied (Thomas et al., 1987; Strand et al., 2007 and references therein). At reservoir temperatures, seawater tends to weaken chalk and consequently the recovery rate (Madland et al., 2011). It is important to understand how fluids interact with rocks because textural changes in the pore space affect how water will absorb and expel oil from the rock (Zimmermann et al., 2015). Fluid injection is therefore often used for EOR research. Experiments on onshore chalk aim to identify mineralogical and chemical impact after flooding processes. Onshore chalk is used as an analogue to reservoir chalk.

Two samples of chalk, which have been flooded with $MgCl_2$ for 1.5 years and 3 years at the University of Stavanger, were investigated with one specific method with the objective of describing and quantifying the effects of flooding processes. These are the first long-term tests on chalk with the injection of $MgCl_2$ under reservoir conditions, although several long-term experiments have been reported before (Hellmann et al., 2002). For further information about flooding processes, the reader is referred to Madland et al. (2011) or Hjuler and Fabricius (2007). The intention of this study was to give a more detailed description of Raman spectroscopy, which is one of the most important methods when it comes to identifying mineral phase down to micron level. This possibility is of paramount importance in research (Madland et al., 2013; Zimmermann et al., 2013). Raman spectroscopy was here used in observing mineralogical changes after flooding. This methodology will together with other research methods provide a full range of information on the flooded chalk cores for a broader understanding of chemical and mineralogical changes. This information will be used for further estimation of rock mechanical changes on an even larger scale, the actual field.

With the purpose of implementing research results into EOR, certain steps are essential: (i) an equivalent onshore chalk must be found and used for the research, (ii) a more extensive knowledge concerning the reservoir chalk must be developed, and (iii) mineralogical and chemical processes in the tested onshore chalk must be studied.

1.2. Raman Spectroscopy

The technique of Raman spectroscopy involves focussing a beam of light onto a sample to identify its molecular composition. The majority of the photons will scatter from the sample with no change of energy, but a small number of photons will exchange a tiny amount of energy and cause molecules in the sample to vibrate. Sir Chandrasekhra Venkata Raman discovered this phenomenon, called the Raman effect, in 1928. He used sunlight as the source, a telescope as the collector and his own eyes as the detector (Ferraro et al., 2002). It is remarkable that bare eyes detected such a feeble phenomenon as Raman scattering and Sir C. V. Raman won the 1930 Nobel Prize for Physics for his discovery. The Raman instrumentation was gradually improved.

Raman spectroscopy is a non-destructive method without any sample preparation necessary and therefore preferable for many users (archaeologists, mineralogists, forensic scientists, etc.) and is gaining more and more popularity in the oil industry (e.g. Gorelik et al., 2000; Costa et al., 2006; Sebek et al., 2011; Andrews et al., 2015). A PhD at the University of Stavanger is sponsored by the NIOR, which also proves the increasing interest.

The key advantages and disadvantages of Raman spectroscopy are listed on the next page.

Advantages

- Can analyse solids, liquids, and gases
- A fast technique and a good quality spectrum can be obtained in just a few seconds
- Non-destructive analysis which allows for further investigation with other analyses
- Two- and three-dimensional images of the sample can be generated simultaneously
- Detailed chemical/molecular analysis and can provide ranges of mineral contents
- Provide subtle information such as crystallinity, phase, intrinsic stress/strain and polymorphism
- Vacuum is not necessary
- The spectrometer takes up little space

Disadvantages

- Cannot analyse metals
- Fluorescence may obscure the Raman spectrum
- An accurate database is necessary in order to interpret the spectrum
- The Raman effect is very weak, which leads to low sensitivity. Low concentration of a substance may therefore prove challenging to measure, e.g. phyllosilicates
- Heating from the laser radiation can destroy the sample or cover the Raman spectrum
- Not as quantitative as a probe by now, but this is constantly being improved. Closer to being semi-quantitative now

1.3. Previous Work

Mineralogical and geochemical composition of chalk has been systematically studied for more than 40 years (Scholle, 1974; Hancock, 1975; Scholle, 1977; Fabricius, 2007). Until now, the small grain size of chalk and the too-coarse spatial resolution of observation techniques have impeded the progress. Raman spectroscopy is a quick analytical technique that can investigate the composition of micro-sized (nano-sized with nano-Raman) particles that requires little sample material and open new possibilities in the understanding of chalk. To the writer's knowledge, Borromeo et al. (2015a; in prep.) is the first study to apply Raman spectroscopy analysis to chalk, in which the results of this thesis will be included. The writer is also privileged to become the second author of Borromeo et al. (2015a; in prep.).

1.4. Objectives

The objectives of this study were to describe one specific research method in detail, i.e. Raman spectroscopy, and to use this methodology to identify and analyse mineralogical and chemical effects after two samples of chalk have been injected with $MgCl_2$.

1.5. Implications of Raman Spectroscopy in the Oil Industry

Raman spectroscopy is a very information-rich technique, which not only confirms molecular identity, but also is highly sensitive to the physical form in which the compound is present. Differentiation of polymorphs is therefore possible. Raman spectroscopy is a robust method, which will give high-resolution results, even when used offshore. The spectrometer is cheap in comparison to other analytical methods (60000-120000 EUR) and the methodology is very fast as a good quality spectrum can be obtained in just a few seconds.

2. METHODOLOGY

2.1. Mechanical Flow Through Experiment

Before this study was initiated, two chalk cores were injected with $MgCl_2$ for 516 days (1.5 years) and 1072 days (3 years) under reservoir conditions. The chalk cores were mounted into triaxial cells (Figure 2) that allow for measurements of axial and radial strains while flooding of reactive fluids at elevated pressures, stresses, and temperatures. The confining pressure and pore pressure were simultaneously increased from 0.5 and 0 MPa to 1.2 and 0.7 MPa, respectively, with a constant stress difference of 0.5 MPa. The triaxial cell was equipped with a heating jacket and a regulation system that kept the temperature constant at 130 ± 0.1°C during the experiment. Distilled water was injected to ensure a clean pore system and to clean the sample. 0.0219 M $MgCl_2$ brine was then injected at a constant injection rate of 32.4 ml/day (i.e. 1 initial PVs/day). The injection rate was constant throughout the experiment. The flooding rate varied between 33.12 cm^3/day and 99.36 cm^3/day.

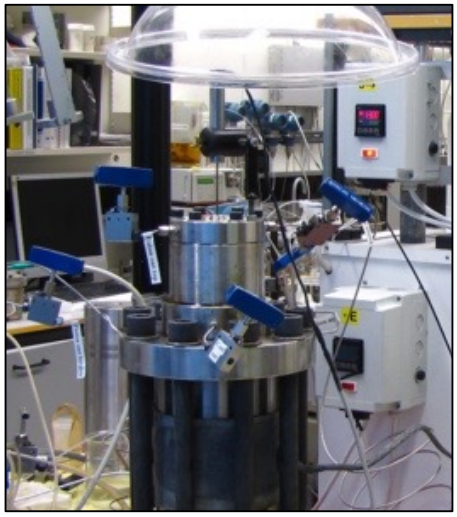

Figure 2: One of the triaxial cells in a laboratory at the University of Stavanger where the rocks were exposed to mechanical compression tests under reservoir conditions (University of Stavanger, 2013).

Each of the 70 mm long cores was cut into six slices with thicknesses of about 1 cm (Figure 3). The diameter of 38 mm allows probing of the sample with different methods, where Raman spectroscopy is one of the methods.

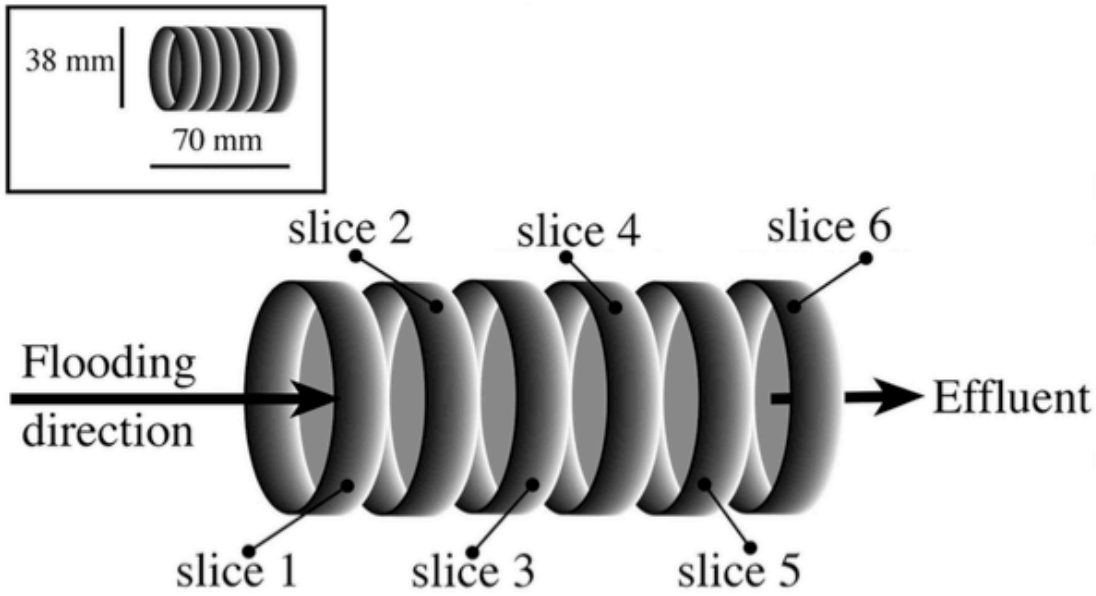

Figure 3: Sketch of the cutting of the two samples. $MgCl_2$ fluid was injected from left into sample core and the effluent collected on the right. Dimensions of the samples are also indicated. The cores are ca. 70 mm long, have diameters of 38 mm, and were cut into six slices, which are illustrated as separated units (Zimmermann et al., 2015).

2.2. The Raman Spectrometer

The technique of Raman spectroscopy relies on focussing a monochromatic light source, i.e. a laser, on a sample and detecting the scattered light (Figure 4). The majority of the photons will scatter from the sample with no change of energy. Frequency is proportional to energy and the photons will therefore have the same frequency as the incident light (v_0). This is called Rayleigh scattering. A small number of photons (1/1000000) will however exchange a tiny amount of energy, causing molecules in the sample to vibrate. This is called Raman

scattering. Raman scattering is characterised by frequencies $v_0 \pm v_m$, where v_m is the vibrational frequency of a molecule. The $v_0 - v_m$ and $v_0 + v_m$ are called Stokes and anti-Stokes scattering, respectively (Figure 5) (Ferraro et al., 2002). A Raman spectrometer measures the vibrational frequency (v_m) as a shift from the frequency of the incident light (v_0) (Ferraro et al., 2002) and the observed Raman shift of the Stokes and anti-Stokes scattering is a direct measure of the vibrational energies of the molecules under investigation.

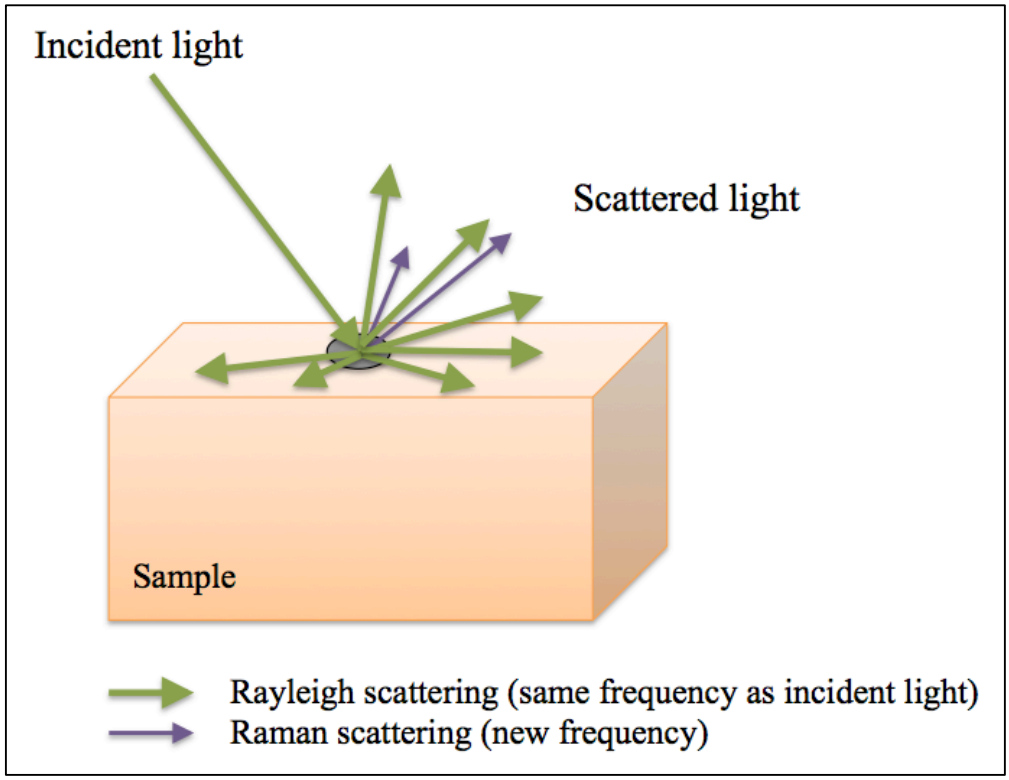

Figure 4: Most photons will scatter from the sample with no change in frequency, called Rayleigh scattering. A small number (1/1000000) of photons will however change frequency and this phenomenon is called Raman scattering. The line thickness represents the intensity of the signal (modified after Lawrence Berkeley National Laboratory, 2007).

It is important to now state the relationship between frequencies and wavelengths. In vibrational spectroscopy, it is rather unusual to express the photon energy by the frequency or

wavelength of the light. Frequencies and wavelengths are therefore generally transformed into wavenumbers ($\tilde{\nu}$). The wavenumber is defined as

$$\tilde{\nu} = \frac{v}{c} = \frac{1}{\lambda},$$

where v is the frequency, c is the speed of light, λ is the wavelength, and the unit of the wavenumber is cm^{-1}. A Raman spectrum is obtained when the light intensity (counts) is plotted against Raman shift (cm^{-1}).

In Rayleigh scattering, a photon interacts with a molecule, to further polarise the electron cloud and raise it to a virtual energy state (Figure 5). The molecule quickly drops back down to its ground state and a photon is released. Since the molecule drops back to its initial state, the energy released in the photon has to be the same as the energy from the initial photon. The frequency and wavelength is therefore the same and since the photon can be released in any direction, scattering is the result. In Raman scattering, a photon lose or gain energy resulting in a changed frequency and wavelength. The vibrational energy levels in the ground state of the molecule controls the energy increase or decrease. When the molecule rises from a ground state to a virtual state and drops back to a (higher energy) vibrational state then the scattered photon has less energy than the incident photon ($v_0 - v_m$), and therefore a longer wavelength. This is called Stokes scattering. When the molecule is positioned in a vibrational state to begin with and drops back to its ground state then the scattered photon has more energy ($v_0 + v_m$), and therefore a shorter wavelength. This is called anti-Stokes scattering. Stokes and anti-Stokes provide the same information, and it is therefore customary to measure only the Stokes half of the spectrum due to its greater intensity.

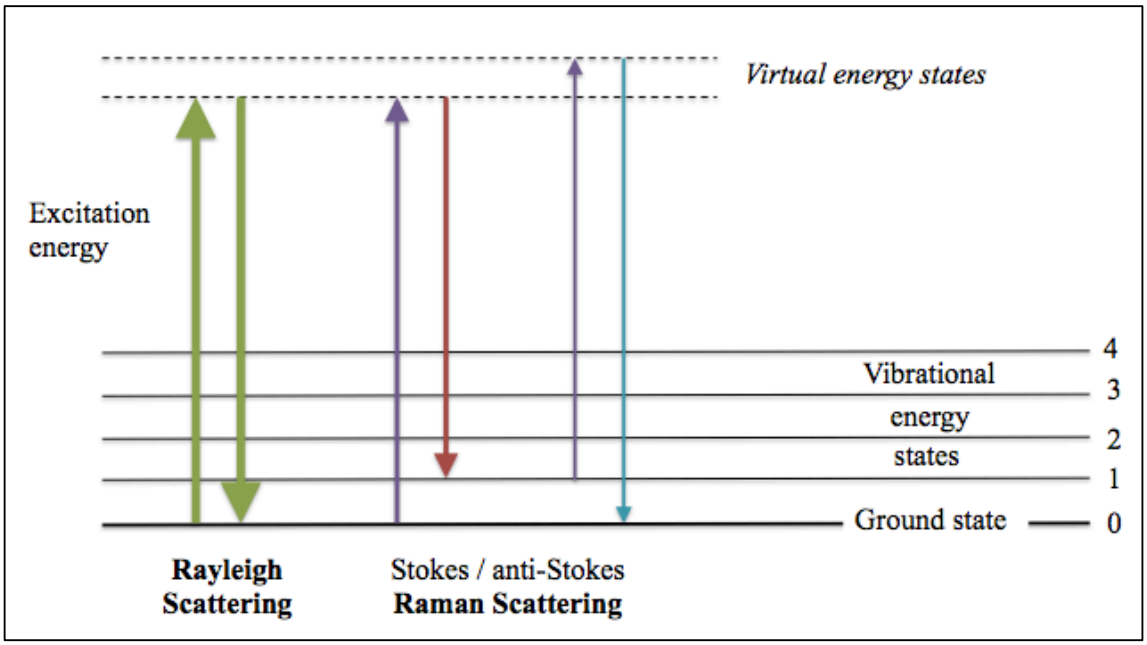

Figure 5: Three different forms of scattering are indicated. Those are Rayleigh and Raman scattering, where Stokes and anti-Stokes are two varieties of Raman scattering. The line thicknesses represent the intensity of the signal. Explanations of arrows: green = Rayleigh scattering, purple = Raman Scattering, red = Stokes scattering, and blue = anti-Stokes scattering (modified after DoITPoMS, 2007b).

Raman is a non-destructive method used to characterize any substance in any physical state. The spatial resolution that can be obtained by Raman spectroscopy is down to 1-2 microns in common applications. There are however, several analytical arrangements where the resolution is far below 1 micron and the observation field can be studied during penetration with an atomic force microscope (AFM). Figure 6 illustrates the construction of a typical Raman spectrometer. The monochromatic light is beamed through a window and filters lead the light to the sample. Optical filters are used to selectively block Rayleigh scatter whilst allowing Raman scatter to pass through to the spectrometer. A set of mirrors gathers the reflected light from the sample and focus it through the entrance slit to the double grating monochromator. A Charge-Coupled Device (CCD) detects the scattered light, transforms the light into a spectrum, and records the intensity of Raman scattering in arbitrary units by wavelength. This intensity is then normalized by the strongest or most defined peak and can

provide a qualitative explanation of the molecular structure. In other words, when a laser is focussed onto a molecule, the molecule starts to vibrate. This vibration is characteristic for the structure of that particular mineral. The vibration modes change the way the wavelength of light is perceived. If this information is plotted where y-axis represents the intensity of the light and x-axis the wavelength of that light, a specific pattern occur. The entire spectral pattern can normally be associated with a specific mineral or a specific substance.

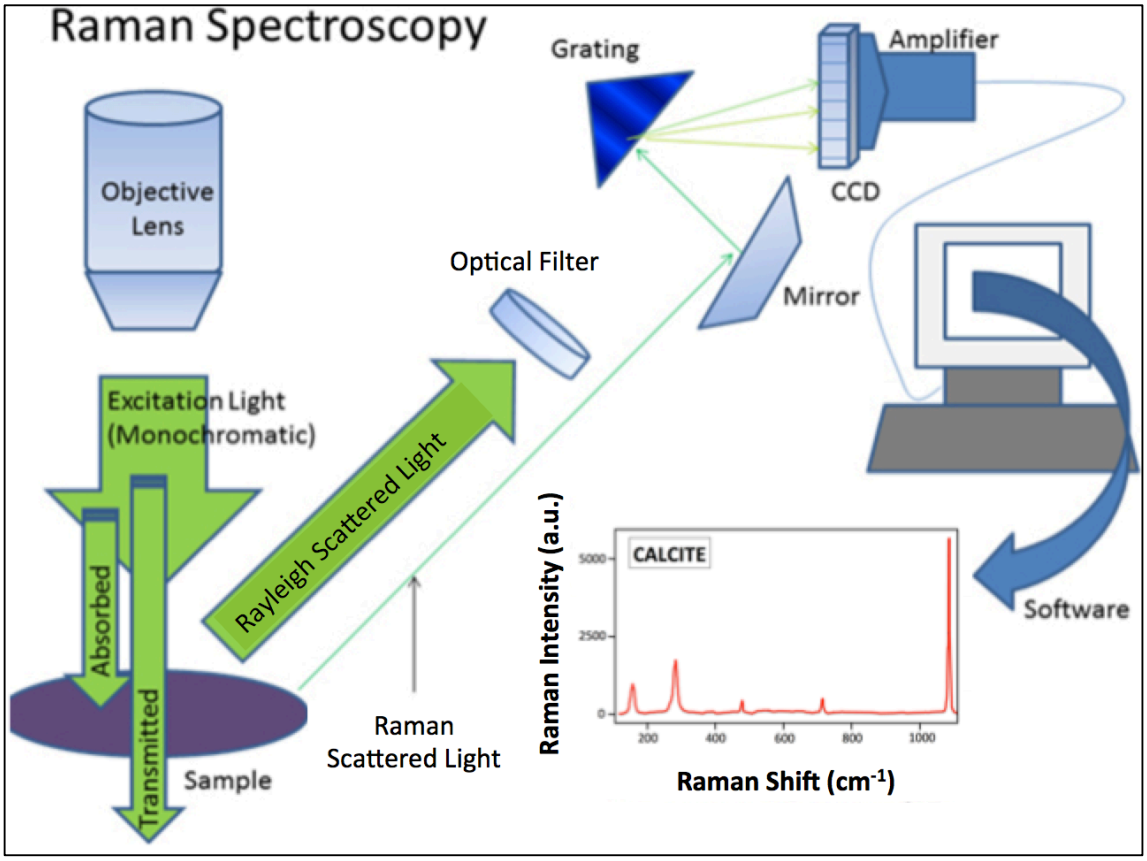

Figure 6: The construction of a typical Raman spectrometer. A laser is beamed onto the sample and optical filters block Rayleigh scatter whilst allowing Raman scatter to pass to the detector. The result is a Raman spectrum that can provide a qualitative explanation of the molecular structure (modified after The Prashant Kamat Laboratory, 2012).

In the next subchapters, the reader will find more information around the most important elements of a Raman spectrometer. The subchapters are arranged after their order within the spectrometer. Fluorescence is a phenomenon that may obscure the Raman spectrum. More details around fluorescence are mentioned in subchapter 2.2.5.

2.2.1. Laser

The wavelength of the monochromatic light used in Raman spectroscopy varies; the most common light sources have a wavelength from 532 to 785 nm. The intensity of Raman scattering is proportional to λ^{-4} (λ is the laser wavelength) and the choice of laser is therefore important for the sensitivity of desired analysis. An infrared laser will actually decrease the scattering intensity by a factor of 15 or more in comparison with blue/green visible lasers. The choice of laser is also important concerning the fact that certain wavelengths interact better with certain vibrational modes of a substance, and some substances could be fluorescent with one wavelength and not with other wavelengths. Each laser wavelength requires an individual filter.

2.2.2. Optical Filters

The main challenge in Raman spectroscopy is preventing overlapping of the relatively weak Raman signal by stray light from the far more prominent Rayleigh scattering. Different types of filter are therefore used to block Rayleigh scattering from reaching the detector. The four basic types of filters are (Figure 7): long-wave-pass (LWP) edge filter, short-wave-pass (SWP) edge filter, notch filter, and laser line filter (Semrock, 2000). The notch filter transmits both Stokes and anti-Stokes Raman signal while blocking out the laser, and is commonly used together with a laser line filter, which transmits the laser, but blocks all other light. The notch

filter cuts the lowest region of the spectrum, have a finite lifetime, and will degrade with time. The edge filter offers the narrowest transition to see Raman signals very close to the laser line, which makes the edge filter the superior alternative. It transmits either Stokes (long pass) or anti-Stokes (short pass). The edge filter is environmentally stable and has a near infinite lifetime.

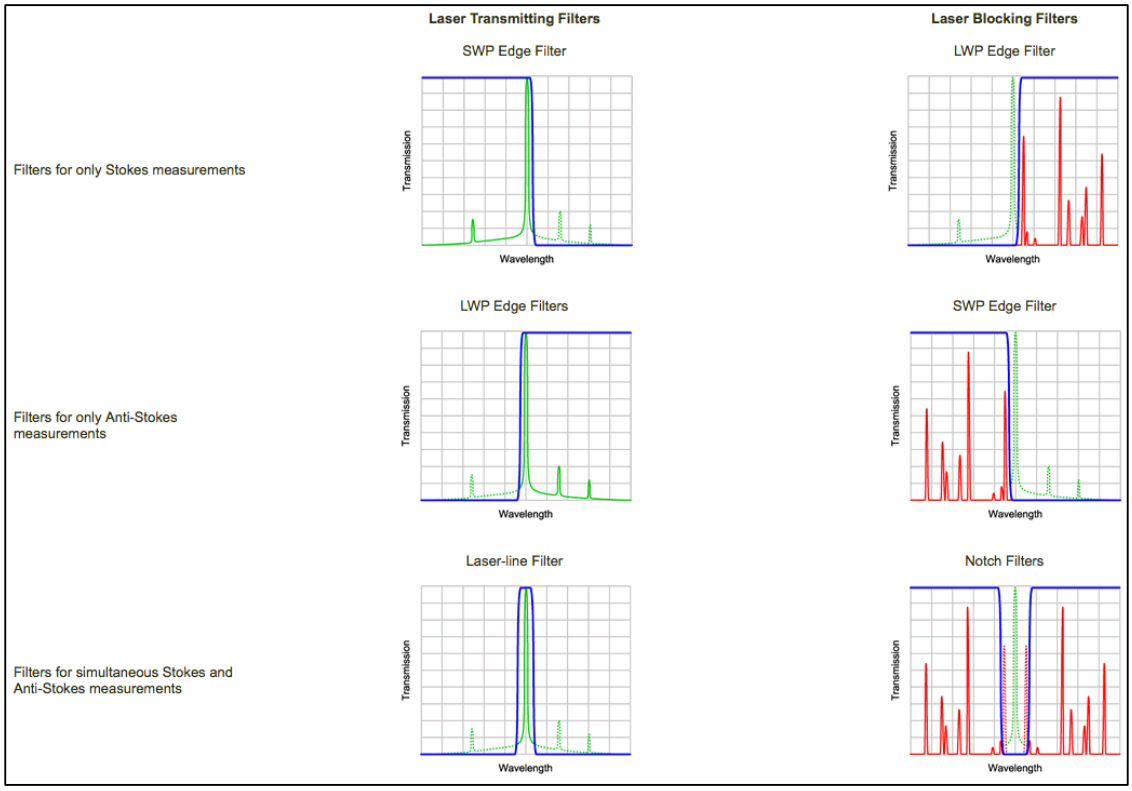

Figure 7: Illustration of how different filters can be used in a Raman spectrometer. The blue lines represent the filter transmission spectra, the green lines represent the laser spectrum, and the red lines represent the Raman signal (Semrock, 2000).

2.2.3. Diffraction Grating

Diffraction is the optical operation that makes it possible to separate the different wavelengths of Raman scatter. The diffraction grating is an array of finely spaced lines on a reflective

surface and is used to reduce stray light, which is generated by dispersion in the spectrometer. The two most common types of grating are holographic and ruled diffraction grating. Raman spectrometers typically use holographic gratings, as these normally have much less manufacturing defects in their structure than the ruled ones and result in much less stray light. When the light hits the diffraction grating, the light is dispersed and further projected onto the CCD (Figure 8) (Subchapter 2.2.4).

The spectral resolution, the ability to resolve features within the spectrum, is important. Increasing the focal length or changing the grating can increase the spectral resolution. If the focal length (e.g. the distance between the diffraction grating and the CCD) is doubled, the spectral resolution is (approximately) doubled as well. Similarly, if the density of the lines on the grating is doubled, the dispersion i.e. the spectral resolution is doubled.

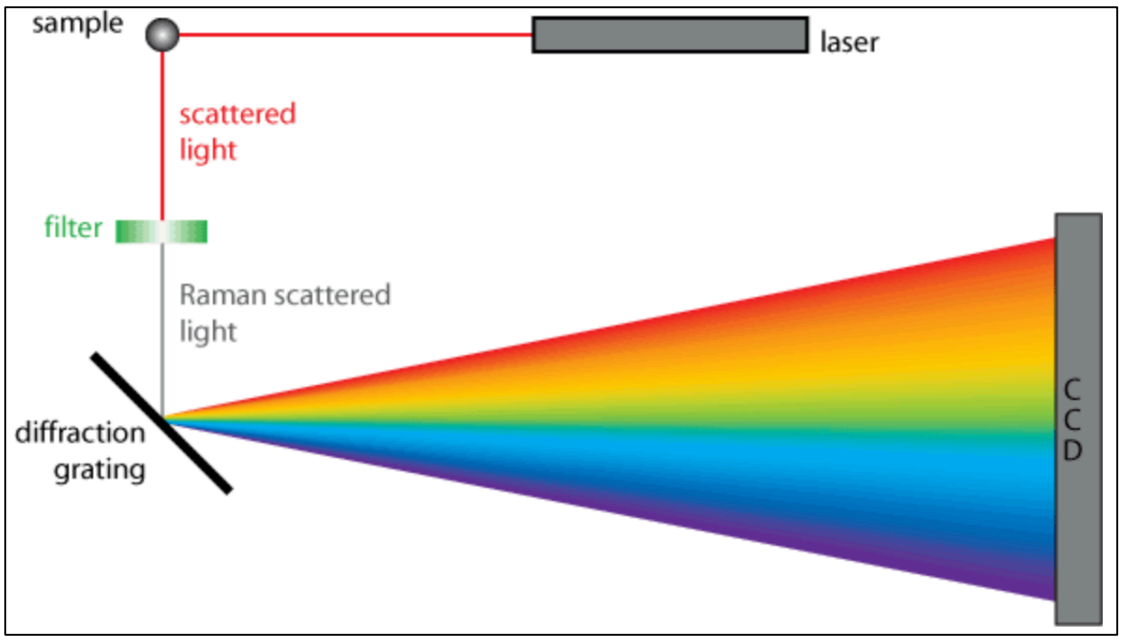

Figure 8: A diffraction grating is often used in Raman spectrometers to reduce stray light. When the light hits the diffraction grating, the light is dispersed and further projected onto the CCD. Changing the focal length or the grating can increase the spectral resolution (DoITPoMS, 2007a).

2.2.4. Charge-Coupled Device (CCD)

The diffraction grating disperses the light and it is then projected onto the CCD array. As CCDs are extremely sensitive to light, they are used as detectors in Raman spectrometers. It is a silicon based multichannel array of thousands or millions of individual detector elements that allows the entire Raman spectrum to be detected in one single acquisition. Each element interacts with light and charge is built up. The brighter the light, and/or the longer the interaction, the more charge is registered. The point of each measured charge reading is then collected. The different elements will detect light from each corresponding cm^{-1} edge of the spectrum, pixel 1 from the low cm^{-1} edge, and pixel 1024 from the high cm^{-1} edge of the spectrum (Figure 9).

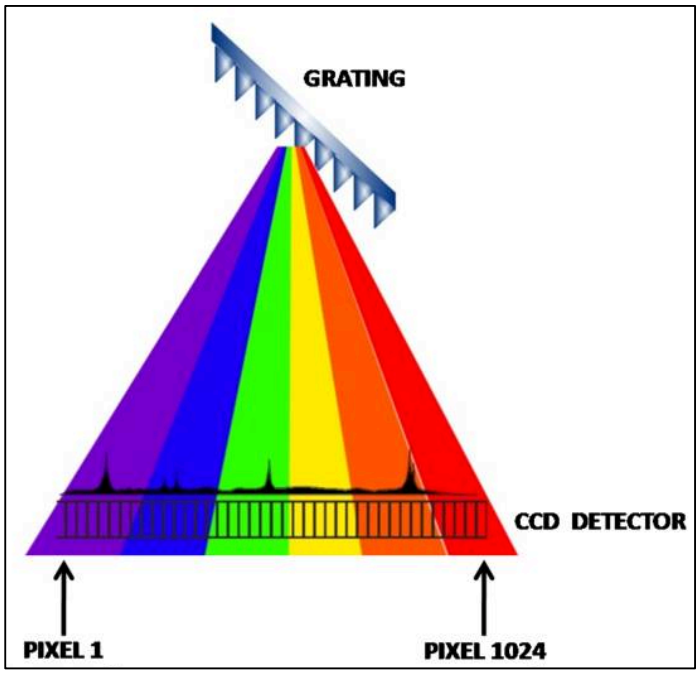

Figure 9: A CCD is an array that consists of thousands of detector elements. The first element will detect light from the low cm^{-1} edge of the spectrum, the second element of the next spectral position, and so on. The last element will detect light from the high cm^{-1} edge of the spectrum (Horiba Scientific, 2005).

2.2.5. Fluorescence

Some molecules are capable of being excited because of absorption of light energy. If the energy absorbed from the external light source is sufficient, the molecule reaches a higher energy state (Figure 10). There are multiple high-energy states that the molecule can attain depending on the wavelength and energy of the external light source. The molecule is however unstable at these high-energy configurations and will always seek the lowest energy excited state, where it is semi-stable. In that process, energy is lost. From the semi-stable state, the molecule will return to its ground state and excess energy is released and emitted as light on the way. As the energy has decreased, the wavelength of the emitted light will always be longer than the absorbed light, thus the emitted light will have a different colour than the absorbed light. This process is called fluorescence.

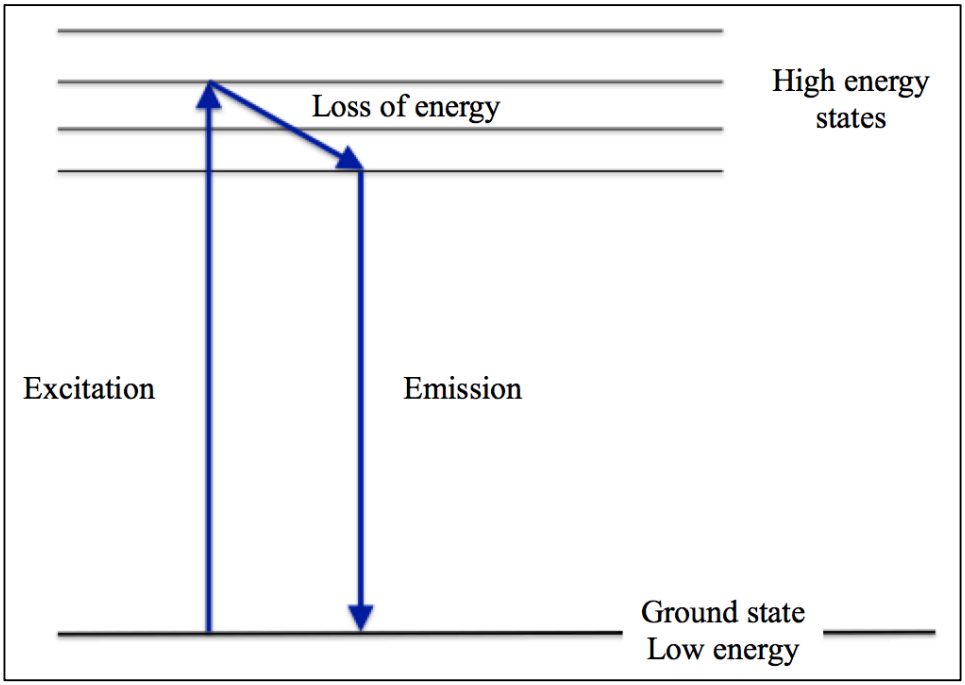

Figure 10: The process of fluorescence. A molecule is excited to a higher energy level through absorption of light. The molecule is unstable and will seek the lowest energy excited state and lose some energy on the way. From there, the molecule will return to its ground state and emit light (modified after Jablonski diagram of fluorescence by Jaffe and Miller, 1966).

If the sample or its impurities absorb the laser radiation and reemit it as fluorescence, a broad, strong fluorescence band can obscure the Raman spectrum (Figure 11). Spectra of samples with organic content are often influenced by fluorescence. The intensity of the fluorescence band could be as much as 10^4 greater than the Raman signal. There are several ways to minimize the problem. A high-power laser beam can bleach out fluorescent impurities in the sample. If the sample itself is fluorescent, the exciting wavelength can be changed. A longer wavelength may reduce the fluorescence significantly.

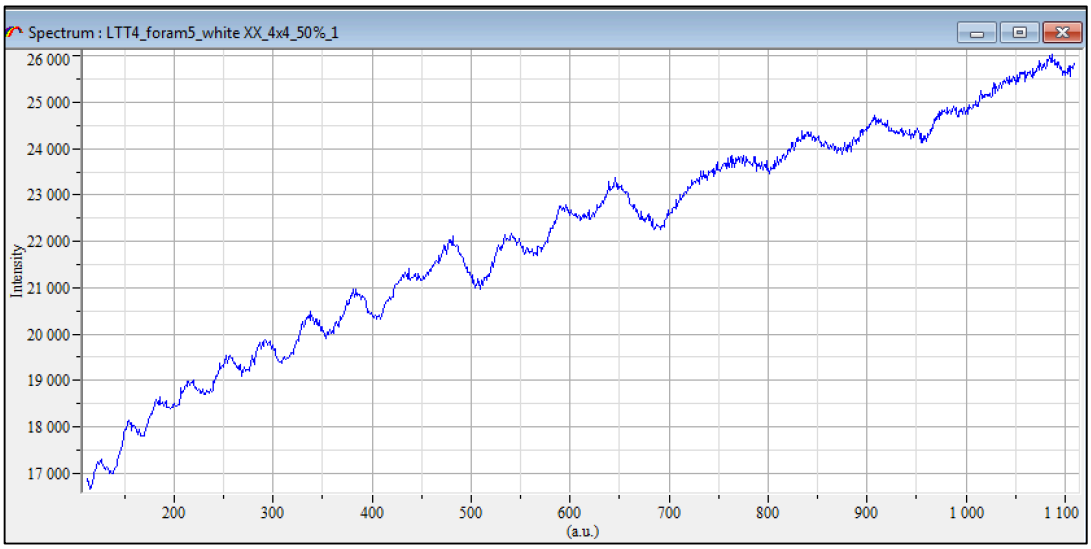

Figure 11: Fluorescence is obscuring the spectrum. The intensity of the fluorescence is covering the secondary peak (L). The main peak (v_1) can barely be identified.

2.3. Carbonate minerals

Carbonate minerals has the carbonate ion CO_3^{2-} as the basic structural and compositional unit and are the principal constituents of many sedimentary rocks. These minerals can be found in every possible geological setting (organic sedimentary, metamorphic, magmatic,

extraterrestrial) and are among the most widely distributed minerals in the Earth's upper crust. Carbonates represent approximately 30 % of the Phanerozoic sedimentary rock record after diagenesis (Urmos et al., 1991). Crystallization of calcium carbonate ($CaCO_3$) is a ubiquitous process in nature and $CaCO_3$ crystallizes in three different forms: calcite, aragonite, and vaterite with trigonal, orthorhombic, and hexagonal structure, respectively. Nucleation and growth of calcium carbonate crystals normally take place in nature, most often due to biomineralisation (Deer et al., 1992) as calcium carbonate is the major constituent of reefs. Calcite is the most stable polymorph of calcium carbonate and the other two associated polymorphs are aragonite and vaterite. Carbonate minerals are in general soluble in slightly acidic waters and they often have high porosity and permeability, which makes them ideal petroleum reservoirs.

Calcite shows a trigonal system and scalenohedral structure with two molecules per unit cell. The structure of calcite crystals allow for impurities of magnesium, iron, and manganese. Aragonite is the relatively common orthorhombic polymorph of calcite and can crystallize by biological (coral reefs and shells) and geological processes (hot springs, stalactite and stalagmite cave formations). Dandeu et al. (2006), Carteret et al. (2013) and De La Pierre et al. (2014) used Raman spectroscopy to study aragonite. Hexagonal vaterite is the most rare and least known polymorph (Gabrielli et al., 2000; Wehrmeister et al., 2010; De La Pierre et al., 2014). Vaterite is metastable but can be found as micrometric crystals in fresh water biological environments and mineral springs.

Magnesite ($MgCO_3$) is isomorphous with calcite and shows the same trigonal structure as calcite. Magnesite can be found in sedimentary and metamorphic (serpentinites) settings.

Magnesite crystals are often massive and colorless, but euhedral crystals are relatively rare, which makes Raman analysis useful in identification of this mineral.

Dolomite ($CaMg(CO_3)_2$) is another important and common carbonate mineral, usually formed by diagenesis or hydrothermal metasomatism of limestone. The structure of dolomite crystals are similar to calcite, but alteration of calcium and magnesium layers results in the hexagonal symmetry of dolomite being lower than that of calcite (Bischoff et al., 1985; Gunasekaran et al., 2006; Sun et al., 2014).

2.4. Raman spectra of carbonate minerals

Raman spectra of carbonate minerals were first collected by Krishnan (1945) and Krishnamurti (1956), students of Sir C. V. Raman who first discovered the Raman effect (Raman, 1928). During the last decades several authors have contributed in the pioneering work of analysing Raman shifts and width of associated bands of carbonate minerals (e.g. Porto et al., 1966; Rutt and Nicola, 1974; Frech et al., 1980; Bischoff et al., 1985; Kuebler et al., 2001; Edwards et al., 2005; Korsakov et al., 2009; Carteret et al., 2013; Sun et al., 2014). Carbonates commonly show dispersion and good Raman signals, and have therefore undergone investigation particularly with regard to thermodynamic properties and vibrational spectra.

The CO_3^{2-} group is characterized by four main Raman vibrational modes, v_1-v_4, and two lattices modes, T and L. Their assignments and ranges are listed in Table 1.

	Assignment	Range
T	Translation mode	From 155 to 235 cm^{-1}
L	Libration mode	From 270 to 345 cm^{-1}
v_1	Symmetric stretching	From 1024 to 1100 cm^{-1}
2 x v_2	Asymmetric deformation	From 1700 to 1765 cm^{-1}
v_3	Asymmetric stretching	From 1390 to 1460 cm^{-1}
v_4	Symmetric deformation	From 710 to 745 cm^{-1}

Table 1: The CO_3^{2-} group is characterized by four main vibrational Raman modes, v_1-v_4, and two lattices modes, T and L. Their assignments and ranges are listed (Bischoff et al., 1985).

Modes present in the 500 to 100 cm^{-1} region are associated with external vibrations of the CO_3^{2-} group. The strongest main peak of any spectra is called v_1 and the secondary peak L (Libration lattice mode). A very strong and sharp band at 1086 cm^{-1} (v_1) together with other subsidiary bands at 156 (T), 283 (L) and 713 cm^{-1} (v_4) characterize a calcite spectrum. Higher band positions have been observed in high-pressure and –temperature calcites (Gillet et al., 1993). The v_1 of aragonite is also located at 1086 cm^{-1}. It is however possible to differentiate aragonite from calcite due to the presence of a weak band at 704 cm^{-1} and several weak bands in the lowest region. An additional vibrational mode at approximately 335 cm^{-1} is found in dolomite due to its lattice structure. The v_1 of dolomite is located at 1097 cm^{-1} (Bischoff et al., 1985). Magnesite and calcite have similar lattice and therefore similar spectra (Krishnamurti, 1956). The frequencies of magnesite are higher than the frequencies of calcite, which is explained by shorter distance between the ions in magnesite. Shorter interionic distances generate increased interionic forces. Edwards et al. (2005) compared spectra of mixtures of known aragonite-calcite ratios and Dandeu et al. (2006) used Raman spectroscopy to study mixtures containing all three polymorphs. Korsakov et al. (2009) also studied the spectra of different $CaCO_3$ polymorphs.

2.5. Sample Preparation

Preparations necessary to perform Raman spectroscopy are very few. Samples can be analysed as they are, as grains, larger fragments, or as whole rocks. In general, carbonate grains show strong signals and good spectra, but several whole-rock analyses of carbonates have shown spectra strongly influenced by fluorescence and noise. One can speculate in whether this problem is related to the amount of organic matter, in which the surrounding carbonates might show too strong Raman signals, or difficulties concerning focusing. This was also partly the fact for the studied samples, and grains were therefore scraped off from the samples and placed on a slide. A needle was used to further crush and smear out the grains. The slide was then placed under the laser of the Raman spectrometer and ready to be analysed. Pictures were taken of the samples in order to keep track of spots where grains were scraped off. One of the samples was analysed with a Scanning Electron Microscope (SEM), mounted, and coated with carbon. Graphite prevents the laser from reaching the sample's surface and therefore had to be polished off before the sample could be analysed with a Raman spectrometer.

Figure 12: As whole rock analyses showed spectra strongly obscured by fluorescence, grains were scraped off from the sample and smeared out on a slide using a needle.

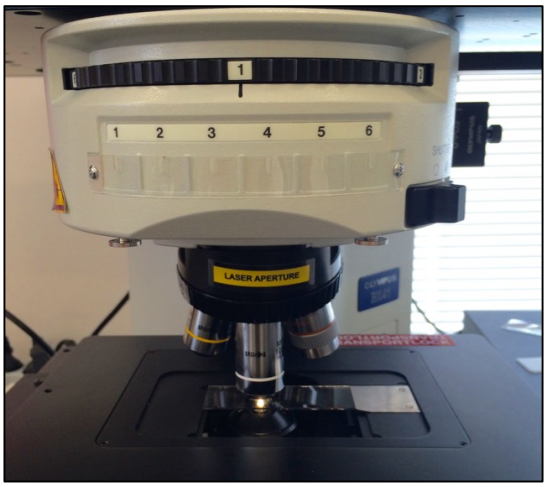

Figure 13: The slide was placed under the laser of the Raman spectrometer and ready to be analysed.

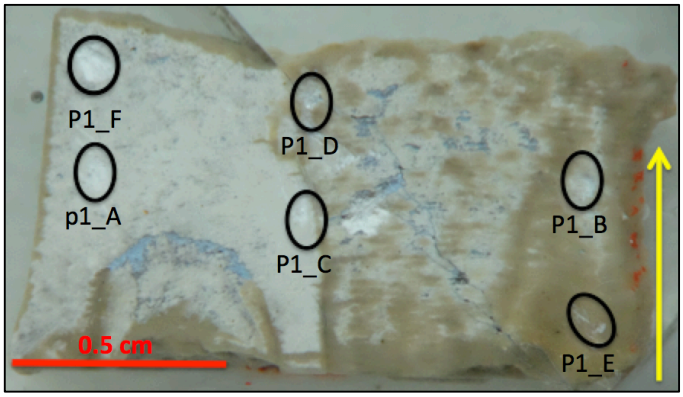

Figure 14: Sample maps were created for each sample in order to keep track of the spots were grains were scraped off. The yellow arrow in this sample map indicates the flooding direction.

2.6. Technical Specifications for Raman Spectrometer

A table of specifications and settings for the Raman spectrometer used in this study is listed in Table 2.

Raman Spectrometer	**XploRA One™ Horiba Scientific**
Laser	Green, solid state, 532 nm high brightness laser. Confocal hole: 300 μm, slit: 100 μm.
Diffraction grating	2400 grid/mm
Microscope	Olympus BX41, light from bottom, 10 % and 100 % enlargement
Optical filter	Edge
Detector	1024x256 TE air-cooled scientific CCD
Coloured camera	Resolution: <1 micron (XY) and <2 microns (Z)
Joystick	Märzhäuser Sensotech GmbH Tango
Power	50 mW (adjustable)
Computer	Desktop PC with monitor, keyboard and mouse, Windows 7 32-bit and LabSpec 6 spectral software suite
Average time of obtaining one spectra	44 seconds
Acquisition time (s) x Accumulation	10x5, 5x4 and 5x15
Error in data	±1 cm^{-1}

Table 2: The technical specifications for the Raman spectrometer used in this study.

Chalk consists mainly of microfossils that range in size from 1-100 microns. As the laser spot size is 1-2 microns, the spectrometer was reaching the limit of resolution in this study.

3. DATA

In order to test the methodology of Raman spectroscopy on EOR related research two core samples of outcrop chalk were selected. Chalk is a sedimentary rock composed predominantly of shells of microfossils and therefore has a high calcium carbonate ($CaCO_3$) content. The studied chalk was sampled at Liège in Belgium from the earliest Late Campanian to early Late Maastrichtian Gulpen Formation. The sample originates from the basal succession, the Zeven Wegen Member (Robaszynski et al., 2001) with an age of 75.5-78.0 Ma, Late Campanian. The $CaCO_3$ concentration of the Liège chalk has been measured and calculated by Hjuler and Fabricius (2009), Megawati et al. (2012) and Zimmermann et al. (2015). The reported values range from 91 to 95 %. Liège chalk has a relatively pure composition of calcite and contains not more than 5 wt.% of noncarbonated phases (Zimmermann et al., 2015). Liège chalk was only subjected to shallow burial and still contains approximately 40-45 % primary porosity (Hjuler and Fabricius, 2009). It is considered mechanically comparable to reservoir chalk (e.g. Collin et al., 2002) and is therefore suggested as the best match for the reservoir successions in the North Sea (Hjuler and Fabricius, 2009). This chalk has, like several other Cretaceous outcrop chalk exposures, been used as analogues in the study of rock-fluid interactions at elevated stresses and temperatures in reservoir chalks (Hjuler and Fabricius, 2007; Strand et al., 2007). One of the two cores was flooded for 3 years and therefore called Ultra Long Term Test (ULTT), while the other core was flooded for 1.5 years and called Long Term Test (LTT). The ULTT proves how quickly results can be obtained using Raman spectroscopy. The LTT sample was particularly challenging for the methodological set-up as it will be shown and enhances the understanding of the application of Raman spectroscopy to chalk significantly.

3.1. Ultra Long Term Test (ULTT)

Raman spectroscopy was applied to a chalk core (ULTT), which has been flooded with $MgCl_2$ for 1072 days (3 years). During the last hundred days of flooding, the calcium effluent production was low, which led to an implication of a complete chemically re-worked chalk. Based on the calcium loss and magnesium gain, it was predicted that magnesite (or dolomite) was the major newly grown mineral phase (Nermoen et al., 2015). However, a mismatch of 0.16 mole additional magnesium being produced, pointed to the presence of other mineral phases associated with the non-carbonates. This was confirmed with a Raman spectrometer in 5 minutes. The ULTT has not been investigated with any other geological methods prior this study.

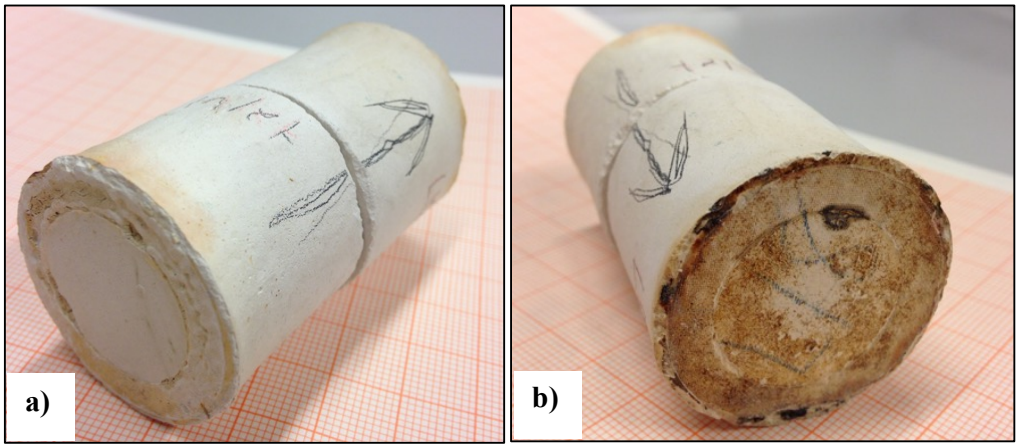

Figure 15: a) Inlet of ULTT. Arrow indicates flow direction. **b)** Outlet of ULTT. Arrow indicates flow direction. When inlet and outlet is compared, one can clearly see that chemical and mineralogical changes have taken place as the outlet has a different colour than inlet.

3.2. Long Term Test (LTT)

Raman spectroscopy was also applied to another chalk core (LTT), which has been flooded with $MgCl_2$ for 516 days (1.5 years). Clear signs of recrystallization, contact cements, overgrowth, preserved intrafossil porosity, and many well-preserved coccolithosphores have been identified by Hjuler and Fabricius (2009). This sample has been investigated with several analytical methods. Previous research showed a nonuniform degree of chemical alteration throughout the LTT and magnesite was identified as the major newly grown mineral phase with a decreasing abundancy along the core (Zimmermann et al., 2015). The first two slices (LT1 and -2) showed severe alteration while magnesite could not be detected in LT4. Lattice Boltzmann geochemical model was used to predict the effluent curve of the flooding experiment and a sharp alteration front was observed between slice 3 and 4 (LT3 and -4) (Zimmermann et al., 2015).

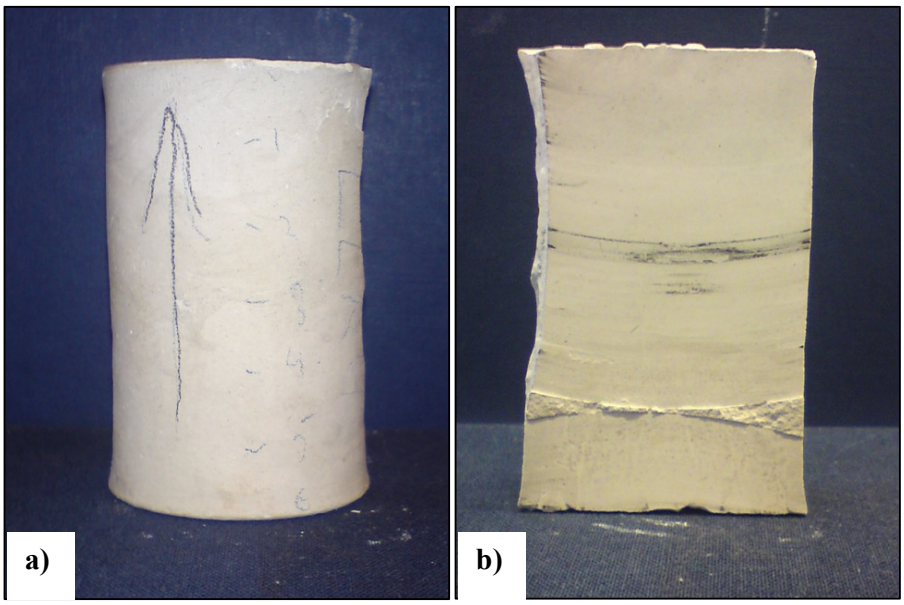

Figure 16: a) The LTT was first longitudinal cut and then further cut into six slices, which is illustrated here. Arrow indicates flow direction (Photo courtesy of Reidar Inge Korsnes). **b)** The inner part of the LTT after longitudinal cut is indicated (Photo courtesy of Reidar Inge Korsnes).

4. THEORY OF CHEMICAL CHANGES

In experiments where chalk is flooded with $MgCl_2$, it is believed that the solid volume changes as calcium carbonate dissolves and new secondary minerals precipitate. Another assumption is that solid volume preserving mechanisms such as solid-diffusion of chemical species do not occur.

Previous studies have shown that certain ions, e.g. Ca^{2+}, Mg^{2+} and SO_4^{2-}, in the injected brine have an impact on the mechanical stability of chalk and consequently the oil recovery factor of carbonate fields (Austad and Standnes, 2003; Strand et al., 2003; Heggheim et al., 2005; Korsnes et al., 2006; Madland et al., 2006; Madland et al., 2008; Korsnes et al., 2008a; Korsnes et al., 2008b; Zangiabadi et al., 2009). The complexity of the tested systems must be taken into account. The injected seawater might be exposed to several mechanisms such as precipitation, dissolution, ion exchange, adsorption, and desorption, at the same time. As the translation of these mechanisms to a larger scale is of a completely different manner, a need for simplification of the system has been identified. Each ion of importance has therefore been studied individually. The focus of this study concerned the presence of magnesium and $MgCl_2$ brine was used for the long-term flow-through experiment.

When a brine of chalk is injected with $MgCl_2$, ion exchange will take place. If the Mg^{2+} ions bond with CO_3^{2-}, magnesite ($MgCO_3$) will grow as a new mineral phase (Figure 17). Another mineral that might grow as a result of this ion exchange is dolomite ($CaMg(CO_3)_2$).

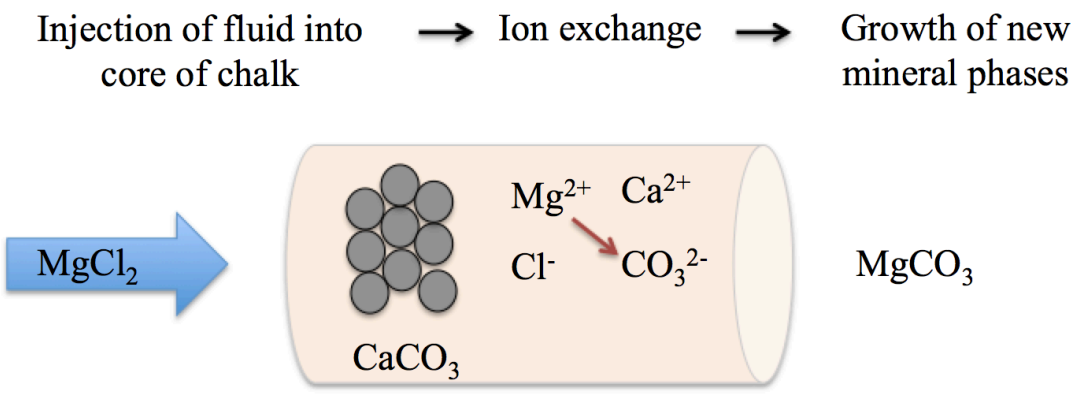

Figure 17: When a core of chalk is injected with $MgCl_2$, ion exchange will take place. If Mg^{2+} ions bond with CO_3^{2-}, magnesite ($MgCO_3$) will grow as a new mineral phase.

Growth of new mineral phases was observed in experiments on short-term tests (Madland et al., 2011), but the presented core scale experiment in this study is unique with regard to its duration under reservoir temperature (130°C) and values of effective stresses (12.6MPa) (Zimmermann et al., 2015).

5. RESULTS

Previous research on the LTT sample have proven dramatic mineralogical and geochemical changes with scanning electron microscopy, energy-dispersive X-ray spectroscopy, nano-secondary ion mass spectrometry, X-ray diffraction, and whole-rock geochemistry (Madland et al., 2013; Zimmermann et al., 2013; 2015). The ULTT sample has on the other hand not been investigated with other geological methods before this study.

5.1. Data Analyses

Both the LTT and ULTT samples were investigated with Raman spectroscopy. 470 spectra of LTT and 90 of ULTT were collected and analysed. LabSpec 6 was used to analyse the spectra. All spectra were threated with baseline correction to avoid fluorescence and calibrated by neon correction (Neon = 476.79 cm^{-1}). In order to identify single minerals under investigation, spectra for different minerals were collected from literature (please see Appendix). The unknown Raman spectrum was then compared to spectra in a chemical and calibrated database including certified standards provided by M.A.C. (Micro-Analysis Consultants). Raman shift (cm^{-1}) is plotted against intensity (counts) (Figure 18). When v_1 and L bands were plotted against each other for each sample, one can clearly see the differentiation between calcite and magnesite minerals in LTT (Figure 19-21). A general trend where the slope is close to 1 can be seen in the three slices (LT1, -2 and -4) of LTT. This means that if the Mg-content rise, the two main peaks will shift to higher Raman shifts with the same length of movement. Please note that there is an error of ±1 cm^{-1} in the data.

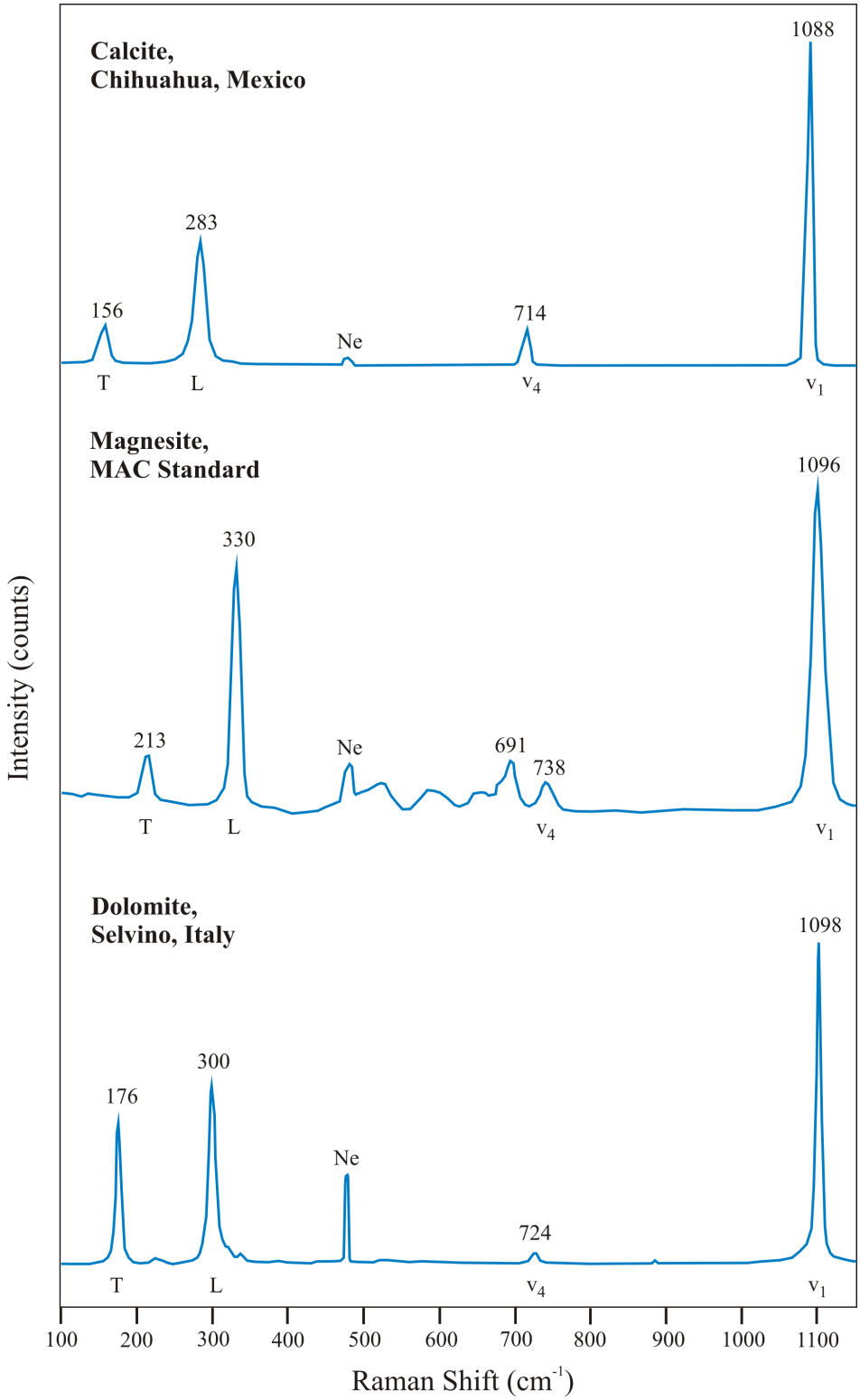

Figure 18: These are three of the standards (calcite, magnesite and dolomite) from the calibrated database used to identify single minerals under investigation in this study.

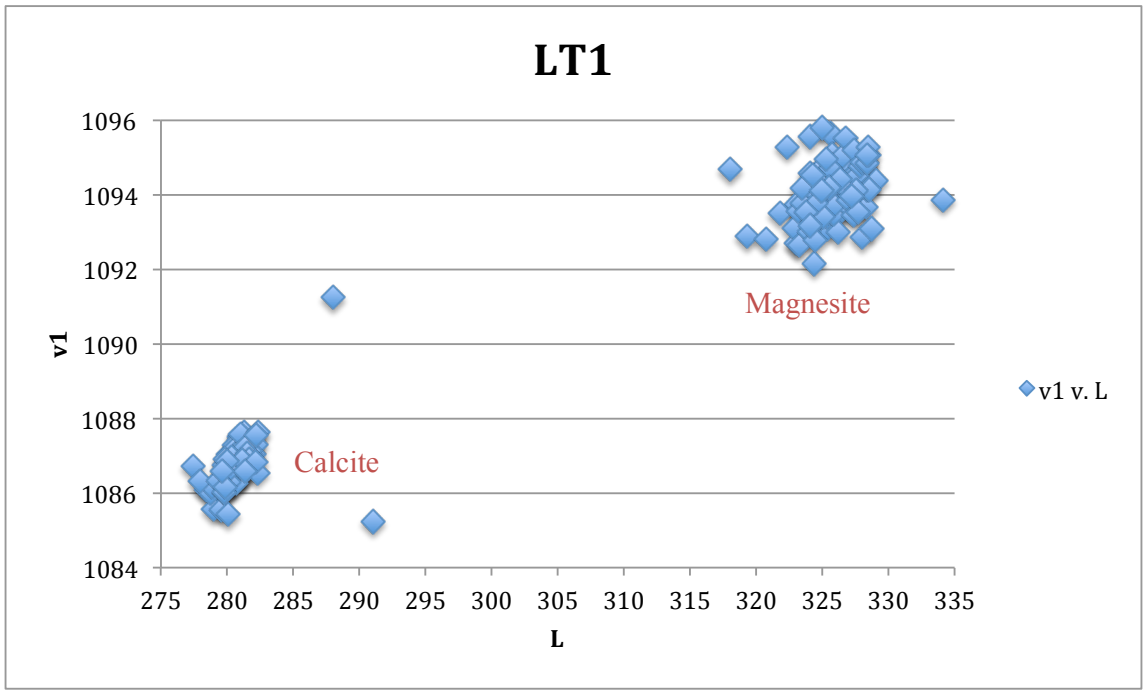

Figure 19: The main band (v_1) is plotted against the secondary band (L) for LT1 (see **Figure 26** where the mineral content of LT1 is given in percentages), which shows differentiation between calcite and magnesite clearly. The plot of LT1 shows a higher content of magnesite than calcite.

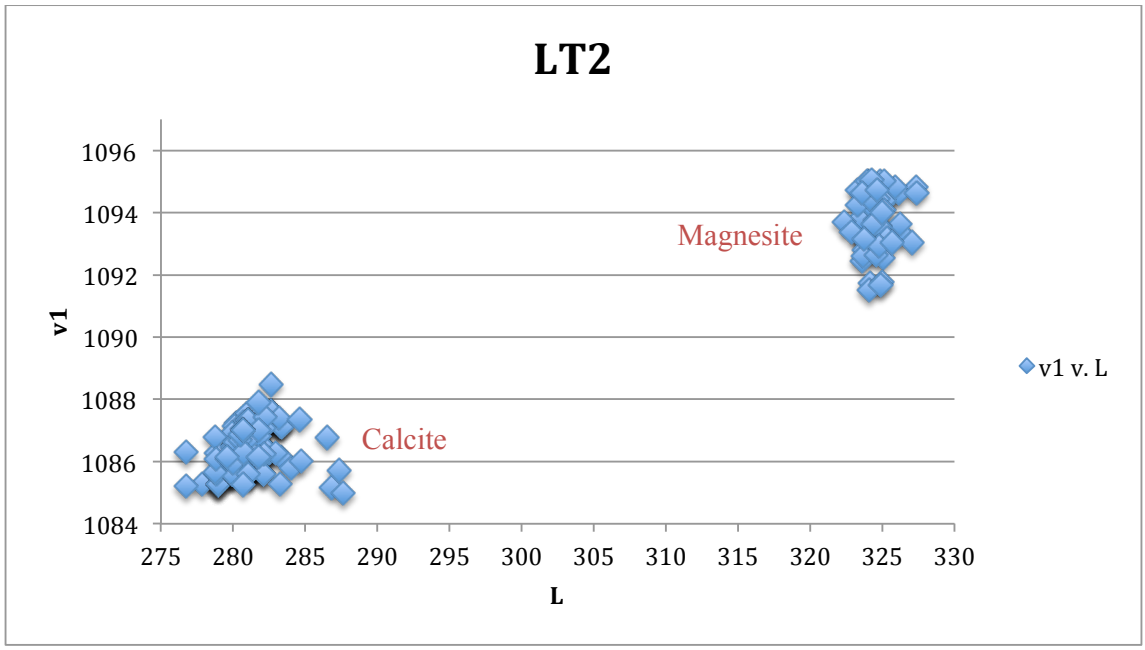

Figure 20: v_1 plotted against L for LT2 with the same distinctions as in **Figure 19**. The plot of LT2 shows a higher content of calcite than magnesite (see **Figure 27** where the mineral content of LT2 is given in percentages).

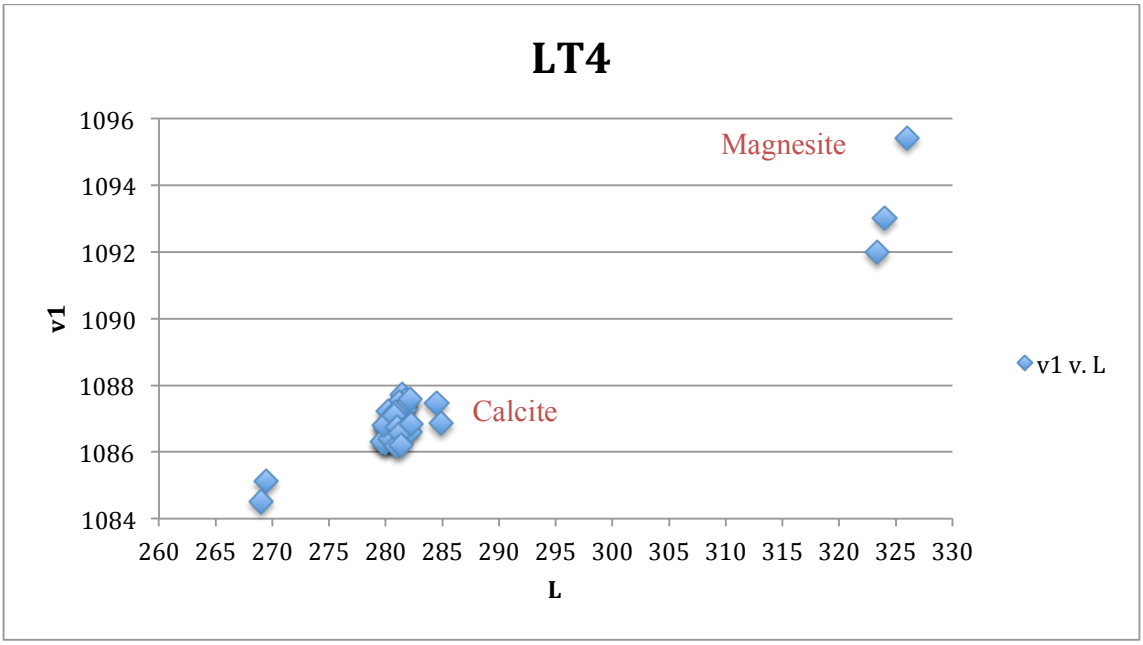

Figure 21: v_1 plotted against L for LT4 and the differentiation between calcite and magnesite is still beyond doubt. The plot of LT4 shows a much higher content of calcite than magnesite than calcite (see **Figure 28** where the mineral content of LT4 is given in percentages).

The fact that calcite will show a solid solution from 0 mol% to 20 mol% $MgCO_3$ makes it challenging to differentiate between calcite and magnesian calcite. Peak position limits for classification in this study was based on Raman spectra and EDS data collected by Borromeo et al. (2015b). The limits were based on an evaluation of v_1 and L together and are the following:

	v_1	L
Calcite	$x \leq 1087.5$	$x \leq 282.5$
Mg-rich calcite	$x > 1087.5$	$x > 282.5$
Magnesite	$x \geq 1093$	$x \geq 322$

Table 3: The peak position limits used in in this study for classification of calcite, Mg-rich calcite, and magnesite were based on an evaluation of v_1 and L together and are listed here.

Figure 22 and Figure 23 show spectra of the three minerals of highest abundance in this study: calcite, Mg-rich calcite, and magnesite. The spectra are presented with their associated vibrational modes (T, L and v_1) aligned with a photo of fragment under investigation.

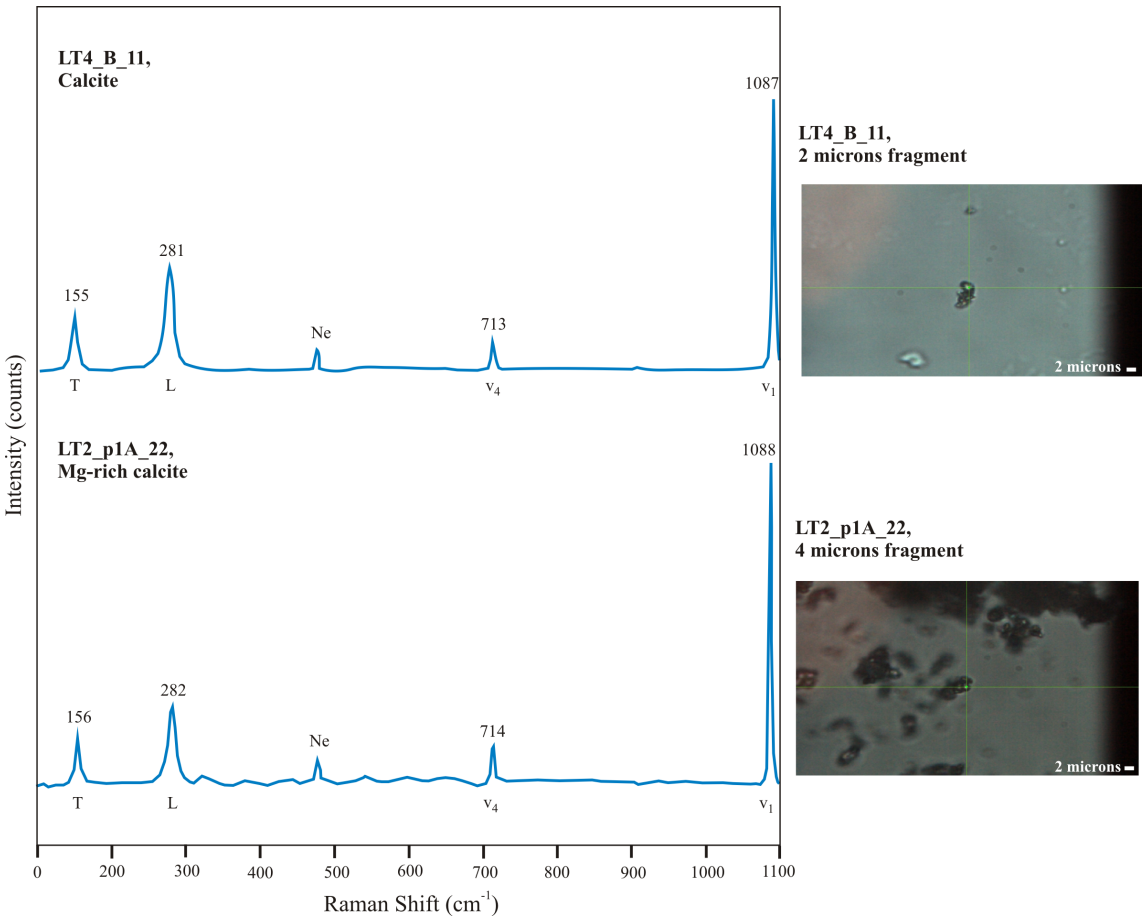

Figure 22: LT4_B_11 is one example of a typical calcite spectrum, while LT2_p1A_22 is a typical Mg-rich calcite spectrum and was identified as Mg-rich calcite based on the limits mentioned in Table 3.

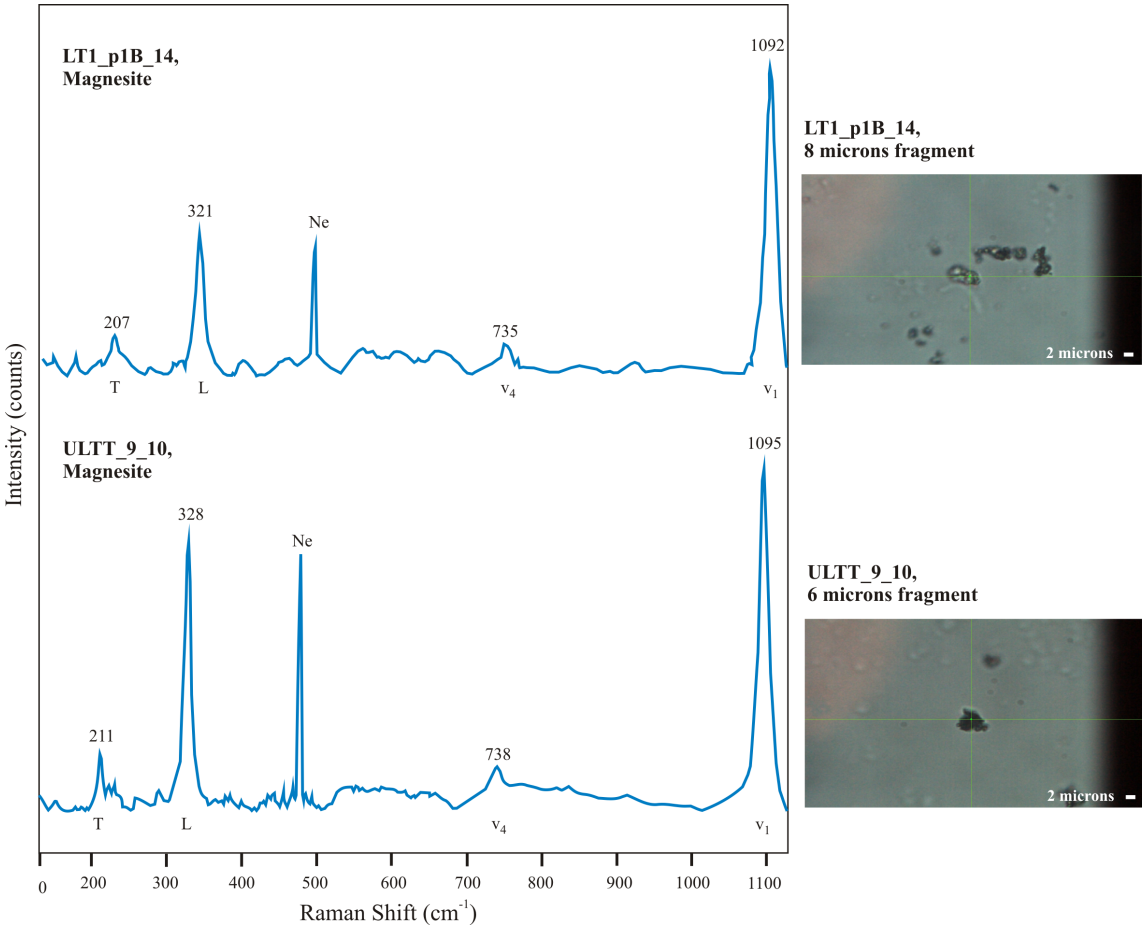

Figure 23: LT1_p1B_14 and ULTT_9_10 are both typical examples of magnesite spectra.

The abundances of each mineral in LTT and ULTT are presented in pie charts in subchapter 5.2 and 5.3. Please note that all spectra where two or more minerals were indicated, all minerals were counted in the percentages given in each pie chart. Samples were taken from several places on each slice in order to detect any lateral changes through the samples. Sample maps with associated results can also be found in the same subchapters.

5.2. Ultra Long Term Test (ULTT)

Although ULTT had not been investigated with other methods prior this study, predictions of its mineralogical changes were made based on the much more investigated LTT and modelling by colleagues (pers. com. M. Minde, 2015; A. Nermoen, 2015). Both of these samples were injected with $MgCl_2$ under reservoir conditions (T = 130°C, confining pressure 1.2 MPa, pore pressure = 0.7 MPA, flooding rate varied between 33.12 cm^3/day and 99.36 cm^3/day), but with different extent of the experiment. Previous research of LTT has shown decreasing chemical alteration in flooding direction. Magnesite was identified as the major newly grown mineral phase and could be traced up to slice 3, while magnesite could not be detected in slice 4 (LT4). This phenomenon is in the rest if this thesis called an *alteration front*. The reader is referred to subchapter 5.3 for more details. As both the LTT and ULTT are cores of 7 cm, split in six slices, and the ULTT was injected for 3 years (double amount of days compared to LTT; please see chapter 3) it was predicted that no alteration front would be found and that the sample consists mainly of magnesite (Nermoen et al., 2015). In this study, 90 spectra were collected from different sample locations of the ULTT and Figure 24 shows the percentages of minerals identified. The mineralogy consists of 81 % magnesite, 16 % Mg-rich calcite, and 3 % unidentified minerals. Figure 25 shows the location of different samples of ULTT and their associated results. There is no distinct trend in magnesian calcite content, but the magnesite content is slightly decreasing with the flooding direction. At the outlet, some spectra that have not yet been identified and therefore denoted as “Unknown” in Figure 25 were also collected. These spectra might be related to the presence of other mineral phases associated with the non-carbonates as Nermoen (2015) suggested. Thus, the predictions already made were extraordinary quickly confirmed with a Raman spectrometer.

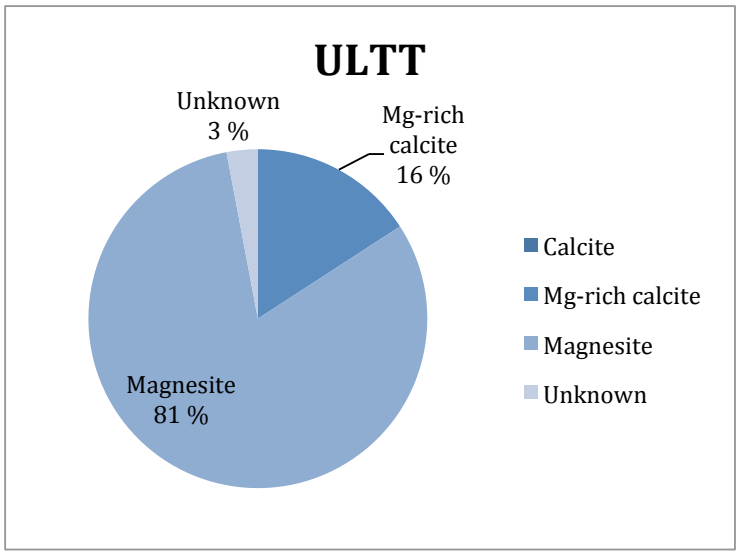

Figure 24: The mineralogical composition of ULTT is 81 % magnesite, 16 % Mg-rich calcite, and 3 % unknown minerals.

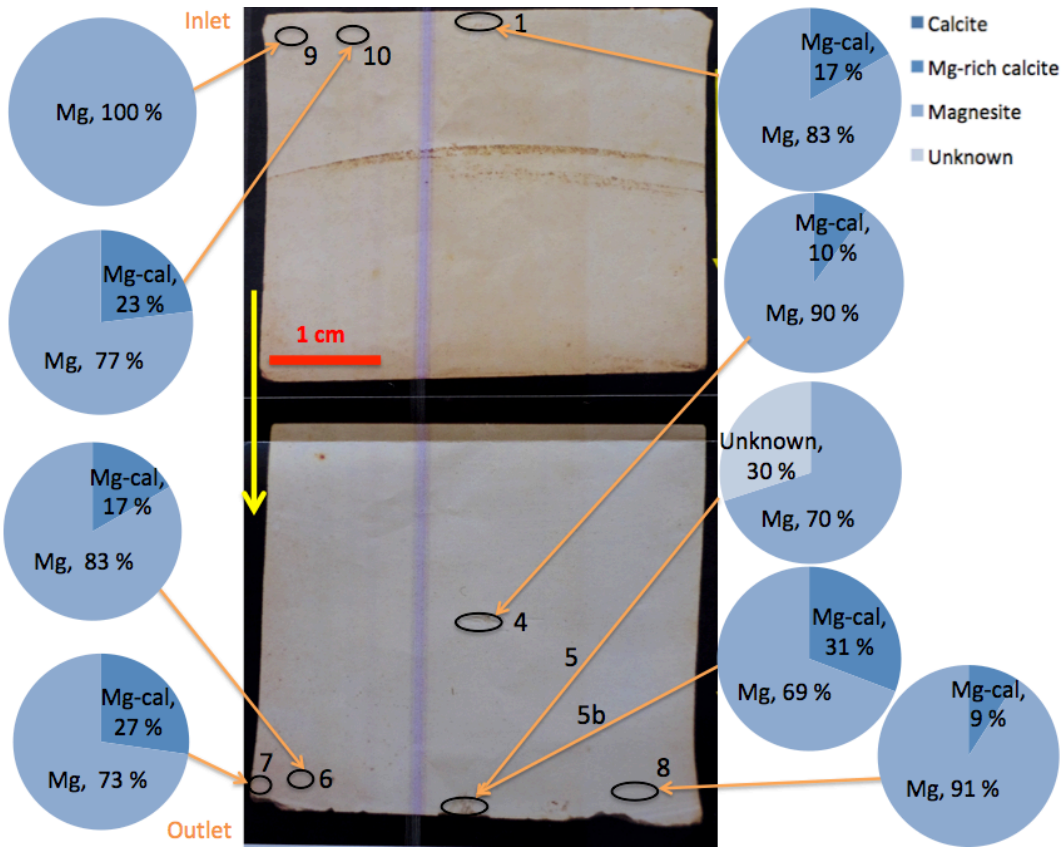

Figure 25: ULTT was cut longitudinal and sample map with sample locations and associated results are indicated. Yellow arrow indicates flooding direction. Cal = Calcite, Mg-cal = magnesian calcite, Mg = Magnesite, Unknown = minerals that have not yet been identified.

5.3. Long Term Test (LTT)

Previous research showed a nonuniform degree of chemical alteration throughout the LTT. Magnesite was identified as the major newly grown mineral phase with a decreasing occurrence along the core. The first two slices (LT1 and -2) show severe alteration while magnesite could not be detected in LT4. With the aim to further investigate the chemical and mineralogical changes in this sample with a new method, three slices of LTT were chosen: LT1, -2 and -4.

Chemical analyses of the effluent brine showed that the amount of Cl^- remained unchanged during the entire injection period, whereas Mg^{2+} was depleted and Ca^{2+} enriched. The Mg^{2+} and Ca^{2+} concentrations remained approximately constant around 0.195 and 0.022 mol/L respectively, with a total Mg^{2+} + Ca^{2+} concentration of 0.217 mol/L, close to the original magnesium concentration of the injected brine of 0.219 M $MgCl_2$. This proves the Mg-Ca exchange as the most important player in the stoichiometric calculations of rock-fluid interactions (Zimmermann et al., 2015). The loss of Ca^{2+} and gain in Mg^{2+} are attributed to precipitation of new minerals and leaching the tested core by approximately 20 %.

The degree of chemical alteration is not uniform throughout the sample. LT1 shows an increase in MgO by approximately 100, from 0.33 to 33.03 wt.% and a corresponding depletion of CaO by more than 70 % from 52.22 to 24.43 wt.% (Zimmermann et al., 2015). The abundance of magnesite is 51 % in LT1 according to the spectra analysed in this study (Figure 26). LT2 shows a magnesite abundance of 32 % (Figure 27).

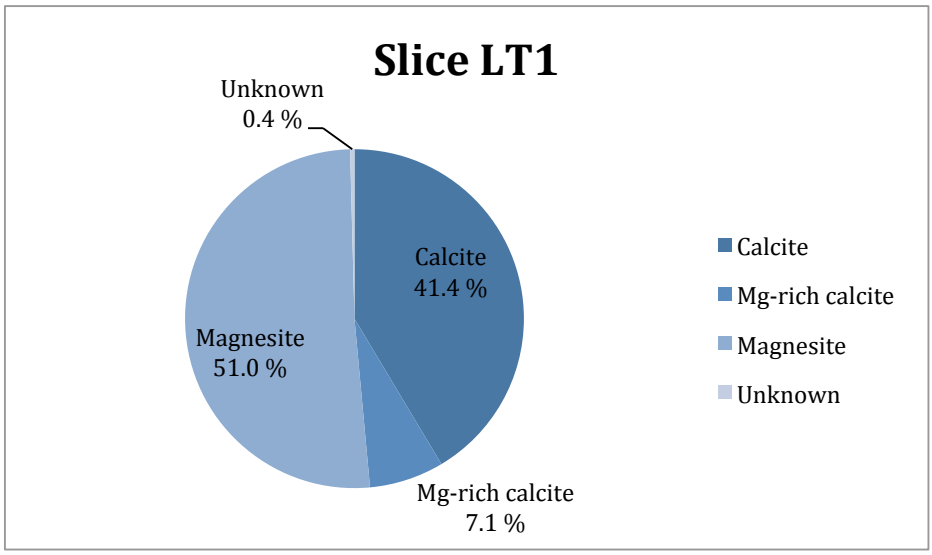

Figure 26: The mineralogical composition in slice LT1 of LTT is 51.0 % magnesite, 41.4 % calcite, 7.1 % Mg-rich calcite and 0.4 % unknown minerals.

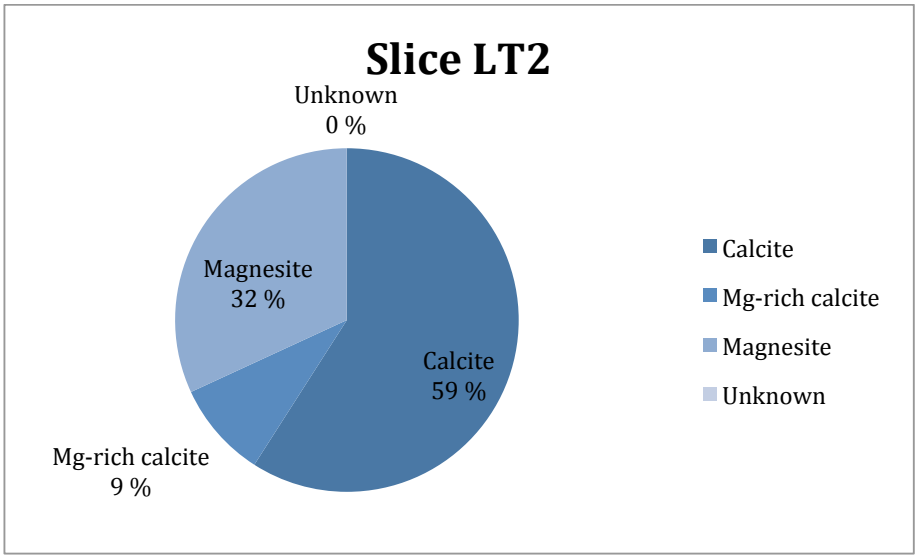

Figure 27: The mineralogical composition in slice LT2 of LTT is 59 % calcite, 32 % magnesite and 9 % Mg-rich calcite.

With the methods used in previous analyses of LTT, magnesite could be traced up to the third slice (LT3), while magnesite was not detected in LT4 using XRD and scarce amounts of tilleyite ($Ca_5Si_2O_7(CO_3)_2$) were detected in LT4 only (Zimmermann et al., 2015). A magnesite content of 15 % in LT4 was detected with the Raman spectrometer (Figure 28), which

confirms the still 10x increase of MgO in comparison to unflooded chalk from Liège (Zimmermann et al., 2015), but the scarce amounts of tilleyite were not detected. Calcite was the dominating mineral in LT5 and LT6. The dissolution of quartz was observed in all the flooded samples. Madland et al. (2013) detected dolomite at the rim of LT1 as intrafossil filling of foraminifera shells, but no dolomite was detected using XRD in Zimmermann et al. (2015) or Raman spectroscopy in this study. It is believed that the amount of dolomite is below the detection limit of XRD and would need intensive and time consuming search by Raman application. Geochemical data suggests that the injection of fluid changed more than 50 % of the mineralogy of LT1, which is supported by results from SEM, XRD (Zimmermann et al., 2015) and Raman datasets.

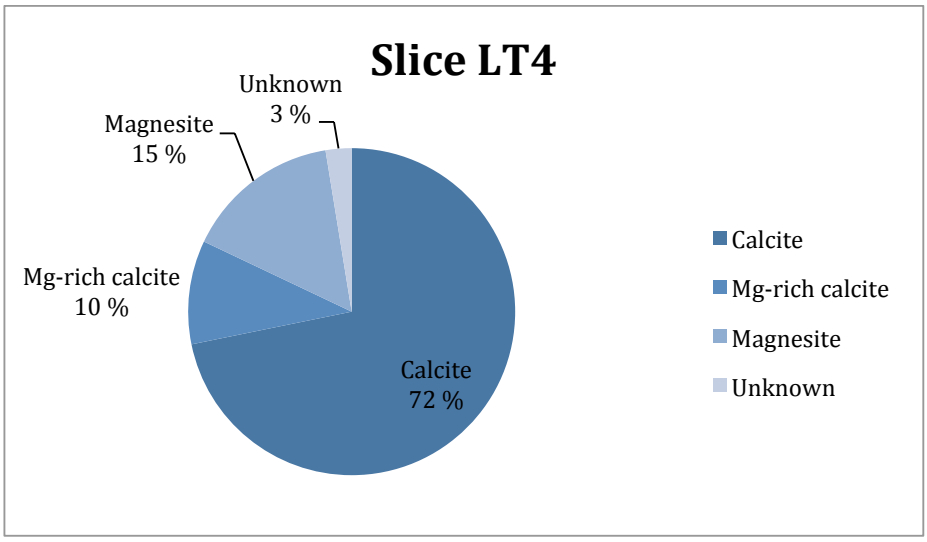

Figure 28: The mineralogical composition in slice LT4 of LTT is 72 % calcite, 15 % magnesite, 10 % Mg-rich calcite and 3 % unknown minerals.

Lattice Boltzmann geochemical model (Hiorth et al., 2013) was used to predict the effluent curve in this experiment. A sharp alteration front where the first part is nearly completely altered from calcite to magnesite is observed from the model (Figure 29) (Zimmermann et al.,

2015). Magnesite does not occur in unflooded Liège chalk, but Zimmermann et al. (2015) proved the proposed mineralogical growth of magnesite in LT1-LT4 using nanoSIMS applications.

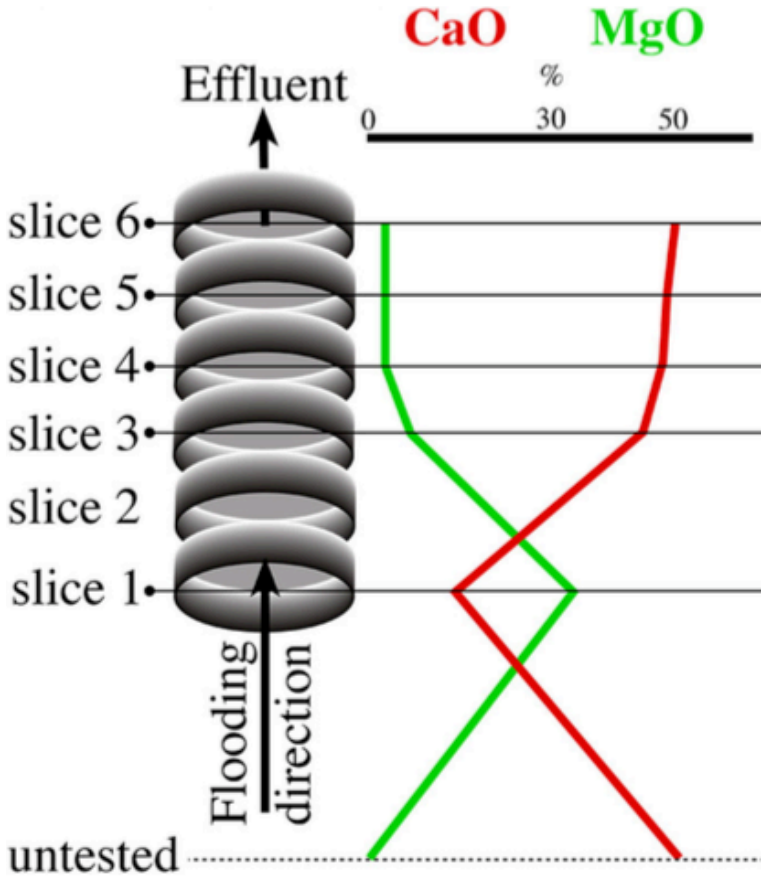

Figure 29: Cross section of LTT with associated changes in geochemical composition. % = Weight percent (Modified after Zimmermann et al., 2015).

From effluent measurements using ICP-OES (please see Zimmermann et al., 2015), the total Ca^{2+} production from the rock was approximately 13.5 g and as much as 20 % of the core was dissolved during the experiment. The amount of dissolved calcite is considerable. The final porosity of the core is calculated to be 31.5 %, which corresponds to a relative reduction of approximately 20 % compared to its original value of 40.5 %. The sample maps of LT1, -2 and -4 with associated results follow in the next subchapters.

5.3.1. LT1

LT1 was split into two fragments denoted LT1_p1 and LT1_p2. The rim of the core is on the left side of LT1_p1 and LT1_p2. A lateral variation in the Mg-Ca exchange perpendicular to the flooding direction can be seen in Figure 30. This was however not observed in LT1_p2, where the magnesite abundance was decreasing with flooding direction. There seems to be a gap between the two fragments and they are not necessarily placed exactly on top of each other.

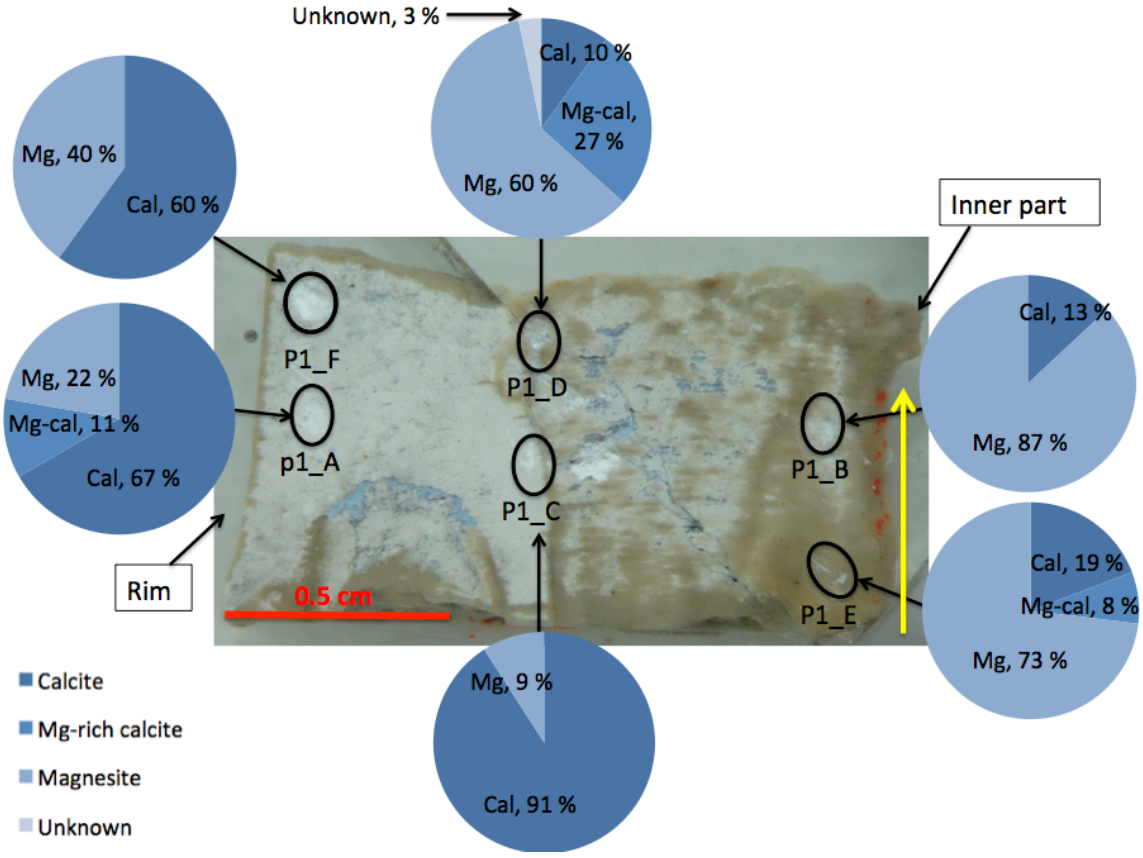

Figure 30: Sample map of LT1_p1 with sample locations and associated results indicated. Yellow arrow indicates flooding direction. Cal = Calcite, Mg-cal = magnesian calcite, Mg = Magnesite, Unknown = minerals that have not yet been identified. The rim of the core is indicated on the left side.

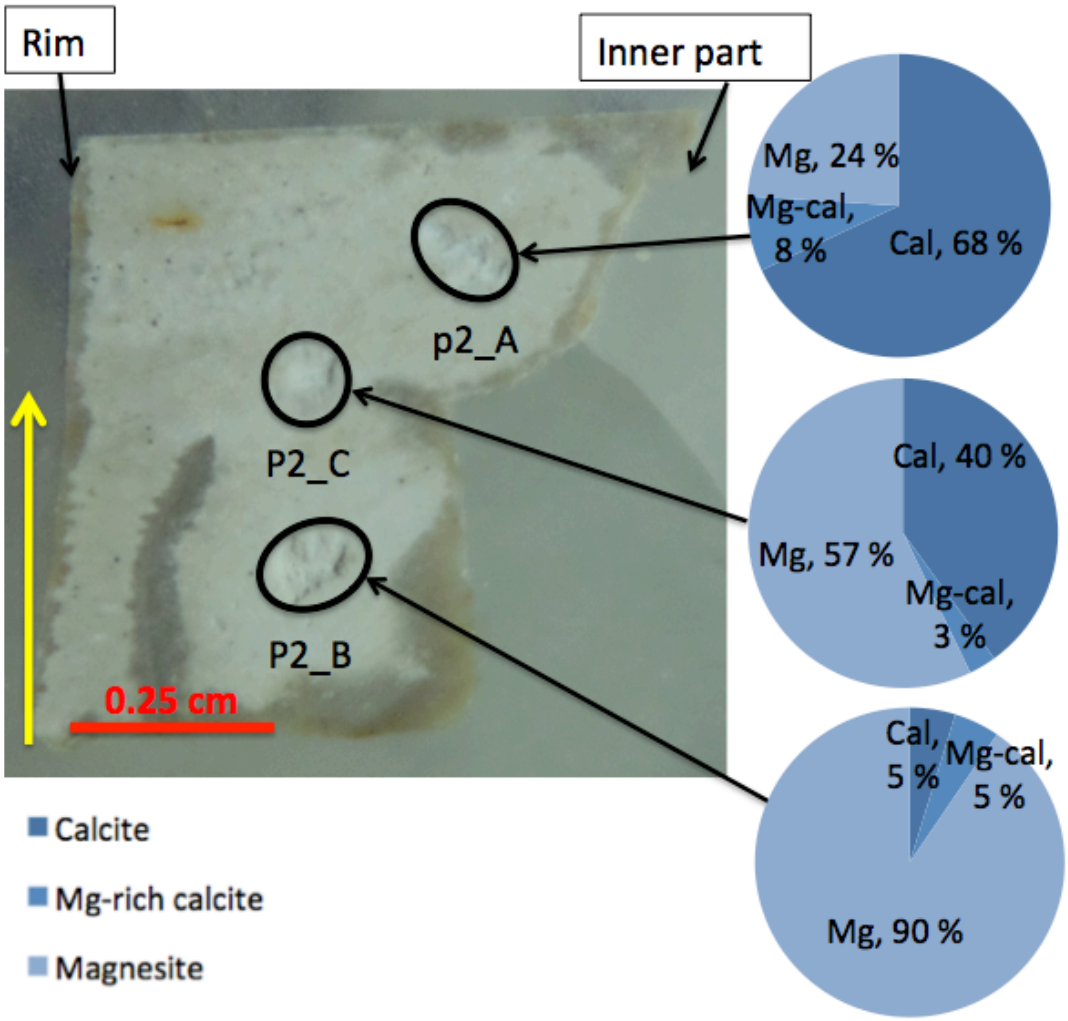

Figure 31: Sample map of LT1_p2 with sample locations and associated results indicated. Yellow arrow indicates flooding direction. Cal = calcite, Mg-cal = magnesian calcite, Mg = magnesite. The rim of the core is indicated on the left side.

5.3.2. LT2

Only fragments of LT2 were available and flooding direction was therefore not known. One fragment was chosen, which explains the notation p1. The calcite abundance was slightly higher in p1B (Figure 32), but is generally decreasing upwards in the figure, while the magnesite occurrence is increasing upwards. This could point to a flooding direction from top to bottom in Figure 32.

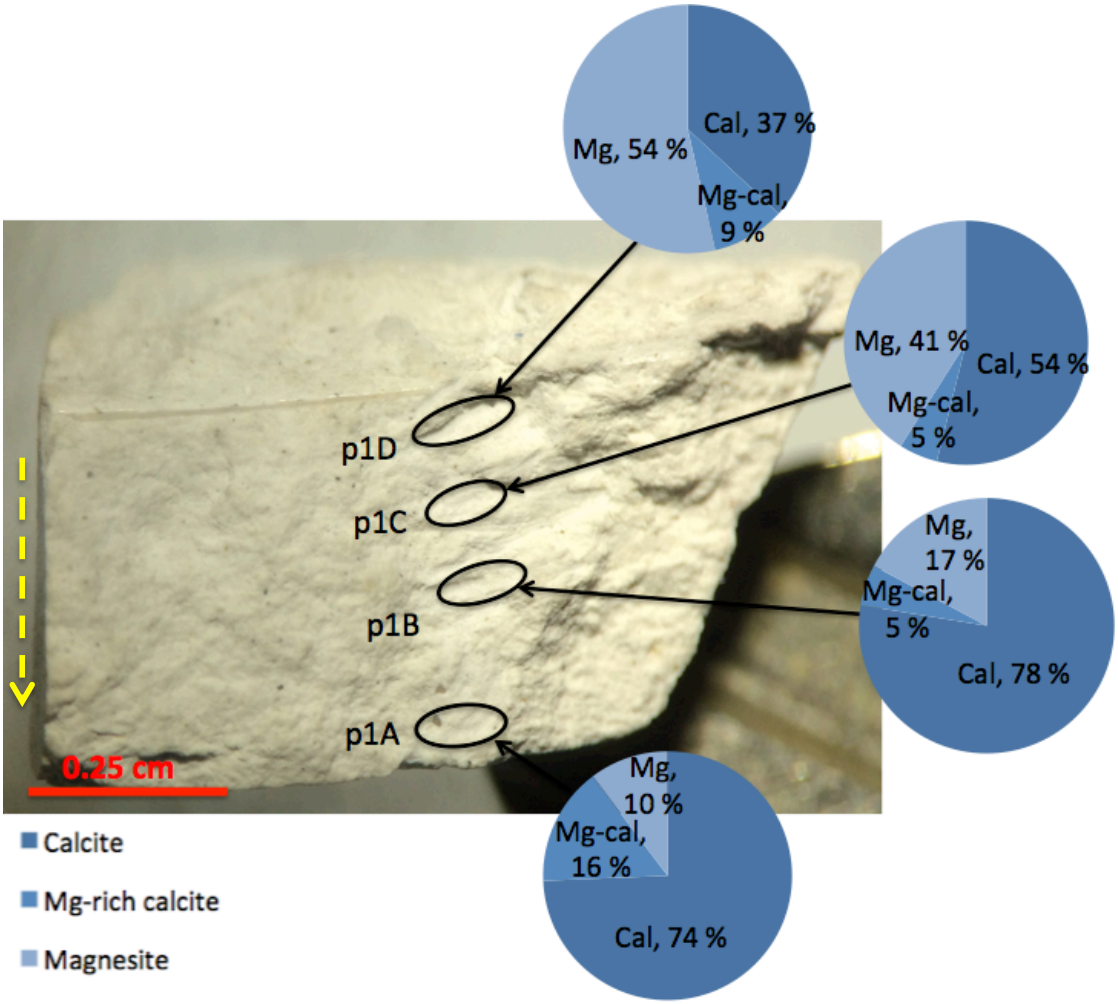

Figure 32: Sample map of LT2 with sample locations and associated results indicated. Only fragments of this slice were available and flooding direction is therefore not known. The dotted arrow indicates proposed flooding direction. Cal = Calcite, Mg-cal = magnesian calcite, Mg = Magnesite.

5.3.3. LT4

The spectra collected from sample location A and B in LT4 show similar results (Figure 33). The aim of investigating this slice was to see if any other minerals than calcite could be detected. From Figure 33 one can see that magnesite was detected both in the first 2 mm of LT4 (location A) and in the last 5 mm of the slice (location B). The foraminifers proved to be challenging to obtain good spectra from, especially of the internal fillings of the shells. Five

foraminifers were analysed and the average calcite content was 79 %, 17 % magnesian calcite, and 4 % magnesite.

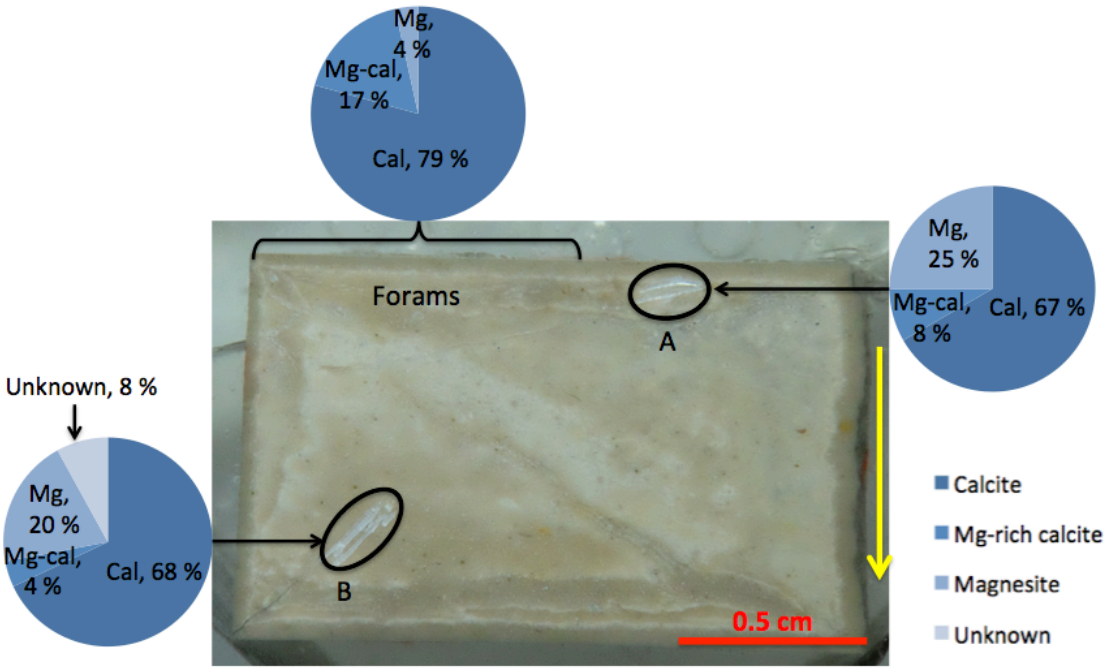

Figure 33: Sample map of LT4 with sample locations and associated results indicated. Yellow arrow indicates flooding direction. Cal = calcite, Mg-cal = magnesian calcite, Mg = magnesite, Unknown = minerals that have not yet been identified. This piece is not taken along the rim of the core.

6. DISCUSSION

The ULTT sample proves how quickly results can be obtained using Raman spectroscopy. Its mineralogical and chemical changes after injection of $MgCl_2$ were identified in 5 minutes only. In order to obtain a more descriptive analysis, several spectra were made. As 81 % of the spectra indicated magnesite content and no distinct trend could be found in the Mg-rich calcite content, it was quickly confirmed that the alteration front was no longer present within the ULTT due to the extent of the injection period. In other words, sufficient amount of Mg^{2+} was exposed to ion exchange to form magnesite throughout the whole injection period. This can all be done in one day without sample preparation.

The LTT sample has, on the other hand, already been investigated with several methods before and data available is therefore of another magnitude. The alteration front was suggested between LT3 and LT4. However, the results in this study suggest that the alteration front is somewhere within the LT4 as magnesite was identified both within the first 2 mm and the last 5 mm of LT4. The writer suggests for the future a more thorough analysis with Raman spectroscopy of LT4 in order to determine exactly where the alteration front is located. LTT is considered a more complex sample in comparison to the quite homogenous ULTT. Sometimes two small grains (1-3 microns) with different mineralogy (calcite + magnesite) are very close and the spatial resolution of the Raman spectrometer is not high enough to focus on only one of the two grains. The laser spot is too large to get the spectrum of one mineral only, resulting in a spectrum that is the mathematical sum of spectra of the two minerals. In all three slices (LT1, -2 and -4), there were several Raman spectra where the v_1 (main peak) was either showing a main peak with a shoulder of a different mineral or a set of double peaks together (Figure 34). The L peaks were in these cases often indicating the presence of both

calcite and magnesite, which is an indication of that the laser is focused on two very close grains of different mineralogy. All of these spectra went through analyses that are more thorough and both minerals have been counted in the percentages given for each slice. The mineralogical analyses of LT1, -2 and -4 show decreasing alteration with flooding direction, which is supported by Zimmermann et al. (2015).

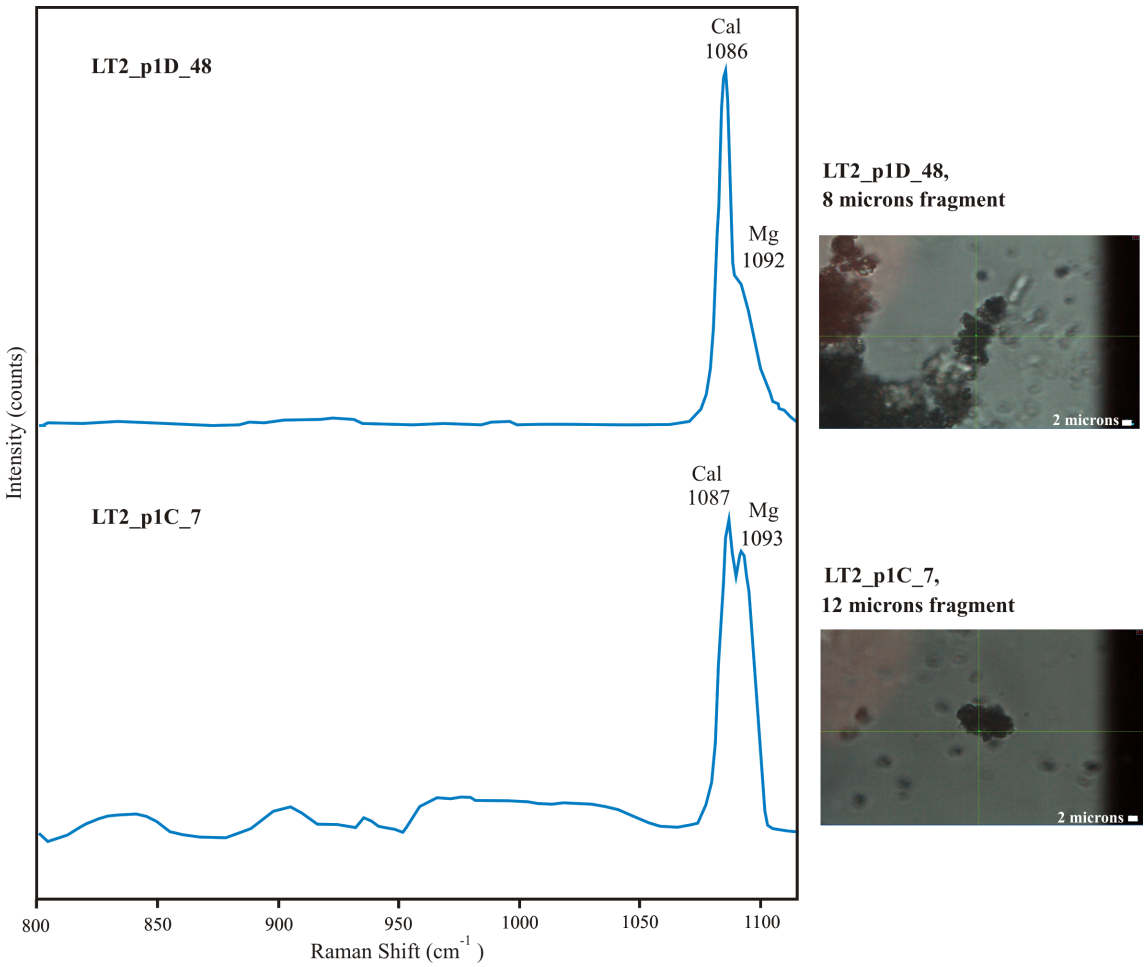

Figure 34: Two spectra with v_1 showing both calcite and magnesite. LT2_p1D_48 is showing calcite with a shoulder of magnesite. LT2_p1C_7 v_1 is showing two clear peaks, calcite is the highest and magnesite the second highest. Cal = calcite, Mg = magnesite.

Figure 35 illustrates the challenges related to resolution that may arise with application of Raman spectroscopy to chalk. A fragment consisting of four grains (Grain 4-7) were beamed at and analysed. v_1 of Grain 4 and 5 show magnesite with a discrete shoulder of calcite. Both

minerals can also be identified from the T and L vibrational modes of the two grains, but the peaks representing magnesite are of higher intensities compared to those of calcite. v_1 of Grain 6 and 7 do however show calcite with a shoulder of magnesite. The other vibrational modes, T, L and v_4, confirm the presence of two minerals as the intensities of the peaks are more balanced.

The results of this study have shown that future analyses of chalk by Raman spectroscopy would benefit from finding an optimized methodology for more complex samples such as the LTT. Significant compositional changes were produced when Liège chalk was injected with $MgCl_2$ for 516 days under Ekofisk reservoir stresses and 130°C. Large amounts of magnesite grew and much of the calcite was dissolved in the first two centimetres of the sample (LT1 and LT2). Massive enrichment of MgO and depletion of CaO in the tested core was demonstrated by ICP-MS whole rock analyses and effluent measurements via ICP-OES. The new growth of magnesite is accompanied by depletion of Sr proportional to CaO (Zimmermann et al., 2015). Sr could possibly in the future represent a more sensitive marker of mineralogical changes than CaO and is therefore proposed as a future topic of study.

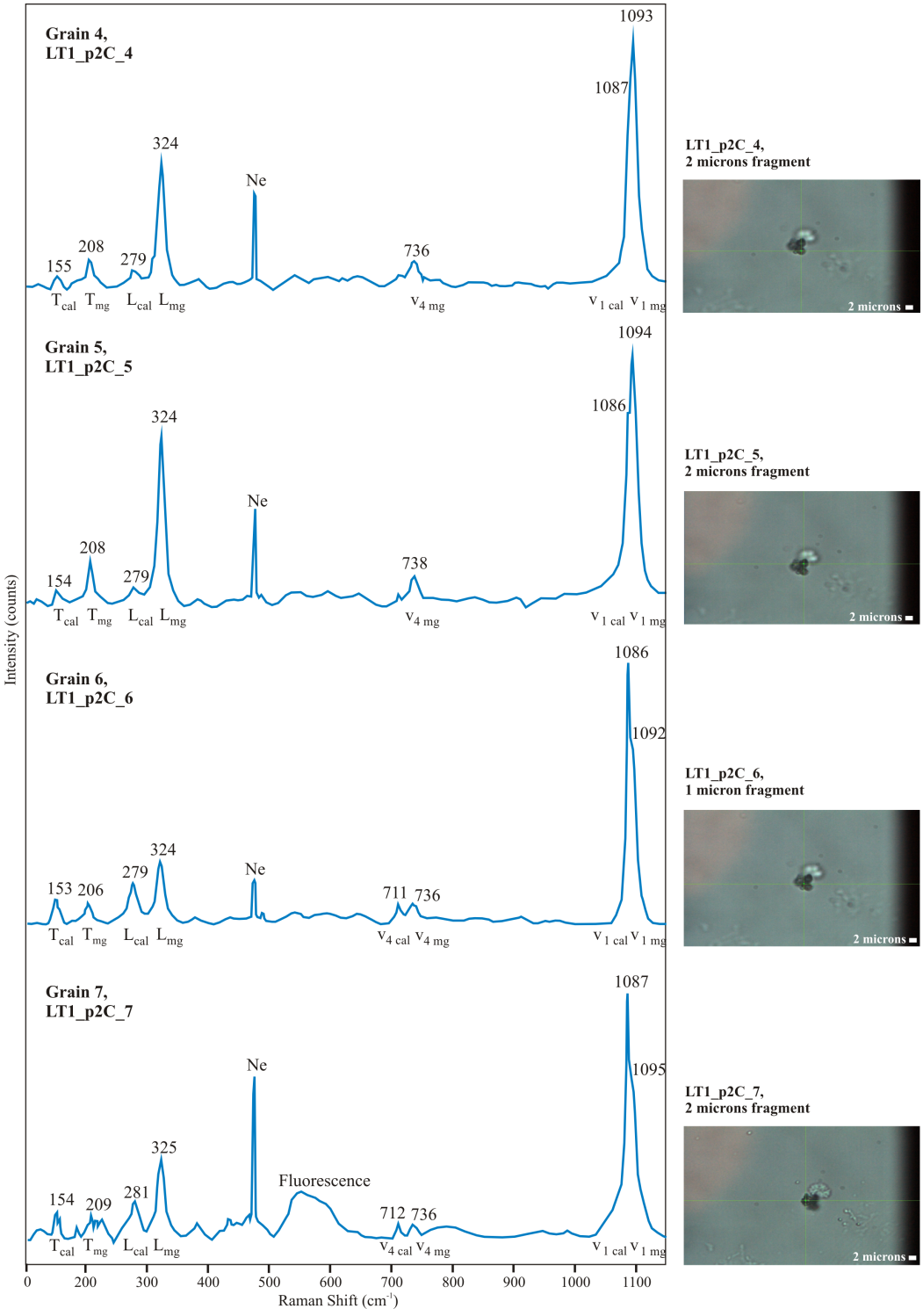

Figure 35: A fragment consisting of four closely surrounded grains (Grain 4-7) was analysed. Grain 4 and 5 show magnesite with a discrete shoulder of calcite. Both minerals can also be identified from the T and L vibrational modes of the two grains, but the peaks representing magnesite are of higher intensities compared to those of calcite. v_1 of Grain 6 and 7 show calcite with a shoulder of magnesite. The other vibrational modes, T, L and v_4, confirm the presence of two minerals as the intensities of the peaks are more balanced. The locations of the different grains are given in the photos aligned with corresponding spectra. Spectrum of grain 7 is influenced by fluorescence. Cal = calcite, mg = magnesite, Ne = neon.

7. CONCLUSIONS

Understanding the mineralogical and chemical changes induced by brine injection proves especially important for EOR research for several reasons. Compaction increases with dissolution of chalk. Formation of secondary minerals will affect rock surface properties and flow pathways for oil and water may be altered. Such textural changes in chalk allow different fluid flow mechanisms to play a role in reservoirs. Raman spectroscopy has in this study proven to be a non-destructive, quick analytical method that allows for identification of mineral phases down to micron level. The spectrometer can obtain high-resolution spectra in only a few seconds, which is a major advantage in comparison to other methodologies where the results are obtained over weeks. The methodology itself is simple, but it requires experience in order to analyse and interpret the spectra collected. The writer believes that the methodology of Raman spectroscopy is desirable for many users and will become an important method for investigation of mineral phases in EOR research. These proposals can be made because the LTT and ULTT have been sampled and injected with $MgCl_2$ for EOR purposes. The chalk here studied had been partially already subject of investigation in regard of mineral changes, which affects rock mechanical parameters in earlier studies. The chalk was sampled close to Liège from a large quarry and has an Upper Cretaceous age. It could be shown in the LTT that the occurrence of newly formed magnesite is decreasing with the flooding direction. The occurrence of magnesian calcite and calcite is increasing with the flooding direction. The magnesite occurrence decreases from 51 % in LT1 to 15 % in LT4, while magnesian calcite increases from 7 % to 10 % and calcite increases from 41 % to 72 % in slice LT1 to LT4. The mineralogical changes of samples of the yet not described ULTT after flooding were extraordinary quickly confirmed by Raman application. The sample consists of mainly magnesite (81 %), which coincides with predictions made prior the study.

The remaining consists of 16 % magnesian calcite and 3 % unidentified minerals. The results of this study prove how quick mineralogical analyses can be achieved by Raman spectroscopy.

REFERENCES CITED

Andrews A. B., D. Wang, K. M. Marzec, O. C. Mullins, and K. B. Crozier, 2015, Surface enhanced Raman spectroscopy of polycyclic aromatic hydrocarbons and molecular asphaltenes: Chemical Physics Letters, v. 620, p. 139-143, doi: 10.1016/j.cplett.2014.12.014.

Austad T., and D. C. Standnes, 2003, Spontaneous imbibition of water into oil-wet carbonates: Journal of Petroleum Science and Engineering, v. 39, p. 363-376, doi: 10.1016/S0920-4105(03)00075-5.

Bischoff W. D., S. K. Sharma, and F. T. Mackenzie, 1985, Carbonate ion disorder in synthetic and biogenic magnesian calcites: a Raman spectral study: American Mineralogist, v. 70, p. 581-589.

Borromeo L., N. Egeland, M. Minde, U. Zimmermann, and S. Andò, 2015a, Quick, easy and economic studies of flooded chalk for EOR experiments using Raman spectroscopy: a snapshot of on-going research (in prep.).

Borromeo L., U. Zimmermann, S. Andò, G. Coletti, D. Bersani, D. Basso, P. Gentile, and E. Garzanti, 2015b, Raman spectroscopy as a tool for magnesium estimation in Mg-calcites (in prep.).

Carteret C., M. De La Pierre, M. Dossot, F. Pascale, A. Erba, and R. Dovesi, 2013, The vibrational spectrum of CaCO3 aragonite: A combined experimental and quantum-mechanical investigation: Journal of Chemical Physics, v. 138, p. 14201-14212, doi: 10.1063/1.4772960.

Collin F., Y. J. Cui, C. Schroeder, and R. Charlier, 2002, Mechanical behaviour of Lixhe chalk partly saturated by oil and water: experiment and modelling: International Jorunal for Numerical and Analytical Methods in Geomechanics, v. 26, p. 897-924, doi: 10.1002/nag.229.

Costa J. C. S., A. C. Sant'Ana, P. Corio, and M. L. A. Temperini, 2006, Chemical analysis of polycyclic aromatic hydrocarbons by surface-enhanced Raman spectroscopy: Talanta, v. 70, p. 1011-1016, doi: 10.1016/j.talanta.2006.01.036.

Dandeu A., B. Humbert, C. Carteret, H. Muhr, E. Plasari, and J. M. Bossoutrot, 2006, Raman Spectroscopy – A Powerful Tool for the Quantitative Determination of the Composition of Polymorph Mixtures: Application to CaCO3 Polymorph Mixtures: Chemical Engineering & Technology, v. 29, p. 221-225, doi: 10.1002/ceat.200500354.

De La Pierre M., C. Carteret, L. Maschio, E. Andre, R. Orlando, and R. Dovesi, 2014, The Raman spectrum of CaCO3 polymorphs calcite and aragonite: A combined experimental and computational study: Journal of Chemical Physics, v. 140, doi: 10.1063/1.4871900.

Deer W. A., R. A. Howie, and J. Zussman, 1992, An introduction to the rock-forming minerals: Harlow, Longman.

DoITPoMS, 2007a, Method (dispersive Raman spectroscopy), http://www.doitpoms.ac.uk/tlplib/raman/index.php, (accessed May 1st, 2015).

DoITPoMS, 2007b, Raman scattering, http://www.doitpoms.ac.uk/tlplib/raman/index.php, (accessed May 4, 2015).

Edwards H. G. M., S. E. J. Villar, J. Jehlicka, and T. Munshi, 2005, FT–Raman spectroscopic study of calcium-rich and magnesium-rich carbonate minerals: Spectrochimica Acta Part A: Molecular and Biomolecular Spectroscopy, v. 61, p. 2273-2280, doi: 10.1016/j.saa.2005.02.026.

Fabricius I. L., 2007, Chalk: Composition, diagenesis and physical properties: Bulletin of the Geological Society of Denmark, v. 55, p. 97-128.

Ferraro J. R., K. Nakamoto, and C. W. Brown, 2002, Introductory Raman spectroscopy: Amsterdam, Academic Press, p. 1, 15-17, 159.

Frech R., E. C. Wang, and J. B. Bates, 1980, The i.r. and Raman spectra of CaCO3 (aragonite): Spectrochimica Acta Part A: Molecular and Biomolecular Spectroscopy, v. 36, p. 915-919.

Gabrielli C., R. Jaouhari, S. Joiret, G. Maurin, and G. Joiret, 2000, In situ Raman spectroscopy applied to electrochemical scaling. Determination of the structure of vaterite: Journal of Raman Spectroscopy, v. 31, p. 497-501, doi: 10.1002/1097-4555(200006)31:6<497::AID-JRS563>3.0.CO;2-9.

Gillet P., C. Biellmann, B. Reynard, and P. McMillan, 1993, Raman spectroscopic studies of carbonates part I: High-pressure and high-temperature behaviour of calcite, magnesite, dolomite and aragonite: Physics and Chemistry of Minerals, v. 20, p. 1-18, doi: 10.1007/BF00202245.

Gorelik V. S., A. V. Chervyakov, L. V. Kol'tsova, and S. S. Veryaskin, 2000, Raman Spectra of Saturated Hydrocarbons and Gasolines: Journal of Russian Laser Research, v. 21, p. 323-334.

Gunasekaran S., G. Anbalagan, and S. Pandi, 2006, Raman and infrared spectra of carbonates of calcite structure: Journal of Raman Spectroscopy, v. 37, p. 892-899, doi: 10.1002/jrs.1518.

Hancock J. M., 1975, The petrology of the chalk: Proceedings of the Geological Association, v. 86, p. 499-535, doi: 10.1016/S0016-7878(75)80061-7.

Heggheim T., M. Madland, R. Risnes, and T. Austad, 2005, A chemical induced enhanced weakening of chalk by seawater: Journal of Petroleum Science and Engineering, v. 46, p. 171-184, doi: 10.1016/j.petrol.2004.12.001.

Hellmann R., P. J. N. Renders, J. P. Gratier, and R. Guiguet, 2002, Experimental pressure solution compaction of chalk in aqueous solutions. Part 1. Deformation behavior and chemistry: The Geochemical Society. Special Publication, v. 7, p. 129-152.

Hiorth A., E. Jettestuen, L. M. Cathles, and M. V. Madland, 2013, Precipitation, dissolution, and ion exchange processes coupled with a lattice Boltzmann advection diffusion solver: Geochimica et Cosmochimica Acta, v. 104, p. 99-110, doi: 10.1016/j.gca.2012.11.019.

Hjuler M. L., and I. L. Fabricius, 2007, Diagenesis of Upper Cretaceous onshore and offshore chalk from the North Sea area: Ph.D. thesis, Technical University of Denmark, Kgs. Lyngby, 70 p.

Hjuler M. L., and I. L. Fabricius, 2009, Engineering properties of chalk related to diagenetic variations of Upper Cretaceous onshore and offshore chalk in the North Sea area: Journal of Petroleum Science and Engineering, v. 68, p. 151-170, doi: 10.1016/j.petrol.2009.06.005.

Horiba Scientific, 2005, What is a CCD detector?, http://www.horiba.com/in/scientific/products/raman-spectroscopy/raman-academy/raman-faqs/what-is-a-ccd-detector/, (accessed May 4, 2015).

Jaffe H. H., and A. L. Miller, 1966, The fates of electronic excitation energy: Journal of Chemical Education, v. 43, p. 469, doi: 10.1021/ed043p469.

Korsakov A. V., K. De Gussem, V. P. Zhukov, M. Perraki, P. Vandenabeele, and A. V. Golovin, 2009, Aragonite-calcite-dolomite relationships in UHPM polycrystalline carbonate inclusions from the Kokchetav Massif, northern Kazakhstan: European Journal of Mineralogy, v. 21, p. 1301-1311, doi: 10.1127/0935-1221/2009/0021-1992.

Korsnes R. I., M. V. Madland, T. Austad, S. Haver, and G. Rosland, 2008a, The effects of temperature on the water 761 weakening of chalk by seawater: Journal of Petroleum Science and Engineering, v. 60, p. 183-193, doi: 10.1016/j.petrol.2007.06.001.

Korsnes R. I., S. Strand, Ø. Hoff, T. Pedersen, M. V. Madland, and T. Austad, 2006, Does the chemical interaction between seawater and chalk affect the mechanical properties of chalk?, *in* A. V. Cotthem, Charlier R., Thimus J. F., and Tshibangu J. P., eds., Multiphysics Coupling and Long Term Behaviour in Rock Mechanics, London, Taylor & Francis, p. 427-434.

Korsnes R. I., E. Wersland, M. V. Madland, and T. Austad, 2008b, Anisotropy in chalk studied by rock mechanics: Journal of Petroleum Science and Engineering, v. 62, p. 28-35, doi: 10.1016/j.petrol.2008.06.004.

Krishnamurti D., 1956, Raman spectrum of magnesite: Proceedings of the Indian Academy of Sciences - Section A, v. 43, p. 210-212, doi: 10.1007/BF03052736.

Krishnan R. S., 1945, Raman spectra of the second order in crystals: Proceedings of the Indian Academy of Sciences - Section A, v. 22, p. 182-193, doi: 10.1007/BF03170928.

Kuebler K., A. Wang, K. Abbott, and L. A. Haskin, 2001, Can we detect carbonate and sulfate minerals on the surface of Mars by Raman spectroscopy?: 32nd Annual Lunar and Planetary Science Conference, Houston, Texas, p. 1889.

Lawrence Berkeley National Laboratory, 2007, Batteries of the Future II Building Better Batteries Through Advanced Diagnostics, Environmental Energy Technologies Division, http://eetd.lbl.gov/newsletter/nl27/eetd-nl27-2-better.html, (accessed May 4, 2015).

Madland M. V., A. Finsnes, A. Alkafadgi, R. Risnes, and T. Austad, 2006, The influence of CO2 gas and carbonate 783 water on the mechanical stability of chalk: Journal of Petroleum Science and Engineering, v. 51, p. 149-168, doi: 10.1016/j.petrol.2006.01.002.

Madland M. V., A. Hiorth, E. Omdal, M. Megawati, T. Hildebrand-Habel, R. I. Korsnes, S. Evje, and L. M. Cathles, 2011, Chemical Alterations Induced by Rock-Fluid

Interactions When Injecting Brines in High Porosity Chalks: Transport in Porous Media, v. 87, p. 679-702, doi: 10.1007/s11242-010-9708-3.

Madland M. V., K. Midtgarden, R. Manafov, R. I. Korsnes, T. Kristiansen, and A. Hiorth, 2008, The Effect of Temperature and Brine Composition on the Mechanical Strength of Kansas Chalk: International Symposium of the Society of Core Analysts, Abu Dhabi, p. 6, UAE, October 29 - November 2, 2008.

Madland M. V., U. Zimmermann, S. Haser, J. N. Audinot, and P. Gysan, 2013, Neoformed Dolomite in Flooded Chalk for EOR Processes: EAGE Annual Conference & Exhibition incorporating SPE Europec, London, June 10, 2013, WE-15-03.

Megawati M., A. Hiorth, and M. V. Madland, 2012, The impact of surface charge on the mechanical behaviour of high-porosity chalk: Rock Mechanical Engineering, v. 46, p. 1073-1090, doi: 10.1007/s00603-012-0317-z.

Nermoen A., R. I. Korsnes, A. Hiorth, and M. V. Madland, 2015, Porosity and permeability development in compacting chalks during flooding of nonequilibrium brines: Insights from long-term experiment: Journal of Geophysical Research: Solid Earth, v. 120, doi: 10.1002/2014JB011631.

Norwegian Petroleum Directorate, 2011, The shelf in 2010 – Press releases, http://www.npd.no/en/news/news/2011/the-shelf-2010--press-releases/, (accessed May 7, 2015).

Norwegian Petroleum Directorate, 2014, Recovery from producing fields, http://www.npd.no/en/Publications/Resource-Reports/2014/Chapter-2/, (accessed May 7, 2015).

Norwegian Petroleum Directorate, 2015, Distribution of oil reserves and resources for the largest oil producing fields as of 31 December 2014, http://www.norskpetroleum.no/en/production/resource-management-in-mature-areas/, (accessed May 7, 2015).

Porto S. P. S., J. A. Giordmaine, and T. C. Damen, 1966, Depolarization of Raman Scattering in Calcite: Physical Review, v. 147, p. 608-611, doi: 10.1103/PhysRev.147.608.

Raman C. V., 1928, A new radiation*: Indian Journal of Physics, v. 2, p. 387-398.

Robaszynski F., A. V. Dhondt, and J. W. M. Jagt, 2001, Cretaceous lithostratigraphic units (Belgium): Geologica Belgica, v. 4, p. 121-134.

Rutt H. N., and H. Nicola, 1974, Raman spectra of carbonates of calcite structure: Journal of Physics C: Solid State Physics, v. 7, p. 4522-4528, doi: 10.1088/0022-3719/7/24/015.

Scholle P. A., 1974, Diagenesis of Upper Cretaceous chalks from England, Northern Ireland, and the North Sea, *in* K. J. Hsü, and Jenkyns H. C., eds., Pelagic Sediments: On land and under the sea, v. 1: Oxford, Blackwell Scientific Publications, p. 177-210, doi: 10.1002/9781444304855.ch8.

Scholle P. A., 1977, Chalk diagenesis and its relationship to petroleum exploration: Oil from chalks, a modern miracle?: AAPG Bulletin, v. 61, p. 982-1009, doi: 10.1306/C1EA43B5-16C9-11D7-8645000102C1865D.

Sebek J., L. Pele, E. O. Potma, and R. Benny Gerber, 2011, Raman spectra of long chain hydrocarbons: anharmonic calculations, experiment and implications for imaging of biomembranes: Physical Chemistry Chemical Physics, v. 13, p. 12724-12733, doi: 10.1039/C1CP20618D.

Semrock, 2000, Filter Types for Raman Spectroscopy Applications, http://www.semrock.com/filter-types-for-raman-spectroscopy-applications.aspx, (accessed May 2, 2015).

Strand S., M. L. Hjuler, R. Torsvik, J. I. Pedersen, M. V. Madland, and T. Austad, 2007, Wettability of chalk: Impact of silica, clay content, and mechanical properties: Petroleum Geosciences, v. 13, p. 69-80, doi: 10.1144/1354-079305-696.

Strand S., D. C. Standnes, and T. Austad, 2003, Spontaneous Imbibition of Aqueous Surfactant Solutions into Neutral to Oil-Wet Carbonate Cores: Effects of Brine Salinity and Composition: Energy & Fuels, v. 17, p. 1133-1144, doi: 10.1021/ef030051s.

Sun J., Z. Wu, H. Cheng, Z. Zhang, and R. L. Frost, 2014, A Raman spectroscopic comparison of calcite and dolomite: Spectrochimica Acta Part A: Molecular and Biomolecular Spectroscopy, v. 117, p. 158-162, doi: 10.1016/j.saa.2013.08.014.

The Prashant Kamat Laboratory, 2012, Spectroscopic Characterization, University of Notre Dame, http://www3.nd.edu/~kamatlab/facilities_spectroscopy.html, (accessed October 23, 2014).

Thomas L. K., T. N. Dixon, C. E. Evans, and M. E. Vienot, 1987, Ekofisk Waterflood Pilot: Journal of Petroleum Technology, v. 39, p. 221-232, doi: 10.2118/13120-PA.

University of Stavanger, 2013, Rock Mechanics Lab, University of Stavanger, http://www.uis.no/research-and-phd-studies/research-areas/oil-gas-and-renewable-energy/petroleum-engineering/reservoir-engineering/research-facilities-labs/rock-mechanics-labs/, (accessed October 23, 2014).

Urmos J., S. K. Sharma, and F. T. Mackenzie, 1991, Characterization of some biogenic carbonates with Raman spectroscopy: American Mineralogist, v. 76, p. 641-646.

Wehrmeister U., A. L. Soldati, D. E. Jacob, T. Häger, W. Hofmeister, W. Wehrmeister, and W. Häger, 2010, Raman spectroscopy of synthetic, geological and biological vaterite: A Raman spectroscopic study: Journal of Raman Spectroscopy, v. 41, p. 193-201, doi: 10.1002/jrs.2438.

Zangiabadi B., R. I. Korsnes, T. Hildebrand-Habel, A. Hiorth, I. K. Surtarjana, A. Lian, and M. V. Madland, 2009, Chemical water weakening of various outcrop chalks at

elevated temperature, in H. I. Ling, Smyth A., and Betti R., eds., Poromechanics IV: The 4th Biot Conference on Poromechanics, p. 543-548.

Zimmermann U., M. V. Madland, S. A. R. Bertolino, T. Hildebrand-Habel, A. Hiorth, and R. I. Korsnes, 2013, Tracing Fluid Flow in Flooded Chalk under Long Term Test Conditions: EAGE Annual Conference & Exhibition incorporating SPE Europec, London, June 10, 2013, WE-17-10.

Zimmermann U., M. V. Madland, A. Nermoen, T. Hildebrand-Habel, S. A. R. Bertolino, A. Hiorth, R. I. Korsnes, J. N. Audinot, and P. Grysan, 2015, Evaluation of the compositional changes during flooding of reactive fluids using scanning electron mincroscoy, nano-secondary ion mass spectroscopy, x-ray diffraction, and whole-rock geochemistry: AAPG Bulletin, v. 99, p. 791-805, doi: 10.1306/12221412196.

APPENDIX

In the appendix the reader will find an overview of literature where relevant spectra for this study have been collected from, the standards used in this study, and the dataset containing all analyzed spectra.

Collected spectra from literature relevant for this study

Calcite																		
Krishnamurti, 1956			156			**284**				712				**1086**	1434			
Porto et al., 1966			156			**283**				714				**1088**				
Rutt & Nicola, 1974			155			**281**				711				**1085**	1435	1748		
Bischoff et al., 1985			154			**281**				711				**1085**	1434	1748		
Herman et al., 1987			154			**283**				714				**1087**	1438	1750		
Gillet et al., 1993			156			**281**				711				**1085**	1434	1748		
Gabrielli et al., 2000						**284**				712				**1086**	1434	1747		
Kubler et al 2001			156			**282**				713				**1086**	1436	1749		
Perez & M.Friaz, 2003			156			**282**				713				**1086**	1433			
Howell et al., 2005			156			**283**				713				**1086**	1436	1749		
Gunasekaran et al., 2006	89		162			**288**				716				**1092**	1437	1754		
White et al., 2006	86		155			**281**				711				**1085**	1435	1748		
Valenzano et al., 2007			156			**284**				712				**1086**	1434			
Sun et al., 2014			157			**278**				715	1047	1069		**1088**	1361	1613		
Borromeo et al., 2015a			154			**281**				712				**1086**	1437	1751		
Aragonite																		
Herman et al., 1987			**150**			205				704				**1085**				
Unvros et al., 1991		143	**153**	190		247	261	284		701	705			**1085**	1462	1574		
Gillet et al., 1993			**155**	180		209	217		275	702		710		**1084**	1463	1575		
Gabrielli et al., 2000			**151**			206				701	704		853	910	**1085**	1460	1570	
Kubler et al 2001			**154**			208	250			703					**1086**	1463	1575	
Howell et al., 2005			**154**	191		208	249	261	273	283	704	717	854		**1086**	1462	1574	
Carteret et al., 2013		**141**	**160**	194		214	284				705		853	1060	**1086**	1463		
Borromeo et al., 2015a			**155**	180		207				708					**1087**	1461	2433	
Vaterite																		
Gabrielli et al., 2000						267		300	325	668	682	740	750	1074		**1090**	1445	1550
Wehrmeister et al., 2009 (bio)		120	150	170	210	236	269	303	332		680		748	1075	1079	**1090**		
Wehrmeister et al., 2009 (syn)	106	120	151	175	210	268		303	333	666	685	738	751	1075	1081	**1090**	1440	1557

Collected spectra from literature relevant for this study

Dolomite															
Krishnamurti, 1956		176		**301**	335				724					**1099**	1444	
Bischoff et al., 1985		175		**299**					724					**1097**	1439	1750
Herman et al., 1987		177		**301**										**1099**	1440	1751
Gabrielli et al., 2000		178		**300**	335				733					**1097**	1439	1750
Kubler et al., 2001									724							
Howell et al., 2005	156	177		**300**	339	682	693	713	725	784	882			**1098**	1443	1759
Gunasekaran et al., 2006		187		**309**					725					**1106**	1450	1765
White et al., 2006		179		**304**					729					**1100**	1445	
Valenzano et al., 2007		176		**301**	335			724		880				**1099**	1444	
Sun et al., 2014	157	176	278	**299**								1019	1088	**1098**	1342	1613
Borromeo et al., 2015a		177		**300**	338			725						**1098**	1444	1760
Magnesite																
Krishnamurti, 1956		212		**332**					735					**1096**	1460	
Rutt & Nicola, 1974		212		**329**					739					**1084**	1445	1763
Bischoff et al., 1985		213		**329**					738					**1094**	1444	1762
Herman et al., 1987		216		**332**					738					**1096**	1447	1763
Gillet et al., 1993		213		**329**					738					**1094**	1444	1762
Kubler et al 2001		215		**332**					739					**1095**	1447	1764
Howell et al., 2005	120	213		**330**					738					**1094**	1444	2906
Valenzano et al., 2007		212		**332**					735					**1096**	1460	
Borromeo et al., 2015a		212		**329**	517	591	689		739					**1095**	1452	1763

Standards used in this study

Chemical formula: $CaCO_3$

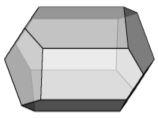

Chemical formula: $MgCO_3$

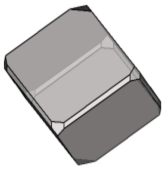

Chemical formula: $CaMg(CO_3)_2$

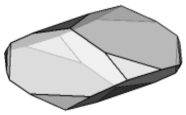

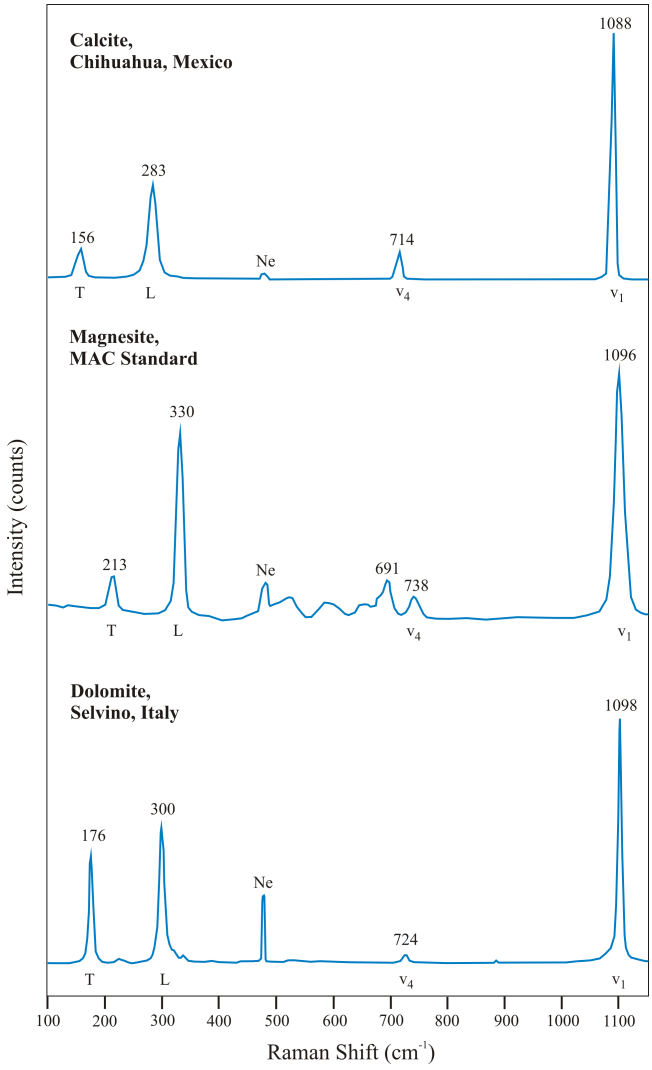

Legend
Cal
Mg-rich cal
Mg
Unknown

Grey numbers = Not sure.

Blue numbers = Spectra including two minerals. The blue numbers show that both minerals have been counted.

Bold numbers = The 2 or 3 strongest peaks per spectrum

From: Bischoff et al. 1985			T_{cal}		T_{mg}		L_{cal}	L_{mg}		Neon			$V_{4\,cal}$	$V_{4\,mg}$			$V_{1\,cal}$	$V_{1\,mg}$		
Name of spectra	**Mineral**	**120 - 151**	**152 - 158**	**159 - 191**	**201 - 216**	**217 - 269**	**270 - 291**	**318 - 345**	**379 - 460**	**Ne = 476,79**	**480 - 550**	**551 - 705**	**710 - 728**	**729 - 745**	**748 - 855**	**856 - 1075**	**1083 - 1092**	**1093-1097**	**Shou-lder**	**Double Peak**
ULTT_1_5x15_100%_1	Mg							327		476,79								**1093**		
ULTT_1_5x15_100%_10	Mg				209			**326**		476,79								**1094**		
ULTT_1_5x15_100%_2	Mg				209			**326**		476,79				738				**1094**		
ULTT_1_5x15_100%_3	Mg				210		288	**327**		476,79				738				**1094**		
ULTT_1_5x15_100%_3	Mg-rich cal						288													
ULTT_1_5x15_100%_4	Mg							326		476,79								**1093**		
ULTT_1_5x15_100%_5	Mg				209			326		476,79				738				**1094**		
ULTT_1_5x15_100%_6	Mg			185				322		476,79								**1094**		
ULTT_1_5x15_100%_7	Mg							325		476,79								**1094**		
ULTT_1_5x15_100%_8	Mg				209			**326**		476,79				738				**1094**		
ULTT_1_5x15_100%_9	Mg					265	288	**325**		476,79				737				**1095**	212	
ULTT_1_5x15_100%_9	Mg-rich cal						288													
ULTT_10_5x15_100%_1	Mg				210			**326**		476,79				737				**1095**		
ULTT_10_5x15_100%_10	Mg				210			**326**		476,79				739				**1096**		
ULTT_10_5x15_100%_2	Mg				212	264	288	**328**		476,79				740				**1096**		
ULTT_10_5x15_100%_2	Mg-rich cal						288													
ULTT_10_5x15_100%_3	Mg				211	263	287	**328**		476,79				739				**1095**		
ULTT_10_5x15_100%_3	Mg-rich cal						287													
ULTT_10_5x15_100%_4	Mg				212		288	328		476,79				740				**1096**		
ULTT_10_5x15_100%_4	Mg-rich cal						288													

From: Bischoff et al. 1985			T_{cal}		T_{mg}		L_{cal}	L_{mg}		Neon			$V_{4\,cal}$	$V_{4\,mg}$			$V_{1\,cal}$	$V_{1\,mg}$		
Name of spectra	**Mineral**	**120 - 151**	**152 - 158**	**159 - 191**	**201 - 216**	**217 - 269**	**270 - 291**	**318 - 345**	**379 - 460**	**NE = 476,79**	**480 - 550**	**551 - 705**	**710 - 728**	**729 - 745**	**748 - 855**	**856 - 1075**	**1083 - 1092**	**1093-1097**	**Shou-lder**	**Double Peak**
ULTT_10_5x15_100%_5	Mg				211			**327**		476,79				740				**1095**		
ULTT_10_5x15_100%_6	Mg-rich cal				209			**325**		476,79				738				**1095**		
ULTT_10_5x15_100%_7	Mg				211			**328**		476,79				740				**1095**		
ULTT_10_5x15_100%_8	Mg				211			**327**		476,79				738				**1095**		
ULTT_10_5x15_100%_9	Mg				210			**327**		476,79				739				**1095**		
ULTT_4_5x15_100%_1	Mg							**326**		476,79								**1094**		
ULTT_4_5x15_100%_2	Mg							326		476,79								**1093**		
ULTT_4_5x15_100%_3	Mg							**325**		476,79								**1093**		
ULTT_4_5x15_100%_4	Mg				208			**325**		476,79				738				**1093**		
ULTT_4_5x15_100%_5	Mg							**325**		476,79								**1093**		
ULTT_4_5x15_100%_6	Mg						288	325		476,79								**1092**		
ULTT_4_5x8_100%_10	Mg							**325**		476,79								**1094**		
ULTT_4_5x8_100%_7	Mg				209			**326**		476,79				736				**1094**		
ULTT_4_5x8_100%_8	Mg				208			**325**		476,79				738				**1093**		
ULTT_4_5x8_100%_9	Mg							326		476,79								**1094**		
ULTT_5_5x15_100%_10	Mg				210			**325**		476,79				737				**1094**		
ULTT_5_5x15_100%_3	Mg				207			324		476,79								**1093**		
ULTT_5_5x15_100%_4	Unknown	126				221		322		476,79						**1026**		**1063**		
ULTT_5_5x15_100%_5	Mg				208			**325**		476,79				737				**1094**		
ULTT_5_5x15_100%_6	Mg				210			326		476,79				736				**1094**		
ULTT_5_5x15_100%_7	Mg							327		476,79								**1093**		
ULTT_5_5x15_100%_8	Mg							325		476,79								**1094**		
ULTT_5_5x15_100%_9	Mg				207			**325**		476,79				737				**1093**		
ULTT_5_XX_5x15_100%_1	Unknown					221		322		476,79		**650**			847	**1002**				
ULTT_5_XX_5x15_100%_2	Unknown					222		322		476,79		**650**			847	**1002**			989	
ULTT_5b_5x8_100%_1	Mg				209		289	**325**		476,79				737				**1094**		

From: Bischoff et al. 1985			T_{cal}		T_{mg}		L_{cal}	L_{mg}		Neon			$V_{4\,cal}$	$V_{4\,mg}$			$V_{1\,cal}$	$V_{1\,mg}$		
Name of spectra	**Mineral**	**120 - 151**	**152 - 158**	**159 - 191**	**201 - 216**	**217 - 269**	**270 - 291**	**318 - 345**	**379 - 460**	**NE = 476,79**	**480 - 550**	**551 - 705**	**710 - 728**	**729 - 745**	**748 - 855**	**856 - 1075**	**1083 - 1092**	**1093-1097**	**Shou-lder**	**Double Peak**
ULTT_5b_5x8_100%_1	Mg-rich cal						289													
ULTT_5b_5x8_100%_10	Mg				207			**324**		476,79								**1093**		
ULTT_5b_5x8_100%_2	Mg					224	289	326		476,79				737				**1093**		
ULTT_5b_5x8_100%_2	Mg-rich cal						289													
ULTT_5b_5x8_100%_3	Mg-rich cal							325		476,79							**1092**			
ULTT_5b_5x8_100%_4	Mg							328		476,79								**1094**		
ULTT_5b_5x8_100%_5	Mg	**147**			201			319	**393**	476,79		**636**		737				**1093**		
ULTT_5b_5x8_100%_6	Mg				207			**324**		476,79				736				**1093**		
ULTT_5b_5x8_100%_7	Mg							327		476,79								**1093**		
ULTT_5b_5x8_100%_8	Mg				209			**325**		476,79								**1094**		
ULTT_5b_5x8_100%_9	Mg				207		289	**325**		476,79				737				**1094**		
ULTT_5b_5x8_100%_9	Mg-rich cal						289													
ULTT_6_5x4_100%_10	Mg				210			**328**		476,79								**1094**		
ULTT_6_5x4_100%_3	Mg				208			325		476,79								**1093**		
ULTT_6_5x4_100%_5	Mg							325		476,79								**1094**		
ULTT_6_5x4_100%_6	Mg					219		325		476,79								**1094**		
ULTT_6_5x4_100%_7	Mg					217		326	**390**	476,79								**1094**		
ULTT_6_5x4_100%_8	Mg							**326**		476,79				738				**1094**		
ULTT_6_5x4_100%_9	Mg		153		207		289	**325**	**385**	476,79				736				**1094**		
ULTT_6_5x4_100%_9	Mg-rich cal						289													
ULTT_6_5x8_100%_1	Mg		153		212			**328**		476,79								1093		
ULTT_6_5x8_100%_2	Mg				209			324		476,79								**1094**		
ULTT_6_5x8_100%_4	Mg					243		326		476,79							1090	**1095**		
ULTT_6_5x8_100%_4	Mg-rich cal																1090			
ULTT_7_5x4_100%_1	Mg				209			**325**		476,79				736				**1094**		
ULTT_7_5x4_100%_10	Mg	149						324	**386**	476,79								**1093**		

From: Bischoff et al. 1985			T_{cal}		T_{mg}		L_{cal}	L_{mg}		Neon			$V_{4\,cal}$	$V_{4\,mg}$			$V_{1\,cal}$	$V_{1\,mg}$		
Name of spectra	**Mineral**	**120 - 151**	**152 - 158**	**159 - 191**	**201 - 216**	**217 - 269**	**270 - 291**	**318 - 345**	**379 - 460**	**NE = 476,79**	**480 - 550**	**551 - 705**	**710 - 728**	**729 - 745**	**748 - 855**	**856 - 1075**	**1083 - 1092**	**1093-1097**	**Shou-lder**	**Double Peak**
ULTT_7_5x4_100%_2	Mg	144			209		288	**326**		476,79				737				**1094**		
ULTT_7_5x4_100%_2	Mg-rich cal						288													
ULTT_7_5x4_100%_3	Mg		154		208			**324**		476,79								**1093**		
ULTT_7_5x4_100%_4	Mg				211			**327**		476,79								**1094**		
ULTT_7_5x4_100%_5	Mg-rich cal					254		323		476,79							**1092**			
ULTT_7_5x4_100%_6	Mg	124	153		207			**325**		476,79				734				**1093**		
ULTT_7_5x4_100%_7	Mg				208			325		476,79				737				**1094**		
ULTT_7_5x4_100%_8	Mg		154		208			**325**		476,79				737				**1094**		
ULTT_7_5x4_100%_9	Mg-rich cal					222		323		476,79							**1090**			
ULTT_8_5x15_100%_1	Mg							**327**	**383**	476,79								1093		
ULTT_8_5x15_100%_10	Mg				208			**325**		476,79				737				**1095**		
ULTT_8_5x15_100%_2	Mg				210			**326**		476,79				737				**1094**		
ULTT_8_5x15_100%_3	Mg				210	261	288	**327**		476,79				738				**1094**		
ULTT_8_5x15_100%_3	Mg-rich cal						288													
ULTT_8_5x15_100%_4	Mg				209			**325**		476,79				738				**1095**		
ULTT_8_5x15_100%_5	Mg				209			325		476,79				739				**1093**		
ULTT_8_5x15_100%_6	Mg				208			**325**		476,79				737				**1094**		
ULTT_8_5x15_100%_7	Mg				209			**325**		476,79				737				**1094**		
ULTT_8_5x15_100%_8	Mg							325		476,79								**1094**		
ULTT_8_5x15_100%_9	Mg				208			**325**	**389**	476,79				737				**1093**		
ULTT_9_5x15_100%_10	Mg				211			**328**		476,79				738				**1095**		
ULTT_9_5x15_100%_2	Mg				210			**326**		476,79				739				**1094**		
ULTT_9_5x15_100%_3	Mg				210			**327**		476,79				739				**1094**		
ULTT_9_5x15_100%_4	Mg				210			**327**		476,79				738				**1095**		
ULTT_9_5x15_100%_5	Mg				209			**324**		476,79				737				**1095**		
ULTT_9_5x15_100%_6	Mg				209			**326**		476,79				738				**1094**		

From: Bischoff et al. 1985			T_{cal}		T_{mg}		L_{cal}	L_{mg}		Neon			$V_{4\,cal}$	$V_{4\,mg}$			$V_{1\,cal}$	$V_{1\,mg}$		
Name of spectra	**Mineral**	**120 - 151**	**152 - 158**	**159 - 191**	**201 - 216**	**217 - 269**	**270 - 291**	**318 - 345**	**379 - 460**	**NE = 476,79**	**480 - 550**	**551 - 705**	**710 - 728**	**729 - 745**	**748 - 855**	**856 - 1075**	**1083 - 1092**	**1093-1097**	**Shou-lder**	**Double Peak**
ULTT_9_5x15_100%_7	Mg				209			**327**		476,79				739				**1095**		
ULTT_9_5x15_100%_8	Mg				211			**327**		476,79								**1095**		
ULTT_9_5x15_100%_9	Mg				208			**325**		476,79				737				**1094**		

Legend	Grey numbers = Not sure.
Cal	Blue numbers = Spectra including two minerals. The blue numbers show that both minerals have been counted.
Mg-rich cal	**Bold numbers** = The 2 or 3 strongest peaks per spectrum
Mg	
Unknown	

From: Bischoff et al. 1985			T_{cal}		T_{mg}		L_{cal}	L_{mg}		Neon			$V_{4\,cal}$	$V_{4\,mg}$			$V_{1\,cal}$	$V_{1\,mg}$		
Name of spectra	**Mineral**	**120 - 151**	**152 - 158**	**159 - 191**	**201 - 216**	**217 - 269**	**270 - 291**	**318 - 345**	**379 - 460**	**NE = 476,79**	**480 - 550**	**551 - 705**	**710 - 728**	**729 - 745**	**748 - 855**	**856 - 1075**	**1083 - 1092**	**1093-1097**	**Shou-lder**	**Double Peak**
LT1_p1A_10x5_100%_10	Mg							**324**												
LT1_p1A_10x5_100%_10	Cal		154		207		281	**324**		476,79			712	736			**1086**		1094	
LT1_p1A_10x5_100%_11	Mg							**325**												
LT1_p1A_10x5_100%_11	Cal		154		207		281	**325**		476,79			712				**1086**			1094
LT1_p1A_10x5_100%_12	Cal		154				281			**476,79**			713				**1087**			
LT1_p1A_10x5_100%_13	Mg							324												
LT1_p1A_10x5_100%_13	Cal		154				280	324		**476,79**							**1087**			1094
LT1_p1A_10x5_100%_14	Mg-rich cal		155				**281**			**476,79**			713				**1088**			
LT1_p1A_10x5_100%_15	Cal		154				**281**			476,79			712				**1087**			
LT1_p1A_10x5_100%_16	Mg							326										1096		
LT1_p1A_10x5_100%_16	Cal		154				**280**	326		476,79			713				**1087**		1096	
LT1_p1A_10x5_100%_17	Cal		154				**280**			476,79			713				**1087**			
LT1_p1A_10x5_100%_18	Cal		154				**280**			476,79			712				**1087**			
LT1_p1A_10x5_100%_19	Cal		154				**281**			476,79			712				**1086**			
LT1_p1A_10x5_100%_1	Cal		155				281			476,79			713				**1087**			
LT1_p1A_10x5_100%_2	Cal		155				281			476,79			713				**1087**			
LT1_p1A_10x5_100%_20	Mg		153		209			**326**		476,79				738				**1094**	1087	
LT1_p1A_10x5_100%_20	Cal																1087			
LT1_p1A_10x5_100%_3	Cal		154				281			476,79			712				**1086**			
LT1_p1A_10x5_100%_4	Mg-rich cal		155				**281**			476,79			713				**1088**			

From: Bischoff et al. 1985			T_{cal}		T_{mg}		L_{cal}	L_{mg}		Neon			$V_{4\,cal}$	$V_{4\,mg}$			$V_{1\,cal}$	$V_{1\,mg}$		
Name of spectra	**Mineral**	**120 - 151**	**152 - 158**	**159 - 191**	**201 - 216**	**217 - 269**	**270 - 291**	**318 - 345**	**379 - 460**	**NE = 476,79**	**480 - 550**	**551 - 705**	**710 - 728**	**729 - 745**	**748 - 855**	**856 - 1075**	**1083 - 1092**	**1093- 1097**	**Shou- lder**	**Double Peak**
LT1_p1A_10x5_100%_5	Cal		154				282			476,79			713				**1087**			
LT1_p1A_10x5_100%_6	Cal		154				280			**476,79**			713				**1086**			
LT1_p1A_10x5_100%_7	Mg							**325**						736				**1093**		
LT1_p1A_10x5_100%_7	Cal		154		208		281	**325**		476,79			712	736			**1087**			**1093**
LT1_p1A_10x5_100%_8	Cal		154				**280**			476,79			712				1087			
LT1_p1A_10x5_100%_9	Cal		154				281			**476,79**			713				**1087**			1092
LT1_p1A_10x5_100%_9	Mg-rich cal																**1092**			
LT1_p1B_10x5_100%_1	Mg				210			326		**476,79**								**1094**		
LT1_p1B_10x5_100%_10	Cal		153		208			324		**476,79**							**1086**			1092
LT1_p1B_10x5_100%_10	Mg							324									1092			
LT1_p1B_10x5_100%_11	Mg				212			327		**476,79**								**1095**		
LT1_p1B_10x5_100%_12	Mg				211			327		**476,79**								**1094**		
LT1_p1B_10x5_100%_13	Mg							325		**476,79**								**1093**		
LT1_p1B_10x5_100%_14	Mg				207			**321**		**476,79**				735				**1092**		
LT1_p1B_10x5_100%_15	Mg							326		**476,79**								**1095**		
LT1_p1B_10x5_100%_16	Mg					260		326		**476,79**								**1095**		1087
LT1_p1B_10x5_100%_16	Cal																1087			
LT1_p1B_10x5_100%_17	Mg				209			326		**476,79**		639		736				**1094**		
LT1_p1B_10x5_100%_18	Mg				209			**326**		476,79				738				**1095**		
LT1_p1B_10x5_100%_19	Mg				210			**327**		476,79				739				**1094**		
LT1_p1B_10x5_100%_2	Mg				207			**322**		476,79								**1094**		
LT1_p1B_10x5_100%_20	Mg				213			328		**476,79**								**1095**		
LT1_p1B_10x5_100%_3	Mg		154		211			**328**		476,79				739				**1095**		
LT1_p1B_10x5_100%_4	Mg		152		211			327		476,79				737				**1095**		1085
LT1_p1B_10x5_100%_4	Cal																1085			
LT1_p1B_10x5_100%_5	Mg				212			325		**476,79**								**1095**		

From: Bischoff et al. 1985			T_{cal}		T_{mg}		L_{cal}	L_{mg}		Neon			$V_{4\,cal}$	$V_{4\,mg}$			$V_{1\,cal}$	$V_{1\,mg}$		
Name of spectra	**Mineral**	**120 - 151**	**152 - 158**	**159 - 191**	**201 - 216**	**217 - 269**	**270 - 291**	**318 - 345**	**379 - 460**	**NE = 476,79**	**480 - 550**	**551 - 705**	**710 - 728**	**729 - 745**	**748 - 855**	**856 - 1075**	**1083 - 1092**	**1093- 1097**	**Shou- lder**	**Double Peak**
LT1_p1B_10x5_100%_6	Mg				210			**326**		476,79				737				**1094**		
LT1_p1B_10x5_100%_7	Mg				211			**327**		476,79								**1094**		
LT1_p1B_10x5_100%_8	Mg	147			209			325		**476,79**		662						**1094**		1098
LT1_p1B_10x5_100%_9	Mg				211			329		**476,79**								**1094**		
LT1_p1C_10x5_100%_1	Cal						282			**476,79**							**1087**			
LT1_p1C_10x5_100%_10	Cal		155				**280**			476,79			713				**1087**			
LT1_p1C_10x5_100%_11	Cal		154				**280**			476,79			712				**1086**			
LT1_p1C_10x5_100%_12	Cal		153				**279**			476,79			712				**1086**			
LT1_p1C_10x5_100%_13	Cal		152				**277**			476,79			713				**1087**			
LT1_p1C_10x5_100%_14	Cal		155				**281**			476,79		589	713				**1087**			
LT1_p1C_10x5_100%_15	Cal		154				**280**			476,79			712				**1087**			
LT1_p1C_10x5_100%_16	Cal		155				**281**			476,79			713				**1087**			
LT1_p1C_10x5_100%_17	Cal		155				**281**			476,79			713				**1087**			
LT1_p1C_10x5_100%_18	Cal		155				**281**			476,79			712				**1086**			
LT1_p1C_10x5_100%_19	Cal		154				**280**			476,79			713				**1087**			
LT1_p1C_10x5_100%_2	Cal		154				280			**476,79**			713				**1087**			
LT1_p1C_10x5_100%_20	Cal		154				**280**			476,79			713				**1087**			
LT1_p1C_10x5_100%_3	Cal		155				281			476,79			712				**1086**			1094
LT1_p1C_10x5_100%_4	Mg							325										1094		
LT1_p1C_10x5_100%_4	Cal		154		208		**280**	325		476,79			712	737			**1087**			1094
LT1_p1C_10x5_100%_5	Mg							325										1093		
LT1_p1C_10x5_100%_5	Cal		155				282	325		**476,79**							**1087**			1093
LT1_p1C_10x5_100%_6	Cal		155				**281**			476,79			713				**1087**			
LT1_p1C_10x5_100%_7	Cal		155				**281**			476,79			713				**1087**			
LT1_p1C_10x5_100%_8	Cal		155				**281**			476,79			713				**1087**			
LT1_p1C_10x5_100%_9	Cal		154				**281**			**476,79**			713				**1087**			

From: Bischoff et al. 1985			T_{cal}		T_{mg}		L_{cal}	L_{mg}		Neon			$V_{4\,cal}$	$V_{4\,mg}$			$V_{1\,cal}$	$V_{1\,mg}$		
Name of spectra	**Mineral**	**120 - 151**	**152 - 158**	**159 - 191**	**201 - 216**	**217 - 269**	**270 - 291**	**318 - 345**	**379 - 460**	**NE = 476,79**	**480 - 550**	**551 - 705**	**710 - 728**	**729 - 745**	**748 - 855**	**856 - 1075**	**1083 - 1092**	**1093-1097**	**Shou-lder**	**Double Peak**
LT1_p1D_10x5_100%_1	Mg				210			326		**476,79**				736				**1094**		
LT1_p1D_10x5_100%_11	Mg-rich cal				208		288	325		**476,79**				738						
LT1_p1D_10x5_100%_11	Mg							325										**1094**		
LT1_p1D_10x5_100%_12	Mg				211			**326**		476,79				737				**1094**		
LT1_p1D_10x5_100%_13	Mg							325		**476,79**		640		735				**1094**	1085	
LT1_p1D_10x5_100%_13	Cal																1085			
LT1_p1D_10x5_100%_14	Mg							**326**		476,79		640		737				**1094**		
LT1_p1D_10x5_100%_15	Mg-rich cal						287	**324**	416	**476,79**										
LT1_p1D_10x5_100%_15	Mg							**324**										**1094**		
LT1_p1D_10x5_100%_16	Mg-rich cal							**326**										**1094**		
LT1_p1D_10x5_100%_16	Mg				210		288	**326**		476,79				736						
LT1_p1D_10x5_100%_17	Mg							323										**1093**		
LT1_p1D_10x5_100%_17	Mg-rich cal						289	323		**476,79**										
LT1_p1D_10x5_100%_18	Mg							323												
LT1_p1D_10x5_100%_18	Mg-rich cal					226	288	323	**417**	**476,79**		645					1091			
LT1_p1D_10x5_100%_19	Mg					218		325	417	**476,79**		640		737				**1094**		
LT1_p1D_10x5_100%_2	Mg-rich cal						290													
LT1_p1D_10x5_100%_2	Mg				210		290	**326**		**476,79**								**1093**		
LT1_p1D_10x5_100%_20	Mg				208			324		**476,79**		640		736				**1094**	1087	
LT1_p1D_10x5_100%_20	Cal																1087			
LT1_p1D_10x5_100%_3	Mg							327		**476,79**		639		735				**1094**	1086	
LT1_p1D_10x5_100%_3	Cal																1086			
LT1_p1D_10x5_100%_4	Mg							318		**476,79**								**1095**	1089	
LT1_p1D_10x5_100%_4	Mg-rich cal																1089			
LT1_p1D_10x5_100%_5	Mg							**328**		476,79										
LT1_p1D_10x5_100%_6	Mg-rich cal									**476,79**							1092			

From: Bischoff et al. 1985			T_{cal}		T_{mg}		L_{cal}	L_{mg}		Neon			$V_{4\,cal}$	$V_{4\,mg}$			$V_{1\,cal}$	$V_{1\,mg}$		
Name of spectra	**Mineral**	**120 - 151**	**152 - 158**	**159 - 191**	**201 - 216**	**217 - 269**	**270 - 291**	**318 - 345**	**379 - 460**	**NE = 476,79**	**480 - 550**	**551 - 705**	**710 - 728**	**729 - 745**	**748 - 855**	**856 - 1075**	**1083 - 1092**	**1093-1097**	**Shou-lder**	**Double Peak**
LT1_p1D_10x5_100%_7	Mg				209			326		476,79		639		735				**1093**		
LT1_p1D_10x5_100%_8	Mg							323		476,79								1093		
LT1_p1D_15x5_100%_10_UFO	Unknown					220	291			476,79	543	599			**850**	957	1091			**818**
LT1_p1D_15x5_100%_9	Mg		155							476,79								1093		
LT1_p1E_10x5_100%_1	Mg				205	219		**322**		476,79				739				1095	1085	
LT1_p1E_10x5_100%_1	Cal																1085			
LT1_p1E_10x5_100%_10	Mg				209			**324**		476,79				740				**1093**		
LT1_p1E_10x5_100%_11	Mg				209			323		476,79								**1093**		
LT1_p1E_10x5_100%_12	Mg							**327**		476,79								**1094**	1086	
LT1_p1E_10x5_100%_12	Cal																1086			
LT1_p1E_10x5_100%_13	Mg				210			326		476,79								**1094**		
LT1_p1E_10x5_100%_14	Mg				213			328		476,79								**1094**		
LT1_p1E_10x5_100%_15	Mg				212			**327**		476,79								1094		
LT1_p1E_10x5_100%_16	Mg	143			211			**327**	387	476,79		640		738				**1095**		
LT1_p1E_10x5_100%_17	Mg				210			326		476,79				737				**1094**		
LT1_p1E_10x5_100%_18	Mg							325	382	476,79								**1095**		
LT1_p1E_10x5_100%_19	Mg				210			327		476,79								**1094**		
LT1_p1E_10x5_100%_2	Mg							319		476,79								**1093**		
LT1_p1E_10x5_100%_20	Mg				212			327		476,79								**1095**	1086	
LT1_p1E_10x5_100%_20	Cal																1086			
LT1_p1E_10x5_100%_3	Mg				209			326	385	476,79				737				**1094**	1086	
LT1_p1E_10x5_100%_3	Cal																1086			
LT1_p1E_10x5_100%_4	Mg				211			**327**		476,79				737				**1094**		
LT1_p1E_10x5_100%_5	Mg				211			326		476,79				740				1095		
LT1_p1E_10x5_100%_6	Mg				216			328		476,79		640				1002		**1095**	1086	
LT1_p1E_10x5_100%_6	Cal																1086			

From: Bischoff et al. 1985			T_{cal}		T_{mg}		L_{cal}	L_{mg}		Neon			$V_{4\,cal}$	$V_{4\,mg}$			$V_{1\,cal}$	$V_{1\,mg}$		
Name of spectra	**Mineral**	**120 - 151**	**152 - 158**	**159 - 191**	**201 - 216**	**217 - 269**	**270 - 291**	**318 - 345**	**379 - 460**	**NE = 476,79**	**480 - 550**	**551 - 705**	**710 - 728**	**729 - 745**	**748 - 855**	**856 - 1075**	**1083 - 1092**	**1093-1097**	**Shou-lder**	**Double Peak**
LT1_p1E_10x5_100%_7	Mg-rich cal							327										**1094**		
LT1_p1E_10x5_100%_7	Mg						289	327		**476,79**										
LT1_p1E_10x5_100%_8	Mg							324										**1093**		
LT1_p1E_10x5_100%_8	Mg-rich cal					218	287	324		**476,79**										
LT1_p1E_10x5_100%_9	Mg				214			328		**476,79**								**1093**		
LT1_p1F_10x5_100%_1	Mg				209			327		**476,79**								**1093**		
LT1_p1F_10x5_100%_10	Mg							325										1095		
LT1_p1F_10x5_100%_10	Cal		154				278	325		**476,79**							**1086**		1095	
LT1_p1F_10x5_100%_11	Cal		155				**281**			476,79			713				**1087**			
LT1_p1F_10x5_100%_12	Mg							326										1094		
LT1_p1F_10x5_100%_12	Cal		154				**279**	326		476,79			712				**1086**		1094	
LT1_p1F_10x5_100%_13	Mg							326												
LT1_p1F_10x5_100%_13	Cal		153				**280**	326		476,79			712				**1086**		1095	
LT1_p1F_10x5_100%_14	Mg							326										1095		
LT1_p1F_10x5_100%_14	Cal		154				**280**	326	385	476,79			713				**1086**		1095	
LT1_p1F_10x5_100%_15	Cal		153				**279**			476,79			713				**1086**			
LT1_p1F_10x5_100%_16	Mg							324										1094		
LT1_p1F_10x5_100%_16	Cal		155				281	324		**476,79**			712				**1087**		1094	
LT1_p1F_10x5_100%_17	Cal		154				**280**			476,79			713				**1087**			
LT1_p1F_10x5_100%_18	Mg							326												
LT1_p1F_10x5_100%_18	Cal		155				281	326		**476,79**			713				**1087**			
LT1_p1F_10x5_100%_19	Mg							**324**										1094		
LT1_p1F_10x5_100%_19	Cal		155		206		281	**324**		476,79			713	735			**1087**		1094	
LT1_p1F_10x5_100%_2	Cal		153							**476,79**							1085			
LT1_p1F_10x5_100%_20	Mg							324										1096		
LT1_p1F_10x5_100%_20	Cal		154				**280**	324		476,79			712				**1086**		1096	

From: Bischoff et al. 1985			T_{cal}		T_{mg}		L_{cal}	L_{mg}		Neon			$V_{4\,cal}$	$V_{4\,mg}$			$V_{1\,cal}$	$V_{1\,mg}$		
Name of spectra	**Mineral**	**120 - 151**	**152 - 158**	**159 - 191**	**201 - 216**	**217 - 269**	**270 - 291**	**318 - 345**	**379 - 460**	**NE = 476,79**	**480 - 550**	**551 - 705**	**710 - 728**	**729 - 745**	**748 - 855**	**856 - 1075**	**1083 - 1092**	**1093-1097**	**Shou-lder**	**Double Peak**
LT1_p1F_10x5_100%_3	Cal		153				279			**476,79**			711				**1086**			
LT1_p1F_10x5_100%_4	Cal		154				**280**			476,79			713				**1085**			
LT1_p1F_10x5_100%_5	Mg							325										1093		
LT1_p1F_10x5_100%_5	Cal		154				**280**	325		476,79			712				**1086**		1093	
LT1_p1F_10x5_100%_6	Cal		154				280			476,79			713				**1087**			
LT1_p1F_10x5_100%_7	Mg		155		208			**325**		476,79				736				**1094**		
LT1_p1F_10x5_100%_8	Mg							327												
LT1_p1F_10x5_100%_8	Cal		154				**280**	327		476,79			712				**1086**			
LT1_p1F_10x5_100%_9	Cal		155				**281**			476,79			713				**1087**			
LT1_p2A_10x5_100%_10	Mg							326										1095		
LT1_p2A_10x5_100%_10	Cal		155				**281**	326		476,79			713				**1087**		1095	
LT1_p2A_10x5_100%_11	Mg							**326**										1095		
LT1_p2A_10x5_100%_11	Cal		155				**282**	**326**		476,79			712				**1087**			1095
LT1_p2A_10x5_100%_12	Cal		155				282			**476,79**			714				**1087**			
LT1_p2A_10x5_100%_13	Cal		154				**282**			476,79			713				**1087**			
LT1_p2A_10x5_100%_14	Cal		155				**281**			476,79			713				**1087**			
LT1_p2A_10x5_100%_15	Cal		154				**282**			476,79			713				**1087**			
LT1_p2A_10x5_100%_16	Cal		154				282			**476,79**			712				**1087**			
LT1_p2A_10x5_100%_17	Cal		155				**281**			476,79			713				**1087**			
LT1_p2A_10x5_100%_18	Mg-rich cal		155				**281**			476,79			713				**1088**			
LT1_p2A_10x5_100%_19	Cal		154							**476,79**							**1087**		1094	
LT1_p2A_10x5_100%_19	Mg																	1094		
LT1_p2A_10x5_100%_2	Mg-rich cal		155				**282**			476,79			714				**1088**			
LT1_p2A_10x5_100%_20	Mg							325										1094		
LT1_p2A_10x5_100%_20	Cal		154		208		281	325		**476,79**			712				**1087**		1094	
LT1_p2A_10x5_100%_3	Cal		154				**282**			476,79			712				**1087**			

From: Bischoff et al. 1985			T_{cal}		T_{mg}		L_{cal}	L_{mg}		Neon			$V_{4\,cal}$	$V_{4\,mg}$			$V_{1\,cal}$	$V_{1\,mg}$		
Name of spectra	**Mineral**	**120 - 151**	**152 - 158**	**159 - 191**	**201 - 216**	**217 - 269**	**270 - 291**	**318 - 345**	**379 - 460**	**NE = 476,79**	**480 - 550**	**551 - 705**	**710 - 728**	**729 - 745**	**748 - 855**	**856 - 1075**	**1083 - 1092**	**1093-1097**	**Shou-lder**	**Double Peak**
LT1_p2A_10x5_100%_4	Cal		155				**281**			476,79			712				**1087**			
LT1_p2A_10x5_100%_5	Cal		154				**280**			476,79			713				**1087**			
LT1_p2A_10x5_100%_6	Mg							327										1096		
LT1_p2A_10x5_100%_6	Cal		154				**280**	327		476,79			712				**1087**		1096	
LT1_p2A_10x5_100%_7	Cal		154		215		**282**			476,79			712				**1087**			
LT1_p2A_10x5_100%_8	Mg							334										1094		
LT1_p2A_10x5_100%_8	Cal		154				282	334		**476,79**	542		713				**1087**		1094	
LT1_p2A_10x5_100%_9	Cal		154				**280**			476,79			712				**1086**			
LT1_p2B_10x5_100%_1	Mg				211			**327**		476,79				739				**1094**		
LT1_p2B_10x5_100%_10	Mg				212			**328**		476,79				739				**1094**		
LT1_p2B_10x5_100%_11	Mg				210			**328**		476,79				737				**1094**		
LT1_p2B_10x5_100%_12	Mg				210			**328**		476,79				738				**1094**		
LT1_p2B_10x5_100%_13	Mg		156		210			**327**		476,79				738				**1095**		
LT1_p2B_10x5_100%_14	Mg				212			328		**476,79**				737				**1094**		
LT1_p2B_10x5_100%_15	Mg				211			**328**		476,79				738				**1095**		
LT1_p2B_10x5_100%_16	Mg				212			**328**		476,79				738				**1095**		
LT1_p2B_10x5_100%_17_UFO	Mg	**146**			210			326	388	476,79		643						**1095**		
LT1_p2B_10x5_100%_18_UFO	Mg	**144**			212			329		476,79		641		738				**1094**		
LT1_p2B_10x5_100%_19	Mg				212			**328**		476,79				738				**1095**		
LT1_p2B_10x5_100%_2	Mg				209			**326**		476,79				738				**1094**		
LT1_p2B_10x5_100%_20	Mg				212			328		**476,79**				738				**1095**		
LT1_p2B_10x5_100%_3	Mg				214			**329**		**476,79**								1093		
LT1_p2B_10x5_100%_4	Mg				212			**328**		476,79				739				**1095**		
LT1_p2B_10x5_100%_5	Cal		152							**476,79**							**1085**			
LT1_p2B_10x5_100%_6	Mg							**328**												
LT1_p2B_10x5_100%_6	Mg-rich cal		152		207		291	**328**		476,79		704					**1085**			1095

From: Bischoff et al. 1985			T_{cal}		T_{mg}		L_{cal}	L_{mg}		Neon			$V_{4\,cal}$	$V_{4\,mg}$			$V_{1\,cal}$	$V_{1\,mg}$		
Name of spectra	**Mineral**	**120 - 151**	**152 - 158**	**159 - 191**	**201 - 216**	**217 - 269**	**270 - 291**	**318 - 345**	**379 - 460**	**NE = 476,79**	**480 - 550**	**551 - 705**	**710 - 728**	**729 - 745**	**748 - 855**	**856 - 1075**	**1083 - 1092**	**1093-1097**	**Shou-lder**	**Double Peak**
LT1_p2B_10x5_100%_7	Mg				211			**328**		476,79				738				**1094**		
LT1_p2B_10x5_100%_8	Mg				210			**327**		476,79				737				**1094**		
LT1_p2B_10x5_100%_9	Mg		152		212			**328**	384	476,79				738				**1095**		
LT1_p2C_10x5_100%_1	Mg		155		207			324		**476,79**				737				**1093**		
LT1_p2C_10x5_100%_10	Mg		154					321		**476,79**				736				**1093**		
LT1_p2C_10x5_100%_11	Mg							**324**										**1094**		
LT1_p2C_10x5_100%_11	Cal		154		207		280	**324**		476,79				736		906	1087		**1094**	
LT1_p2C_10x5_100%_12	Mg				208			**325**		476,79				738				**1095**		
LT1_p2C_10x5_100%_13	Mg		155					325		**476,79**					747			1094	**1087**	
LT1_p2C_10x5_100%_13	Cal																**1087**			
LT1_p2C_10x5_100%_14	Mg							**325**										**1093**		
LT1_p2C_10x5_100%_14	Cal		153		208		282	**325**		476,79				737			1087		**1093**	
LT1_p2C_10x5_100%_15	Mg				206			**323**		476,79				736				**1094**		
LT1_p2C_10x5_100%_16	Cal		153				278			**476,79**			712				**1086**		1094	
LT1_p2C_10x5_100%_17	Mg							323										**1094**		
LT1_p2C_10x5_100%_17	Cal		154		206		279	323		476,79			711	737			**1086**			**1094**
LT1_p2C_10x5_100%_18_UFO	Cal	123		180	213	251				**476,79**						**1071**	1087		1069	
LT1_p2C_10x5_100%_19	Mg							**325**										**1093**		
LT1_p2C_10x5_100%_19	Cal		156		208		281	**325**		476,79				736			1087			**1093**
LT1_p2C_10x5_100%_2	Mg							**324**										**1093**		
LT1_p2C_10x5_100%_2	Cal		154		207		280	**324**		476,79				737			1086		**1093**	
LT1_p2C_10x5_100%_20	Mg				207			325		**476,79**				737				**1094**		
LT1_p2C_10x5_100%_21	Mg				208			**324**		476,79				737				**1095**		
LT1_p2C_10x5_100%_3	Mg							**325**										**1094**		
LT1_p2C_10x5_100%_3	Cal		155		208		282	**325**		476,79				737		906	1087			**1094**
LT1_p2C_10x5_100%_4	Mg							326										**1094**		

From: Bischoff et al. 1985			T_{cal}		T_{mg}		L_{cal}	L_{mg}		Neon			$V_{4\,cal}$	$V_{4\,mg}$			$V_{1\,cal}$	$V_{1\,mg}$		
Name of spectra	**Mineral**	**120 - 151**	**152 - 158**	**159 - 191**	**201 - 216**	**217 - 269**	**270 - 291**	**318 - 345**	**379 - 460**	**NE = 476,79**	**480 - 550**	**551 - 705**	**710 - 728**	**729 - 745**	**748 - 855**	**856 - 1075**	**1083 - 1092**	**1093-1097**	**Shou-lder**	**Double Peak**
LT1_p2C_10x5_100%_4	Cal		154		208		281	326		**476,79**				736			1087		**1094**	
LT1_p2C_10x5_100%_8	Mg		154			225		324		**476,79**								**1094**		
LT1_p2C_10x5_100%_9	Mg							323										1094		
LT1_p2C_10x5_100%_9	Cal		154				280	323	381	**476,79**							**1086**		1094	
LT1_p2C_15x5_100%_4	Mg							**325**										**1093**		
LT1_p2C_15x5_100%_4	Cal		155		208		279	**324**		476,79				736			1087			**1093**
LT1_p2C_15x5_100%_5	Mg		154		208			**324**		476,79				738				**1094**		1086
LT1_p2C_15x5_100%_5	Cal																1086			
LT1_p2C_15x5_100%_6	Mg							**324**									1092			
LT1_p2C_15x5_100%_6	Cal		153		206		279	**324**		476,79			711	736				**1086**	1092	
LT1_p2C_15x5_100%_7	Mg							325										1095		
LT1_p2C_15x5_100%_7	Cal		154		209		281	325		**476,79**			712	736			**1087**		1095	

Legend	Grey numbers = Not sure.
Cal	Blue numbers = Spectra including two minerals. The blue numbers show that both minerals have been counted.
Mg-rich cal	**Bold numbers** = The 2 or 3 strongest peaks per spectrum
Mg	
Unknown	

From: Bischoff et al. 1985			T_{cal}	T_{mg}			L_{cal}	L_{mg}		Neon			$V_{4\,cal}$	$V_{4\,mg}$			$V_{1\,cal}$	$V_{1\,mg}$		
Name of spectra	**Mineral**	**120 - 151**	**152 - 158**	**159 - 191**	**201 - 216**	**217 - 269**	**270 - 291**	**318 - 345**	**379 - 460**	**NE = 476,79**	**480 - 550**	**551 - 705**	**710 - 728**	**729 - 745**	**748 - 855**	**856 - 1075**	**1083 - 1092**	**1093-1097**	**Shou-lder**	**Double Peak**
LT2_p1A_5x15_100%_10	Cal		154				282			**476,79**							**1086**			
LT2_p1A_5x15_100%_17	Cal		155				**281**			476,79			713				**1087**			
LT2_p1A_5x15_100%_18	Cal		154				**281**			476,79			713				**1086**			
LT2_p1A_5x15_100%_19	Cal		154				**281**			476,79			713				**1086**			
LT2_p1A_5x15_100%_31	Cal		155							**476,79**							1087			
LT2_p1A_5x15_100%_49	Cal		154							**476,79**		643					1087			
LT2_p1A_5x15_100%_68	Cal		155				282			**476,79**			713				**1086**			
LT2_p1A_5x4_100%_1	Cal		154				281	326		**476,79**							**1086**			
LT2_p1A_5x4_100%_1	Mg							326												
LT2_p1A_5x4_100%_11	Cal		155							**476,79**							**1086**			
LT2_p1A_5x4_100%_12	Cal		152							**476,79**							**1085**			
LT2_p1A_5x4_100%_13	Cal		152				**278**			476,79			712				**1085**			
LT2_p1A_5x4_100%_14	Cal		154				**280**			476,79			713				**1086**			
LT2_p1A_5x4_100%_15	Cal		154				282			**476,79**							**1086**			
LT2_p1A_5x4_100%_16	Cal									**476,79**							1086			
LT2_p1A_5x4_100%_17	Cal		**154**				**280**			476,79			712				**1086**			
LT2_p1A_5x4_100%_2	Mg-rich cal		154				283	325		**476,79**			712				**1086**			
LT2_p1A_5x4_100%_2	Mg							325												
LT2_p1A_5x4_100%_20	Mg-rich cal		155				283			**476,79**							**1087**			
LT2_p1A_5x4_100%_21	Cal		154				280			**476,79**			712				**1086**			

From: Bischoff et al. 1985			T_{cal}		T_{mg}		L_{cal}	L_{mg}		Neon			$V_{4\,cal}$	$V_{4\,mg}$			$V_{1\,cal}$	$V_{1\,mg}$		
Name of spectra	**Mineral**	**120 - 151**	**152 - 158**	**159 - 191**	**201 - 216**	**217 - 269**	**270 - 291**	**318 - 345**	**379 - 460**	**NE = 476,79**	**480 - 550**	**551 - 705**	**710 - 728**	**729 - 745**	**748 - 855**	**856 - 1075**	**1083 - 1092**	**1093-1097**	**Shou-lder**	**Double Peak**
LT2_p1A_5x4_100%_22	Mg-rich cal		156				**282**			476,79			714				**1088**			
LT2_p1A_5x4_100%_23	Cal		155				280			**476,79**			713				**1086**			
LT2_p1A_5x4_100%_24	Mg-rich cal		154				283			**476,79**							**1087**			
LT2_p1A_5x4_100%_25	Mg-rich cal		156				283			476,79			713				**1088**			
LT2_p1A_5x4_100%_26	Cal		156				**282**			**476,79**			712				**1087**			
LT2_p1A_5x4_100%_27	Mg-rich cal		156				**283**			476,79			713				**1088**			
LT2_p1A_5x4_100%_28	Mg-rich cal		157				**283**			476,79			713				**1088**			
LT2_p1A_5x4_100%_29	Mg-rich cal		156				**283**			476,79			713				**1088**			
LT2_p1A_5x4_100%_3	Mg-rich cal		154				283			**476,79**							**1085**			
LT2_p1A_5x4_100%_30	Cal		154				**281**			**476,79**			713				**1086**			
LT2_p1A_5x4_100%_32	Cal		156				282	325		476,79		693	714				1087			1093
LT2_p1A_5x4_100%_32	Mg							325										1093		
LT2_p1A_5x4_100%_33	Cal		153				**279**	324		**476,79**			712				**1085**			
LT2_p1A_5x4_100%_33	Mg							324												
LT2_p1A_5x4_100%_34	Cal		153				**279**	324		**476,79**			712				**1085**			
LT2_p1A_5x4_100%_34	Mg							324												
LT2_p1A_5x4_100%_35	Cal		155				281			**476,79**			713				**1086**			
LT2_p1A_5x4_100%_36	Cal		155				281			**476,79**			713				**1087**			
LT2_p1A_5x4_100%_37	Cal		155				**281**			476,79			713				**1087**			
LT2_p1A_5x4_100%_38	Cal		153				**277**			476,79			712				**1085**			
LT2_p1A_5x4_100%_39	Cal		154				**280**			476,79			712				**1086**			
LT2_p1A_5x4_100%_4	Cal		153				**279**	321		**476,79**					839		**1085**			
LT2_p1A_5x4_100%_4	Mg							321												
LT2_p1A_5x4_100%_40	Cal		154				280			**476,79**			713				**1086**			
LT2_p1A_5x4_100%_41	Cal		153				280			476,79			712				**1086**			
LT2_p1A_5x4_100%_42	Cal		155				**281**			476,79			713				**1087**			

From: Bischoff et al. 1985			T_{cal}		T_{mg}		L_{cal}	L_{mg}		Neon			$V_{4\,cal}$	$V_{4\,mg}$			$V_{1\,cal}$	$V_{1\,mg}$		
Name of spectra	**Mineral**	**120 - 151**	**152 - 158**	**159 - 191**	**201 - 216**	**217 - 269**	**270 - 291**	**318 - 345**	**379 - 460**	**NE = 476,79**	**480 - 550**	**551 - 705**	**710 - 728**	**729 - 745**	**748 - 855**	**856 - 1075**	**1083 - 1092**	**1093-1097**	**Shou-lder**	**Double Peak**
LT2_p1A_5x4_100%_43	Cal		155				**281**			476,79			713				**1087**			
LT2_p1A_5x4_100%_44	Cal		155				**282**			476,79			713				**1086**			
LT2_p1A_5x4_100%_45	Mg-rich cal		156				**283**		386	**476,79**							**1087**			
LT2_p1A_5x4_100%_46	Cal		154				**281**			476,79			712				**1086**			
LT2_p1A_5x4_100%_47	Cal		155				**281**			476,79			713				**1086**			
LT2_p1A_5x4_100%_48	Mg-rich cal		155				**283**			**476,79**			714				**1087**			
LT2_p1A_5x4_100%_5	Cal		**152**				**277**			476,79			713				**1086**			
LT2_p1A_5x4_100%_50	Cal		155				**281**			476,79			712				**1087**			
LT2_p1A_5x4_100%_51	Cal		154				**280**			476,79			712				**1086**			
LT2_p1A_5x4_100%_52	Cal		154				**281**			476,79			713				**1087**			
LT2_p1A_5x4_100%_53	Cal		154				282			**476,79**	547						**1086**			
LT2_p1A_5x4_100%_54	Cal		153				**279**			476,79			711				**1086**			
LT2_p1A_5x4_100%_55	Cal		155				282			**476,79**							**1087**			
LT2_p1A_5x4_100%_56	Cal		155			223	281	326		476,79							1087		1093	
LT2_p1A_5x4_100%_56	Mg							326										1093		
LT2_p1A_5x4_100%_57	Cal		154				**281**			476,79			712				**1086**			
LT2_p1A_5x4_100%_58	Cal		155				281	327		476,79			712				1087		1095	
LT2_p1A_5x4_100%_58	Mg							327										1095		
LT2_p1A_5x4_100%_59	Cal		155				**281**			476,79			713				**1086**			
LT2_p1A_5x4_100%_6	Cal		153				**279**	323		**476,79**							**1085**			
LT2_p1A_5x4_100%_6	Mg							323												
LT2_p1A_5x4_100%_60	Cal		154				**281**			476,79			713				**1086**			
LT2_p1A_5x4_100%_61	Cal		154				**281**			476,79			713				**1086**			
LT2_p1A_5x4_100%_62	Mg-rich cal		155				283			**476,79**							**1087**			
LT2_p1A_5x4_100%_63	Cal		154				**281**			476,79			713				**1086**			
LT2_p1A_5x4_100%_64	Cal		156				**282**			**476,79**			713				**1087**			

From: Bischoff et al. 1985			T_{cal}		T_{mg}		L_{cal}	L_{mg}		Neon			$V_{4\,cal}$	$V_{4\,mg}$			$V_{1\,cal}$	$V_{1\,mg}$		
Name of spectra	**Mineral**	**120 - 151**	**152 - 158**	**159 - 191**	**201 - 216**	**217 - 269**	**270 - 291**	**318 - 345**	**379 - 460**	**NE = 476,79**	**480 - 550**	**551 - 705**	**710 - 728**	**729 - 745**	**748 - 855**	**856 - 1075**	**1083 - 1092**	**1093-1097**	**Shou-lder**	**Double Peak**
LT2_p1A_5x4_100%_65	Cal		155				**282**			476,79			713				**1087**			
LT2_p1A_5x4_100%_66	Cal		156							476,79		656					**1087**			
LT2_p1A_5x4_100%_67	Cal		154				**281**			476,79			713				**1086**			
LT2_p1A_5x4_100%_69	Cal		155				281			476,79			712				**1086**			
LT2_p1A_5x4_100%_7	Cal		153				**279**			476,79			712				**1085**			
LT2_p1A_5x4_100%_70	Cal		155				**281**			476,79			713				**1087**			
LT2_p1A_5x4_100%_8	Cal									476,79		652			775		**1085**			
LT2_p1A_5x4_100%_9	Cal		154						387	476,79							**1085**			
LT2_p1B_5x15_100%_19	Cal									476,79							**1087**			
LT2_p1B_5x15_100%_2_UFO	Mg							321		476,79									310	
LT2_p1B_5x15_100%_3	Cal		155					322		476,79							**1087**		**311**	
LT2_p1B_5x15_100%_3	Mg							322												
LT2_p1B_5x15_100%_4	Cal		154				**280**	324		476,79			713				**1087**			1093
LT2_p1B_5x15_100%_4	Mg							324										1093		
LT2_p1B_5x15_100%_42	Cal		154				**281**			476,79			712				**1086**			
LT2_p1B_5x15_100%_49	Cal		154				**281**	323		476,79			713				**1087**			1093
LT2_p1B_5x15_100%_49	Mg							323										1093		
LT2_p1B_5x15_100%_50_UFO	Cal	130	154			258			**389**	476,79		689					**1086**			
LT2_p1B_5x4_100%_1	Cal		155			227	**282**			476,79			713				**1087**		**265**	
LT2_p1B_5x4_100%_10	Cal		153				282			476,79			713				**1086**			
LT2_p1B_5x4_100%_11	Cal		154				**281**			476,79			712				**1087**			
LT2_p1B_5x4_100%_12	Mg-rich cal		155				287	324		476,79							**1087**		**1095**	
LT2_p1B_5x4_100%_12	Mg							324										**1095**		
LT2_p1B_5x4_100%_13	Cal		154				**282**			476,79	537		713				**1087**			
LT2_p1B_5x4_100%_14	Cal		154				**282**			476,79	537		713				**1087**			
LT2_p1B_5x4_100%_15	Cal		154				**280**			476,79			712				**1086**			

From: Bischoff et al. 1985			T_{cal}		T_{mg}		L_{cal}	L_{mg}		Neon			$V_{4\,cal}$	$V_{4\,mg}$			$V_{1\,cal}$	$V_{1\,mg}$		
Name of spectra	**Mineral**	**120 - 151**	**152 - 158**	**159 - 191**	**201 - 216**	**217 - 269**	**270 - 291**	**318 - 345**	**379 - 460**	**NE = 476,79**	**480 - 550**	**551 - 705**	**710 - 728**	**729 - 745**	**748 - 855**	**856 - 1075**	**1083 - 1092**	**1093-1097**	**Shou-lder**	**Double Peak**
LT2_p1B_5x4_100%_16	Cal		155				282			**476,79**							**1086**			
LT2_p1B_5x4_100%_17	Cal		154				**280**			476,79			712				**1086**			
LT2_p1B_5x4_100%_18	Cal		154				**281**			476,79			712				**1087**			
LT2_p1B_5x4_100%_20	Mg-rich cal		155				**281**			476,79			713				**1088**			
LT2_p1B_5x4_100%_21	Mg-rich cal		155				**281**			476,79			713				**1086**			1094
LT2_p1B_5x4_100%_21	Mg																	1094		
LT2_p1B_5x4_100%_22	Cal		154				**281**			476,79			712							
LT2_p1B_5x4_100%_23	Cal		154				**281**	326		**476,79**			712				**1087**			
LT2_p1B_5x4_100%_23	Mg							326												
LT2_p1B_5x4_100%_24	Cal		155				**281**			476,79			713				**1086**			
LT2_p1B_5x4_100%_25	Cal		155				**281**			476,79			713				**1086**			
LT2_p1B_5x4_100%_26	Cal		155				**281**			476,79			712				**1087**			
LT2_p1B_5x4_100%_27	Cal		154				**281**			476,79			712				**1086**			
LT2_p1B_5x4_100%_28	Cal		154				**282**			**476,79**			712				**1086**			
LT2_p1B_5x4_100%_29	Cal		154				**281**			476,79			712				**1085**			
LT2_p1B_5x4_100%_30	Cal		155				**281**			476,79			713				**1087**			
LT2_p1B_5x4_100%_31	Cal		155							**476,79**							**1086**			
LT2_p1B_5x4_100%_32	Cal		154				**281**			476,79			713				**1087**			
LT2_p1B_5x4_100%_33	Cal		154				**281**			476,79			713				**1086**			
LT2_p1B_5x4_100%_34	Cal		155				**281**			476,79			713				**1086**			
LT2_p1B_5x4_100%_35	Cal		154				**281**			476,79			713							
LT2_p1B_5x4_100%_36	Cal		154				**280**	324		476,79			712				**1086**			1094
LT2_p1B_5x4_100%_36	Mg							324										1094		
LT2_p1B_5x4_100%_37	Cal		154				**280**	323		476,79			712				**1086**			1094
LT2_p1B_5x4_100%_37	Mg							323										1094		
LT2_p1B_5x4_100%_38	Cal		154				**280**			476,79			712				**1086**			

From: Bischoff et al. 1985			T_{cal}		T_{mg}		L_{cal}	L_{mg}		Neon			$V_{4\,cal}$	$V_{4\,mg}$			$V_{1\,cal}$	$V_{1\,mg}$		
Name of spectra	**Mineral**	**120 - 151**	**152 - 158**	**159 - 191**	**201 - 216**	**217 - 269**	**270 - 291**	**318 - 345**	**379 - 460**	**NE = 476,79**	**480 - 550**	**551 - 705**	**710 - 728**	**729 - 745**	**748 - 855**	**856 - 1075**	**1083 - 1092**	**1093-1097**	**Shou-lder**	**Double Peak**
LT2_p1B_5x4_100%_39	Cal		154				**280**			476,79			712				**1086**			
LT2_p1B_5x4_100%_40	Cal		154				**280**			476,79			713				**1086**			
LT2_p1B_5x4_100%_41	Cal		154				**280**			476,79			713				**1086**			
LT2_p1B_5x4_100%_43	Cal		154				**280**			476,79							**1086**			
LT2_p1B_5x4_100%_44	Cal		155				**281**			476,79			713				**1086**			
LT2_p1B_5x4_100%_45	Cal		154				**281**			476,79			712				**1087**			
LT2_p1B_5x4_100%_46	Cal		154				**282**			476,79			713				**1087**			1092
LT2_p1B_5x4_100%_47	Cal		154				**281**			476,79			713				1092			
LT2_p1B_5x4_100%_48	Cal		154				280	324		**476,79**			712				**1086**			
LT2_p1B_5x4_100%_48	Mg							324												
LT2_p1B_5x4_100%_5	Cal		154				281			**476,79**			717				**1086**			
LT2_p1B_5x4_100%_6	Cal		154				282			**476,79**							**1086**			
LT2_p1B_5x4_100%_7	Cal		154				**279**			476,79			712				**1086**			
LT2_p1B_5x4_100%_8	Cal		154				281			476,79			713				**1087**			
LT2_p1B_5x4_100%_9	Cal		154				**280**			476,79			712					**1093**		**1086**
LT2_p1C_5x15_100%_14	Cal		155			224	282			**476,79**							**1086**			
LT2_p1C_5x15_100%_17	Mg		153		**207**		280	**324**		476,79			**712**	**736**				**1094**		**1087**
LT2_p1C_5x15_100%_17	Cal						280										**1087**			
LT2_p1C_5x15_100%_18	Mg		155		**209**		281	325		**476,79**				**738**			**1086**			1092
LT2_p1C_5x15_100%_18	Cal						281										1092			
LT2_p1C_5x15_100%_2	Cal		154				284	324		**476,79**			**712**				**1086**			1095
LT2_p1C_5x15_100%_2	Mg							324										1095		
LT2_p1C_5x15_100%_21	Cal		153				281	324		**476,79**			**713**				**1086**			
LT2_p1C_5x15_100%_21	Mg							324												
LT2_p1C_5x15_100%_3	Cal		154				281			**476,79**										
LT2_p1C_5x15_100%_39	Cal		155				282	323		**476,79**							**1086**			1095

From: Bischoff et al. 1985			T_{cal}		T_{mg}		L_{cal}	L_{mg}		Neon			$V_{4\,cal}$	$V_{4\,mg}$			$V_{1\,cal}$	$V_{1\,mg}$		
Name of spectra	**Mineral**	**120 - 151**	**152 - 158**	**159 - 191**	**201 - 216**	**217 - 269**	**270 - 291**	**318 - 345**	**379 - 460**	**NE = 476,79**	**480 - 550**	**551 - 705**	**710 - 728**	**729 - 745**	**748 - 855**	**856 - 1075**	**1083 - 1092**	**1093-1097**	**Shou-lder**	**Double Peak**
LT2_p1C_5x15_100%_39	Mg							323										1095		
LT2_p1C_5x15_100%_47	Cal		154				282	326		476,79							**1086**		**1094**	
LT2_p1C_5x15_100%_47	Mg							326										**1094**		
LT2_p1C_5x15_100%_5_UFO	Mg				208			**325**		476,79										
LT2_p1C_5x15_100%_6	Cal		154				281	325		476,79							**1087**			
LT2_p1C_5x15_100%_6	Mg							325										**1093**		
LT2_p1C_5x15_100%_7	Cal		154		**208**		283	**325**		476,79			**713**				**1087**			**1093**
LT2_p1C_5x15_100%_7	Mg							**325**										**1093**		
LT2_p1C_5x4_100%_1	Cal		155				**282**			476,79			**713**							
LT2_p1C_5x4_100%_10	Cal		153				280	**324**		476,79			**712**				**1086**			
LT2_p1C_5x4_100%_10	Mg							**324**												
LT2_p1C_5x4_100%_11	Mg		154				280			476,79			**713**					1095		
LT2_p1C_5x4_100%_11	Cal						280													
LT2_p1C_5x4_100%_12	Cal		152				281	325		476,79							**1087**			1094
LT2_p1C_5x4_100%_12	Mg							325										1094		
LT2_p1C_5x4_100%_13	Mg		154					325		476,79								1093		
LT2_p1C_5x4_100%_15	Cal		154				281	324		476,79			**713**	**735**			**1087**			1093
LT2_p1C_5x4_100%_15	Mg							324										1093		
LT2_p1C_5x4_100%_16	Cal		153				281	324		476,79			**713**				**1086**			
LT2_p1C_5x4_100%_16	Mg							324												
LT2_p1C_5x4_100%_20	Cal		153				280			476,79			**712**				**1086**			
LT2_p1C_5x4_100%_22	Cal		154				281			476,79			**713**					**1094**		1087
LT2_p1C_5x4_100%_23	Cal		**153**				**280**			476,79			**712**				1087			
LT2_p1C_5x4_100%_24	Mg-rich cal		153		**207**		283	**324**		476,79			**713**				**1087**		1093	
LT2_p1C_5x4_100%_24	Mg						**324**											1093		
LT2_p1C_5x4_100%_25	Cal		154				**280**	325		476,79			**712**				**1086**			

From: Bischoff et al. 1985			T_{cal}		T_{mg}		L_{cal}	L_{mg}		Neon			$V_{4\,cal}$	$V_{4\,mg}$			$V_{1\,cal}$	$V_{1\,mg}$		
Name of spectra	**Mineral**	**120 - 151**	**152 - 158**	**159 - 191**	**201 - 216**	**217 - 269**	**270 - 291**	**318 - 345**	**379 - 460**	**NE = 476,79**	**480 - 550**	**551 - 705**	**710 - 728**	**729 - 745**	**748 - 855**	**856 - 1075**	**1083 - 1092**	**1093-1097**	**Shou-lder**	**Double Peak**
LT2_p1C_5x4_100%_25	Mg							325												
LT2_p1C_5x4_100%_26	Cal		154				280			**476,79**							**1086**			
LT2_p1C_5x4_100%_27	Cal		154				**280**			476,79			**713**				**1087**			1094
LT2_p1C_5x4_100%_27	Mg																	1094		
LT2_p1C_5x4_100%_28	Cal		154				**280**			476,79			**712**							
LT2_p1C_5x4_100%_29	Mg		154				280	325		**476,79**			**713**					**1094**		1087
LT2_p1C_5x4_100%_29	Cal						280										1087			
LT2_p1C_5x4_100%_30_UFO	Mg		154		**206**		282	**324**		476,79				**736**			**1086**			
LT2_p1C_5x4_100%_30_UFO	Cal						282										**1086**			
LT2_p1C_5x4_100%_31	Cal		153				**281**			**476,79**			**712**							
LT2_p1C_5x4_100%_32	Cal		153				280	323		**476,79**			**712**				**1086**			1094
LT2_p1C_5x4_100%_32	Mg							323										1094		
LT2_p1C_5x4_100%_33	Cal		154				**281**	325		476,79			**712**				**1087**			
LT2_p1C_5x4_100%_33	Mg							325												
LT2_p1C_5x4_100%_34	Cal		155				281	324		**476,79**			**713**				**1087**			
LT2_p1C_5x4_100%_34	Mg							324												
LT2_p1C_5x4_100%_35	Cal		154				**281**			**476,79**			**713**				**1087**			1095
LT2_p1C_5x4_100%_35	Mg																	1095		
LT2_p1C_5x4_100%_36	Mg		154						460	**476,79**								1095		
LT2_p1C_5x4_100%_37	Cal		155		**208**		**282**	326		476,79			**713**				**1086**			1094
LT2_p1C_5x4_100%_37	Mg							326										1094		
LT2_p1C_5x4_100%_38_UFO	Cal		154		208		**281**	325		476,79			**712**	**735**			**1086**		1094	
LT2_p1C_5x4_100%_38_UFO	Mg							325										1094		
LT2_p1C_5x4_100%_4	Cal		153				279	**322**		**476,79**			**712**				**1087**			1095
LT2_p1C_5x4_100%_4	Mg							**322**										1095		
LT2_p1C_5x4_100%_40	Cal		155				**282**			**476,79**							**1086**			

From: Bischoff et al. 1985			T_{cal}		T_{mg}		L_{cal}	L_{mg}		Neon			$V_{4\,cal}$	$V_{4\,mg}$			$V_{1\,cal}$	$V_{1\,mg}$		
Name of spectra	**Mineral**	**120 - 151**	**152 - 158**	**159 - 191**	**201 - 216**	**217 - 269**	**270 - 291**	**318 - 345**	**379 - 460**	**NE = 476,79**	**480 - 550**	**551 - 705**	**710 - 728**	**729 - 745**	**748 - 855**	**856 - 1075**	**1083 - 1092**	**1093-1097**	**Shou-lder**	**Double Peak**
LT2_p1C_5x4_100%_41	Cal		154				280	325		**476,79**			**713**				**1085**			1095
LT2_p1C_5x4_100%_41	Mg							325										1095		
LT2_p1C_5x4_100%_42	Mg-rich cal	144				264	**288**			**476,79**			**712**				**1085**			
LT2_p1C_5x4_100%_43	Cal		152				279	323		**476,79**			**712**				**1086**			1093
LT2_p1C_5x4_100%_43	Mg							323												1093
LT2_p1C_5x4_100%_44	Cal		154				**281**			476,79			**712**							
LT2_p1C_5x4_100%_45	Cal		154				**279**	323		476,79			**711**				**1086**			
LT2_p1C_5x4_100%_45	Mg							323												
LT2_p1C_5x4_100%_46	Cal									**476,79**							**1086**			
LT2_p1C_5x4_100%_48	Cal		154				**281**			**476,79**							**1087**			
LT2_p1C_5x4_100%_49	Cal		153							**476,79**							**1087**			
LT2_p1C_5x4_100%_50_UFO	Mg		153		209		281	325		**476,79**				**736**			**1086**			1093
LT2_p1C_5x4_100%_50_UFO	Cal						281										**1087**			
LT2_p1C_5x4_100%_8	Cal		155				280			**476,79**			**712**				1086			
LT2_p1C_5x4_100%_9	Cal		154				282	**325**		**476,79**			**713**					**1094**		
LT2_p1C_5x4_100%_9	Mg							**325**										**1094**		
LT2_p1D_5x15_100%_26	Mg	142						325	**436**	476,79		**608**					**1086**		1092	
LT2_p1D_5x15_100%_26	Mg-rich cal																1092			
LT2_p1D_5x15_100%_3	Mg							325		**476,79**							1092			
LT2_p1D_5x15_100%_48	Cal		154		206		**280**	324		476,79			**712**	**731**			**1086**			1092
LT2_p1D_5x15_100%_48	Mg							324									1092			
LT2_p1D_5x15_100%_49	Cal		154				**280**	324		476,79			**712**				**1087**			1093
LT2_p1D_5x15_100%_49	Mg							324										1093		
LT2_p1D_5x15_100%_50	Cal		154		208		281	**325**		**476,79**			**712**	**737**			**1087**		1094	
LT2_p1D_5x15_100%_50	Mg							**325**										1094		
LT2_p1D_5x4_100%_1	Mg-rich cal		157				285	323	378	476,79			**712**					**1094**		

From: Bischoff et al. 1985			T_{cal}		T_{mg}		L_{cal}	L_{mg}		Neon			$V_{4\,cal}$	$V_{4\,mg}$			$V_{1\,cal}$	$V_{1\,mg}$		
Name of spectra	**Mineral**	**120 - 151**	**152 - 158**	**159 - 191**	**201 - 216**	**217 - 269**	**270 - 291**	**318 - 345**	**379 - 460**	**NE = 476,79**	**480 - 550**	**551 - 705**	**710 - 728**	**729 - 745**	**748 - 855**	**856 - 1075**	**1083 - 1092**	**1093-1097**	**Shou-lder**	**Double Peak**
LT2_p1D_5x4_100%_1	Mg							323										**1094**		
LT2_p1D_5x4_100%_10	Mg		153		209			**325**		**476,79**								**1094**		
LT2_p1D_5x4_100%_11	Mg				210			**326**		476,79				**738**			**1086**			
LT2_p1D_5x4_100%_11	Cal																**1086**			
LT2_p1D_5x4_100%_12	Mg-rich cal		155		208			**325**		**476,79**							1092			
LT2_p1D_5x4_100%_12	Mg							**325**												
LT2_p1D_5x4_100%_13_UFO	Mg-rich cal		153			221	283	325		**476,79**			**711**				1087			1094
LT2_p1D_5x4_100%_13_UFO	Mg							325										1094		
LT2_p1D_5x4_100%_14	Cal		153				281	325		476,79			**713**				**1086**			**1093**
LT2_p1D_5x4_100%_14	Mg							325										**1093**		
LT2_p1D_5x4_100%_15	Mg-rich cal		153				287	327		**476,79**							**1087**			1094
LT2_p1D_5x4_100%_15	Mg							327										1094		
LT2_p1D_5x4_100%_16	Mg-rich cal		156				282			**476,79**			**713**				**1088**			
LT2_p1D_5x4_100%_17	Cal		155				**281**	324		476,79			**713**				**1087**		1095	
LT2_p1D_5x4_100%_17	Mg							324										1095		
LT2_p1D_5x4_100%_18	Cal		154		206		280	324		476,79			**712**				**1087**			
LT2_p1D_5x4_100%_18	Mg							324												
LT2_p1D_5x4_100%_19	Cal		156				**282**	325		476,79			**713**				1086			1094
LT2_p1D_5x4_100%_19	Mg							325										1094		
LT2_p1D_5x4_100%_2	Cal		153				279	324		476,79			**712**				**1086**		1095	
LT2_p1D_5x4_100%_2	Mg							324										1095		
LT2_p1D_5x4_100%_20	Cal		153				**280**	324		476,79			**711**				**1086**		1094	
LT2_p1D_5x4_100%_20	Mg							324										1094		
LT2_p1D_5x4_100%_21	Cal		154				**280**	325		476,79			**713**				**1086**		1093	
LT2_p1D_5x4_100%_21	Mg							325										1093		
LT2_p1D_5x4_100%_22	Cal		154				282	325		**476,79**			**712**				1090		**1094**	

From: Bischoff et al. 1985			T_{cal}		T_{mg}		L_{cal}	L_{mg}		Neon			$V_{4\,cal}$	$V_{4\,mg}$			$V_{1\,cal}$	$V_{1\,mg}$		
Name of spectra	**Mineral**	**120 - 151**	**152 - 158**	**159 - 191**	**201 - 216**	**217 - 269**	**270 - 291**	**318 - 345**	**379 - 460**	**NE = 476,79**	**480 - 550**	**551 - 705**	**710 - 728**	**729 - 745**	**748 - 855**	**856 - 1075**	**1083 - 1092**	**1093-1097**	**Shou-lder**	**Double Peak**
LT2_p1D_5x4_100%_22	Mg							325										**1094**		
LT2_p1D_5x4_100%_23	Mg		153		201			323		476,79				**731**				**1094**		
LT2_p1D_5x4_100%_24	Mg		152		209			**325**		476,79						857		**1094**		
LT2_p1D_5x4_100%_25	Mg				205			**323**		**476,79**							**1087**			
LT2_p1D_5x4_100%_25	Cal																**1087**			
LT2_p1D_5x4_100%_27	Cal					251			**428**	476,79		604					**1087**			
LT2_p1D_5x4_100%_28	Cal		154				**281**			**476,79**			713				**1085**			
LT2_p1D_5x4_100%_29	Cal		154				**281**			**476,79**			713					**1093**		
LT2_p1D_5x4_100%_29	Mg																	**1093**		
LT2_p1D_5x4_100%_30	Cal		153				**281**			476,79			712					**1095**		
LT2_p1D_5x4_100%_30	Mg																	**1095**		
LT2_p1D_5x4_100%_31	Mg							**324**		**476,79**								**1095**		**1087**
LT2_p1D_5x4_100%_31	Cal																	**1087**		
LT2_p1D_5x4_100%_32	Mg				209			**326**		476,79						895	**1086**			**1094**
LT2_p1D_5x4_100%_32	Cal																	**1086**		
LT2_p1D_5x4_100%_33	Mg		154					324	387	**476,79**								**1094**		
LT2_p1D_5x4_100%_34	Mg		153					**325**		**476,79**								**1095**		
LT2_p1D_5x4_100%_35	Mg				209			**326**		476,79				**738**			**1086**		1093	
LT2_p1D_5x4_100%_35	Cal																	**1086**		
LT2_p1D_5x4_100%_36	Mg							326		476,79								1093		
LT2_p1D_5x4_100%_37	Cal		153			258	281	324		**476,79**			712				**1086**		1093	
LT2_p1D_5x4_100%_37	Mg							324										1093		
LT2_p1D_5x4_100%_38	Cal		154				285	326		**476,79**							**1087**			1095
LT2_p1D_5x4_100%_38	Mg-rich cal							326										1095		
LT2_p1D_5x4_100%_39	Mg-rich cal		153				287	325	439	**476,79**			714					**1093**		
LT2_p1D_5x4_100%_39	Mg							325										**1093**		

From: Bischoff et al. 1985			T_{cal}		T_{mg}		L_{cal}	L_{mg}		Neon			$V_{4\,cal}$	$V_{4\,mg}$			$V_{1\,cal}$	$V_{1\,mg}$		
Name of spectra	**Mineral**	**120 - 151**	**152 - 158**	**159 - 191**	**201 - 216**	**217 - 269**	**270 - 291**	**318 - 345**	**379 - 460**	**NE = 476,79**	**480 - 550**	**551 - 705**	**710 - 728**	**729 - 745**	**748 - 855**	**856 - 1075**	**1083 - 1092**	**1093-1097**	**Shou-lder**	**Double Peak**
LT2_p1D_5x4_100%_4	Mg							325		**476,79**								**1093,2**		
LT2_p1D_5x4_100%_40	Mg		154		208			**324**		**476,79**							1085	**1093,1**		
LT2_p1D_5x4_100%_40	Cal																	1085		
LT2_p1D_5x4_100%_41	Mg							325		**476,79**							**1086**		1094	
LT2_p1D_5x4_100%_41	Cal																**1086**			
LT2_p1D_5x4_100%_42	Cal		153							**476,79**							1085		1095	
LT2_p1D_5x4_100%_42	Mg																	1095		
LT2_p1D_5x4_100%_43	Cal		153				**280**	325		476,79			**712**				**1087**			1095
LT2_p1D_5x4_100%_43	Mg							325										1095		
LT2_p1D_5x4_100%_44	Cal		154				281	327		**476,79**			**712**		**772**		**1087**		1095	
LT2_p1D_5x4_100%_44	Mg							327										1095		
LT2_p1D_5x4_100%_45	Cal		154				282			**476,79**			**713**				**1087**			
LT2_p1D_5x4_100%_46	Cal		154				**281**			476,79			**713**				**1087**			
LT2_p1D_5x4_100%_47	Cal		154	191			**281**	325		476,79			**712**				**1087**	**1093**		
LT2_p1D_5x4_100%_47	Mg							325										**1093**		
LT2_p1D_5x4_100%_5	Mg							327		**476,79**		646						**1094**		
LT2_p1D_5x4_100%_6	Mg				208			**325**		476,79								**1093**		
LT2_p1D_5x4_100%_7	Mg				208			**325**		476,79								**1094**		
LT2_p1D_5x4_100%_8	Mg							**325**		476,79							**1088**			
LT2_p1D_5x4_100%_8	Mg-rich cal																**1088**			
LT2_p1D_5x4_100%_9	Mg							**326**		476,79							**1086**			
LT2_p1D_5x4_100%_9	Cal																**1086**			

Legend	Grey numbers = Not sure.
Cal	Blue numbers = Spectra including two minerals. The blue numbers show that both minerals have been counted.
Mg-rich cal	**Bold numbers** = The 2 or 3 strongest peaks per spectrum
Mg	
Unknown	

From: Bischoff et al. 1985			T_{cal}		T_{mg}		L_{cal}	L_{mg}		Neon			$V_{4\,cal}$	$V_{4\,mg}$			$V_{1\,cal}$	$V_{1\,mg}$		
Name of spectra	**Mineral**	**120 - 151**	**152 - 158**	**159 - 191**	**201 - 216**	**217 - 269**	**270 - 291**	**318 - 345**	**379 - 460**	**Ne = 476,79**	**480 - 550**	**551 - 705**	**710 - 728**	**729 - 745**	**748 - 855**	**856 - 1075**	**1083 - 1092**	**1093-1097**	**Shou-lder**	**Double Peak**
LT4_A_10x5_100%_1	Cal		155				**282**			476,79			713				**1087**			
LT4_A_10x5_100%_10	Cal		155			219	281			**476,79**		639	711				**1087**			
LT4_A_10x5_100%_11	Mg-rich cal		155				281			**476,79**							**1088**			
LT4_A_10x5_100%_12	Cal		155				282			**476,79**			713				**1087**			
LT4_A_10x5_100%_13	Cal		155				280	325		**476,79**			712				**1087**	1093		
LT4_A_10x5_100%_13	Mg							324										1093		
LT4_A_10x5_100%_14	Cal		154				281			**476,79**			714				**1086**	1095		
LT4_A_10x5_100%_14	Mg																	1095		
LT4_A_10x5_100%_15	Cal		154				280			**476,79**			713				**1086**			
LT4_A_10x5_100%_16	Cal		155				281			**476,79**			713				**1087**			
LT4_A_10x5_100%_17	Cal		155				280			**476,79**			712				**1086**			
LT4_A_10x5_100%_18	Cal		155				281	321		**476,79**		641	713			973	**1087**			
LT4_A_10x5_100%_18	Mg							321												
LT4_A_10x5_100%_19	Cal		155				281	322		**476,79**			714				**1087**			
LT4_A_10x5_100%_19	Mg							322												
LT4_A_10x5_100%_2	Cal		154				**281**			476,79		640	712				**1086**			
LT4_A_10x5_100%_3	Cal		154				**281**			476,79		639	712				**1087**			
LT4_A_10x5_100%_4	Cal		155				280	326		**476,79**		641	712				**1087**	1095		
LT4_A_10x5_100%_4	Mg							326										1095		
LT4_A_10x5_100%_5	Cal		155				280			**476,79**			712				**1087**			
LT4_A_10x5_100%_6	Mg-rich cal		156				**282**			476,79			713				**1088**			

From: Bischoff et al. 1985			T_{cal}		T_{mg}		L_{cal}	L_{mg}		Neon			$V_{4\,cal}$	$V_{4\,mg}$			$V_{1\,cal}$	$V_{1\,mg}$		
Name of spectra	**Mineral**	**120 - 151**	**152 - 158**	**159 - 191**	**201 - 216**	**217 - 269**	**270 - 291**	**318 - 345**	**379 - 460**	**Ne = 476,79**	**480 - 550**	**551 - 705**	**710 - 728**	**729 - 745**	**748 - 855**	**856 - 1075**	**1083 - 1092**	**1093-1097**	**Shou-lder**	**Double Peak**
LT4_A_10x5_100%_7	Cal		154							**476,79**							1086			
LT4_A_10x5_100%_8	Cal		155				**281**			476,79		640	713				**1087**			
LT4_A_10x5_100%_9	Cal		155			224	281	324		**476,79**		604	713				**1087**			
LT4_A_10x5_100%_9	Mg							324												
LT4_B_10x5_100%_1	Cal		154				280	322		**476,79**			712				**1086**			
LT4_B_10x5_100%_1	Mg							322												
LT4_B_10x5_100%_10	Cal	151								**476,79**		704					**1086**			
LT4_B_10x5_100%_11	Cal		155				**281**			476,79			713				**1087**			
LT4_B_10x5_100%_12	Cal		155				282			**476,79**			713				**1087**			
LT4_B_10x5_100%_13	Mg-rich cal							323		**476,79**			713				**1092**		1087	
LT4_B_10x5_100%_13	Cal																1087			
LT4_B_10x5_100%_14	Cal		153				280	323		**476,79**			712				**1086**			
LT4_B_10x5_100%_14	Mg							323												
LT4_B_10x5_100%_15	Cal		155				281	322		**476,79**		640	713				**1087**			
LT_B_10x5_100%_15	Mg							322												
LT4_B_10x5_100%_16	Cal		155				281	322		**476,79**			713				**1087**			
LT4_B_10x5_100%_16	Mg							322												
LT4_B_10x5_100%_17	Cal		154				282	321		**476,79**							**1087**			
LT4_B_10x5_100%_17	Mg							321												
LT4_B_10x5_100%_18	Cal		154				282		385	**476,79**			713				**1087**			
LT4_B_10x5_100%_19	Cal		155				**281**			476,79			713				**1087**			
LT4_B_10x5_100%_20	Cal		154				280		385	**476,79**			713				**1086**			
LT4_B_10x5_100%_4	Cal		155				281			**476,79**		640	713				**1087**			
LT4_B_10x5_100%_5	Cal		154				280			**476,79**			713				**1087**			
LT4_B_10x5_100%_6	Cal		154			222	280			**476,79**	525		714				**1087**			
LT4_B_10x5_100%_7	Cal		155				281			**476,79**			713				**1087**			

From: Bischoff et al. 1985			T_{cal}		T_{mg}		L_{cal}	L_{mg}		Neon			$V_{4\,cal}$	$V_{4\,mg}$			$V_{1\,cal}$	$V_{1\,mg}$		
Name of spectra	**Mineral**	**120 - 151**	**152 - 158**	**159 - 191**	**201 - 216**	**217 - 269**	**270 - 291**	**318 - 345**	**379 - 460**	**Ne = 476,79**	**480 - 550**	**551 - 705**	**710 - 728**	**729 - 745**	**748 - 855**	**856 - 1075**	**1083 - 1092**	**1093-1097**	**Shou-lder**	**Double Peak**
LT4_B_10x5_100%_8	Cal	150				269				**476,79**			712				**1085**			
LT4_B_10x5_100%_9	Cal	146				**269**				476,79			712				**1085**			
LT4_B_15x5_100%_2_UFO	Unknown					223		321		**476,79**		642			853	**1003**				
LT4_B_15x5_100%_3_UFO	Unknown			183				321		**476,79**	489	643			854	**1004**				
LT4_foram1_internal filling_2x5_1	Cal									476,79							**1086**			
LT4_foram1_internal filling_2x5_2	Cal									476,79							**1086**			
LT4_foram1_internal filling_2x5_3	Mg-rich cal						282			476,79							**1088**			
LT4_foram1_shell_2x2_50%_1	Cal									476,79							**1087**			
LT4_foram1_shell_2x5_1	Cal		153							476,79			711				**1086**			
LT4_foram1_shell_2x5_2	Cal		154				281			476,79							**1086**			
LT4_foram1_shell_4x2_50%_1	Cal		154				282										**1087**			
LT4_foram1_shellinternalwall_2x5_2	Mg-rich cal	151					290			**476,79**			710				**1083**			
LT4_foram2_internal filling_2x5_1	Cal									476,79							1085			
LT4_foram2_shell_2x3_2	Cal		154														1085			
LT4_foram2_shell_3x5_1	Cal		154							476,79							1086			
LT4_foram2_shell_3x5_2 Ne ok	Cal		154				**281**			476,79			713				**1087**			
LT4_foram2_shell_3x5_3	Cal		154				282			**476,79**							**1087**			
LT4_foram3_internal filling_2x3_25%_1	Cal		155							476,79							1086			
LT4_foram3_shell_2x5_50%_1	Cal						**281**			476,79			711				**1087**			
LT4_foram3_shell_5x3_50%_2	Cal		154				**281**			476,79							**1087**			
LT4_foram3_shell_3x2_50%_3	Cal		154							476,79			712				**1086**			
LT4_foram5_internal filling_2x2_50%_1	Mg-rich cal		**154**				285			477,19		646					**1087**			
LT4_foram5_internal filling_2x2_50%_2	Cal		153					335		476,79		**646**					**1086**			
LT4_foram5_internal filling_2x2_50%_2	Mg							335												
LT4_foram6_internal filling_2x3_50%_1	Cal		156							476,79						910	**1085**		1088	
LT4_foram6_internal filling_2x3_50%_1	Mg-rich cal																		1088	

From: Bischoff et al. 1985			T_{cal}		T_{mg}		L_{cal}	L_{mg}		Neon			$V_{4\ cal}$	$V_{4\ mg}$			$V_{1\ cal}$	$V_{1\ mg}$		
Name of spectra	**Mineral**	**120 - 151**	**152 - 158**	**159 - 191**	**201 - 216**	**217 - 269**	**270 - 291**	**318 - 345**	**379 - 460**	**Ne = 476,79**	**480 - 550**	**551 - 705**	**710 - 728**	**729 - 745**	**748 - 855**	**856 - 1075**	**1083 - 1092**	**1093-1097**	**Shou-lder**	**Double Peak**
LT4_foram6_shell_4x2_50%_1	Cal		154							476,79							**1086**			
LT4_foram6_shell_4x2_50%_2	Cal		155							**476,79**							**1087**			
LT4_foram6_XX1_4x4_50%_1	Cal		155							476,79							**1087**			
LT4_foram6_XX1_4x4_50%_2	Cal		154				281			476,79			711				**1086**			
LT4_foram6_XX2_4x4_50%_1	Mg-rich cal		155				284			476,79			713				**1087**			
LT4_foram6_XX2_4x4_50%_2	Cal		154				282			476,79			713				**1087**			